University of Bath

UNIVERSITY OF BATH

MPHIL

Towards robust cellulose-based nanofiltration membranes

Wirawan, Remigius

Award date:
2023

Awarding institution:
University of Bath

[Link to publication](#)

Towards Robust Cellulose-based Nanofiltration Membranes

by

Remigius H. Wirawan

Supervisors:

Prof Janet L. Scott (Chemistry)

Dr Darrell A. Patterson (Chemical Engineering)

March 2023

A thesis submitted in partial fulfilment of the requirements
for the MPhil Programme in Chemistry at the University of Bath

Dedicated for my wife, DI, and my sons TW and DW.

And for my parents, AW and SP.

Abstract

The sustainability of cellulose as a material is unquestionable, with it being the most abundant biopolymer on earth. The chemical recalcitrance of cellulose makes its processing challenging but it can also be used as a benefit. This PhD project investigates the recently discovered organic electrolyte solutions (OESs), to dissolve underivatised cellulose and reports the development of cellulose membranes for use in membrane separation applications. Membrane separation processes are well established with many industrial applications. Two examples of membrane separation processes, Nanofiltration (NF) and Ultrafiltration (UF), separate solutes from aqueous feed over a membrane. A challenge for NF and UF is to extend their application range from aqueous to non-aqueous feeds. Meeting this challenge requires solvent stable membrane that preserve their separation characteristics in a wide range of solvents. This emerging technology is termed organic solvent solvent nanofiltration (OSN). Few comercial OSN membranes are stable in dipolar aprotic group of solvents in particular, so cellulose membranes are poised to fill this gap.

This thesis reports investigations on several OESs, with emphasis on cellulose dissolution performance and discovery of efficient co-solvents. These findings were then employed to develop cellulose membranes via Non-solvent Induced Phase Separation (NIPS) methodology and the membranes produced were tested for their permeation, rejection, as well as physical and mechanical properties.

The cellulose membranes developed were shown to be stable and have reasonable flux in wide ranging organic solvents, including dipolar aprotic solvents; can be categorised as UF membranes in terms of their rejection characteristics of non-polar solutes; but are found to be performing at NF range (MW < 1000 Da) for their rejection of polar compounds. Membrane properties can be tuned, to some extent, by using different OESs as the cellulose casting solutions, by changing certain variables such as the non-solvent for the regeneration stage, and by performing chemical crosslinking to the membranes as a post-treatment step.

Table of Contents

Chapter 1 Introduction

1.1 Cellulose as a Sustainable Biopolymer

Cellulose is the most abundant renewable biopolymer on Earth. About a third of all plant matter is cellulose. Cotton is an example of the purest form of natural cellulose and wood contains about 50% of cellulose.[1] Cellulose can also be synthesised by some bacteria, commonly referred to as bacterial cellulose. Since its discovery in 1838, cellulose have been extensively studied and discoveries are being made with respect to its biosynthesis, assembly, and structural features.[2] Derivatised cellulose has many important applications in the fibre, paper, membrane, polymer, and paints industries.[3]

Cellulose is a polysaccharide having a molecular structure similar to starch. It is a high molecular weight homopolymer where its D-glucose units are linked by β(1→4)-glycosidic bonds (Figure 1). Due to this β-glycosidic bond, cellulose molecules adopt an extended and stiff rod-like structure. The number of glucose units or the degree of polymerization (DP) is up to 20000 but typically 400-1000.[4] Shorter cellulose chains are mainly localized in primary cell walls. These chemical and structural properties give cellulose its tough, fibrous, water-insoluble characteristics that play an essential role in maintaining the structure of plant cell walls.
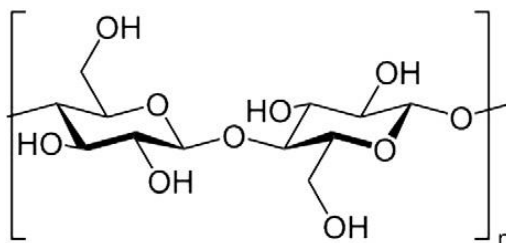
Figure 1. Chemical Structure of Cellulose

(Image from Wikimedia Common licence, public domain)

Cellulosic natural fibres (e.g., abaca, bamboo, jute, flax, and hemp) have long been used as reinforcement fibres in polymer matrices.[5] Compared to traditional reinforcement fibres, e.g., glass and carbon fibres, cellulosic fibres have the advantages of low material cost, low environmental impact (renewable and carbon neutral), competitive strength to density ratio and

biodegradability.[5] The cellulose's relatively good strength is thought to be caused by the high Young's modulus along the chain direction due to the strong glycosidic bonds in oligosaccharide chains.[6] Cellulosic fibres are also almost nonabrasive to processing equipment and safe to handle.[5]

Some disadvantages of using cellulosic fibres include limited thermal stability (<200°C), high moisture absorption (hydrophilic due to the high number of hydroxyl groups), swelling, low microbial resistance and non-flame retardant (e.g. in electronics applications).[7] However, many of these disadvantages can be minimised or even eliminated by appropriate treatment and composite processing.

1.2   Current Cellulose Processing & Dissolution Methods

Generally, the processing of biomass into desired products requires firstly the dissolution of cellulose. Cellulose is difficult to dissolve with common solvents due to its strong intra- and inter-molecular hydrogen bonding.[8]
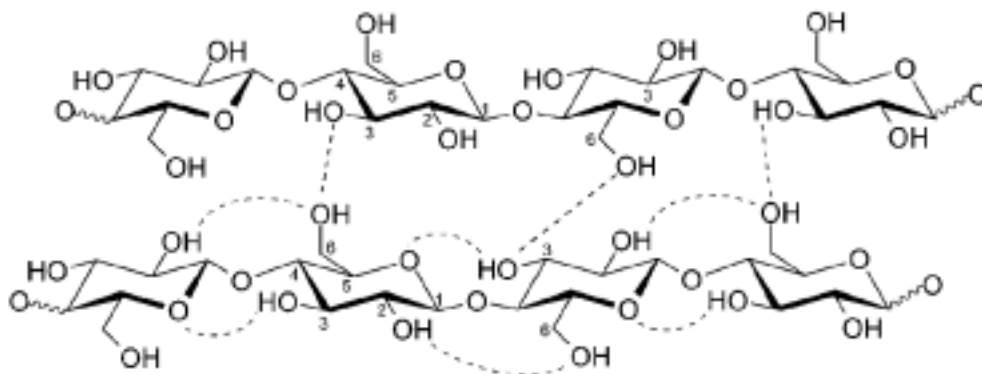
Figure 2. Intra-and inter-molecular hydrogen bonds in cellulose. From Pinkert *et al.*, 2010.[8]

There are currently two methods used commercially to dissolve cellulose in order to produce derivatised products: the viscose and Lyocell processes.[3]

The viscose process is over a hundred years old and has been the dominant production method for reconstituted cellulose, with an annual world production of 5.63 megatons in 2019.[9] However, the process has serious drawbacks from a technological standpoint (see **Figure 3**), requires the highest-quality dissolving pulp, and is decidedly 'non green' due to the use of carbon disulfide, and the resultant by-products.
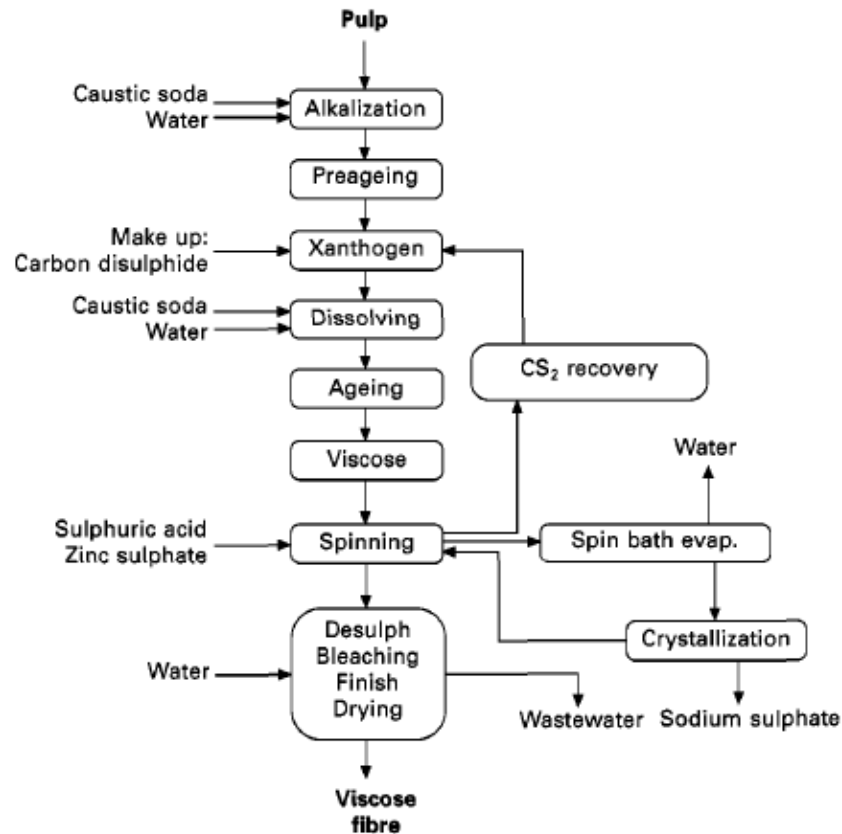
Figure 3. Viscose process flowsheet highlighting its complexity From Ciechanska *et al.*, 2009.[10]

Efforts to make the viscose process free from carbon disulfide have been developed, the most well-known is the CarbaCell/carbamate process which uses urea to convert the cellulose to cellulose carbamate using xylene as a transfer medium.[3] However, the fibre industry has been slow to take it up.

The second commercial process is the Lyocell process which was developed by Austrian company Lenzing AG as a method that is able to dissolve cellulose without prior activation or derivatisation.[3] This process uses *N*-methylmorpholine-*N*-oxide (NMMO) as the solvent; solutions of up to 23% cellulose can be produced and NMMO recovery is close to 100% in industry.[3] The Lyocell process has advantages over the viscose process, namely: greener process due to high recovery of NMMO, higher tolerance to the quality (or lack thereof) the cellulose pulp feedstock and reduced complexity (see Figure 4). Its disadvantages are: process temperatures between 80 and 120 °C are needed in order to lower the viscosity of the cellulose/NMMO/water solution and

as NMMO is an oxidising agent, the process requires stringent temperature control and poses health and safety risks.[3]
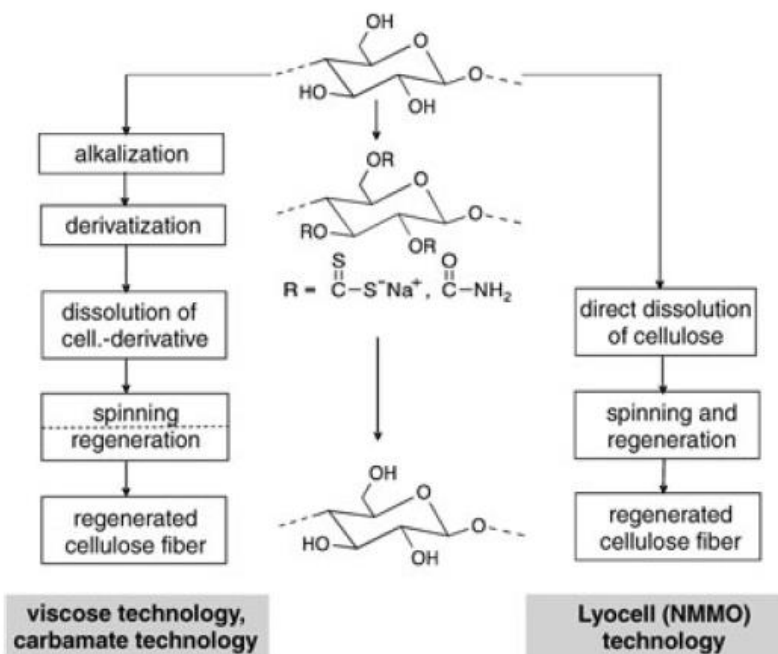
Figure 4. Process principles in regenerated cellulose technologies: left, derivatisation methods; right, direct dissolution method. From Klemm *et al.,* 2005.[3]

With the existing processes used in the cellulose industry posing several drawbacks and inefficiencies as described above, development of new, efficient solvents or solvent systems is the first step for the transformation towards much higher utilisation of cellulose as a renewable material in technologically demanding applications.

1.3   Ionic Liquids and Organic Electrolyte Solutions for Dissolution of Cellulose

The discovery of ionic liquids can credited to Paul Walden in 1863, when he was looking for salts that would melt close to ambient temperature in order to conduct his low temperature studies.[11] In 1934, Graenacher found molten that *N*-ethylpyridinium chloride could dissolve cellulose; however, since the salt was uncommon and has a relatively high melting point (118 °C), the finding was not developed further.[4] These studies of "molten salts" were not particularly linked with the solvating property of ionic liquids, until the interest in these kinds of liquids began to be registered in literature in 1980s and 1990s.[11]

The so-called 'traditional' non-aqueous cellulose solvents emerged in the literature in the 1980s, namely LiCl/DMAc and LiCl/DMI, which can actually be classified as organic electrolyte solutions (OES), a recently coined term referring to a solution of a salt in an organic solvent.

Ionic liquids (ILs) are salts, or mixtures of salts, with melting temperature below 100 °C. As alternative solvents, ionic liquids have many attractive properties, including negligible vapour pressure, non-flammability, thermal stability and recyclability.[11,12,13,14]

By early 2000s, several ionic liquids, especially imidazolium-based ones, were discovered as efficient solvents of cellulose, pioneered by the work of Rogers and co-workers[4]. Feng and Chen[15] offered a possible mechanism of cellulose dissolution in imidazolium-based ionic liquid whereby both the cation and anion interact with the hydroxyl groups of cellulose to effect dissolution. However, despite the efficacy, dissolving cellulose in ILs suffers from several drawbacks, such as slow rate of dissolution, high viscosity of the resultant solution and high costs of ILs.[16]

By 2012 or so, the term or the use of organic electrolyte solution (OES), which is a binary mixtures composed of ionic liquid (IL) and organic solvent, started to appear in literature[16–18] and seen as a potential improvement to using a neat IL as cellulose solvent, driven primarily by motivation to minimise the use of IL to reduce cost and/or viscosity of the resultant solution. Rinaldi[16] and Gericke *et al*.[19] pioneered studies of using binary mixtures composed of ionic liquid and organic solvent –henceforth OES– for cellulose dissolution, in which the systems only contain a minor molar fraction of IL.[16]

Rinaldi used two imidazolium ILs, BMIM Cl and 1-ethyl-3-methylimidazolium acetate (EMIM AcO) coupled with a wide range of organic solvents as his OESs.[16] He noted that replacing BMIM Cl with EMIM AcO makes the dissolution of cellulose instantaneous.[16]
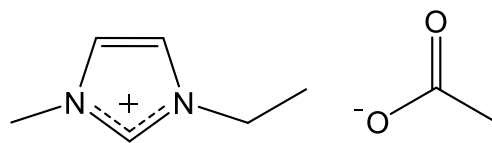
Figure 5. Chemical structure of 1-ethyl-3-methylimidazolium acetate (EMIM AcO)

(Image: own work)

Additionally, Rinaldi also screened a wide range of solvents to be used as a co-solvent with EMIM AcO, and it was found that OESs with DMSO needed the lowest amount of the IL for Avicel (a microcrystalline cellulose product from Sigma-Aldrich) dissolution, Table 1.

Table 1. Molar fraction of EMIM AcO (X_{IL}) required in OESs with different solvent for Avicel dissolution (adapted from Rinaldi, 2011)[16]

Solvent	X_{IL} (molar fraction of IL)
Dimethylsulfoxide	0.08
Dimethylformamide	0.10
N-Methylethylpyrrolidinone	0.16
1,3-Dimethyl-2-imidazolidinone	0.18
Sulfolane	0.23
Dimethylacetamide	0.27
tert-Butanol	0.48

Even though OESs have been demonstrated to be better solvent systems for cellulose than ILs alone, little is known of the mechanism of this phenomenon. Zhao *et al.* studied the interaction of cellulose with OESs by molecular dynamics simulations and quantum chemistry calculations and concluded that the effect of the organic solvents as co-solvents on the solubility of cellulose is indirectly achieved by influencing the hydrogen bond interactions between the anions and the hydroxyl groups of cellulose.[20] The strong preferential solvation of acetate anions by aprotic solvents (e.g. DMSO and DMF) can partially disrupt the ionic attraction of EMIM AcO by solvation of the cations and anions, and the dissociated acetate anions would then interact with cellulose to improve its dissolution.[20]

Kamlet–Taft parameters i.e. α (hydrogen bond donor/acidity), β (hydrogen bond acceptor/basicity) and π* (polarisability) parameters were also analysed in Rinaldi's study in an attempt to relate these parameters with cellulose dissolution performance of different solvent systems. Rinaldi concluded that the basicity of the solvent system is essential for the dissolution of cellulose and that the polymer behaves as a hydrogen-bond donor in solution.[16] In addition, to avoid competition between the organic solvent and cellulose for the hydrogen bond basicity of

the IL, the solvents should show, preferentially, no hydrogen-bond acidity.[16] Thus aprotic solvents are preferred. However, Rinaldi noted that surprisingly, EMIM AcO-based OES containing tetramethylurea (TMU) required much higher X_{IL} (0.59) to instantaneously dissolve cellulose compared to that containing 1,3-dimethyl-2-imidazolidinone (DMI, X_{IL}=0.18), despite the two co-solvents are structural analogues and have very similar Kamlet-Taft parameters, Figure 6. This suggests that there are probably other important parameters to cellulose dissolution that are still overlooked.

DMI, α=0, β=0.79 and π*=0.92   TMU, α=0, β=0.8 and π*=0.83
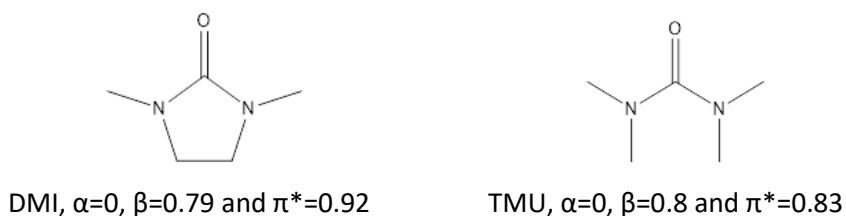
Figure 6. Structures and Kamlet-Taft parameters of DMI and TMU. (Image: own work)

At probably around the same time as Rinaldi's study, Gericke *et al.*[19] investigated the effects of 18 solvents and 3 binary solvent mixtures on cellulose solutions in three ILs with respect to the solution phase behaviour. They concluded that appropriate cellulose co-solvents should be highly polar, have very low "acidity" (α < 0.5), and relatively high "basicity" (β ≥ 0.4).[19]

Gomes and co-workers studied the solubility of microcrystalline cellulose in BMIM AcO/DMSO system and they observed that it enhances the solvent power of the ionic liquid by decreasing the time needed for dissolution.[21] They measured the mass transport properties (viscosity and ionic conductivity) of the OES and assessed the molecular structure and interactions around glucose, the structural unit of cellulose, by means of molecular dynamic simulations. They found that DMSO decreased the viscosity and increased the conductivity of the OES, but without inducing cation–anion dissociation in the ionic liquid.[21] Molecular simulation confirmed the finding by showing that by adding DMSO to an equimolar BMIM AcO/DMSO concentration, the hydrogen-bond network in the ionic liquid was not significantly affected and DMSO did not interact specifically with glucose. They concluded that DMSO, as a co-solvent, improved the OES's dissolution capabilities by facilitating mass transport by decreasing the solvent mixture's viscosity without significantly affecting the specific interactions between cations and anions or between the ionic liquid and cellulose.[21] Their study did not offer a possible explanation as to why co-

solvents that have similar viscosities and conductivities exert vastly different effects on cellulose dissolution as highlighted in the above studies, as well as from the findings revealed in this report.

In a recent 2014 study, Rein and co-workers[22] investigated cellulose dissolution in binary EMIM AcO/co-solvent mixtures and found that cellulose dissolved easier in IL/co-solvent mixtures that exhibit the highest electrical conductivity. Furthermore, the study also showed that for all EMIM AcO/co-solvent mixtures tested (co-solvent: chloroform, DCM, DMF, acetonitrile and propylene carbonate), the electrical conductivities had clear maxima at around X_{IL} range of 0.33 to 0.5.[22] However, the study did not seem to determine the (absolute) solubility of each of the OESs, hence even though electrical conductivity was shown to affect the kinetics of cellulose dissolution in OESs, there's no evidence whether it also had a role in the thermodynamics aspect of the dissolution (which determines the cellulose solubility in OES). Indeed, they found that even though some co-solvents have higher electrical conductivity, their minimum IL content required to dissolve cellulose when paired with EMIM AcO (min. X_{IL}), were higher than those with less electrical conductivity, which seemed contradictory. For example, acetonitrile had higher electrical conductivity than both DMF and DCM, but its min. X_{IL} was considerably higher than both DMF and DCM, Table 2. They concluded that electrical conductivity alone could not explain the fundamental aspect of cellulose dissolution in OESs.[22] This study, however, did seem to confirm the finding from a previous study[19] which suggested that cellulose dissolution in OESs correlates positively with the co-solvent's polarity. Electrical conductivity of a solvent depends on its dielectric constant, which is a relative measure of its chemical polarity, along with its dipole moment.[23,24]

Table 2. Electrical conductivities of co-solvents and min. X_{IL} values for EMIM AcO/co-solvent (adapted from Rein *et al*., 2014)[22]

Co-solvent	Electrical Conductivity (mS cm^{-1})	Min. X_{IL}
Chloroform	0.02	0.5
DCM	0.005	0.2
DMF	0.03	0.1
Acetonitrile	0.07	0.5
Propylene carbonate	0.04	0.25

Investigation of OESs for cellulose dissolution, specifically measurement of dissolution capacities and selection of organic solvents as co-solvents, formed the early part of this project as efficient cellulose solvents are seen as important enablers for the development of cellulose membrane via solution casting method. Chapter 3 reports the findings of the study in cellulose dissolution and OESs whilst the rest of the chapters focus on the cellulose membrane preparation and characterisations.

1.4 Membrane Separation Technologies

A membrane, in membrane separation processes, is a selective barrier that allows the passage of certain constituents and retains other constituents. The influent of a membrane is known as the feed stream, the stream that passes through the membrane is known as the permeate and the stream containing the retained constituents is the retentate or concentrate (Figure 7).
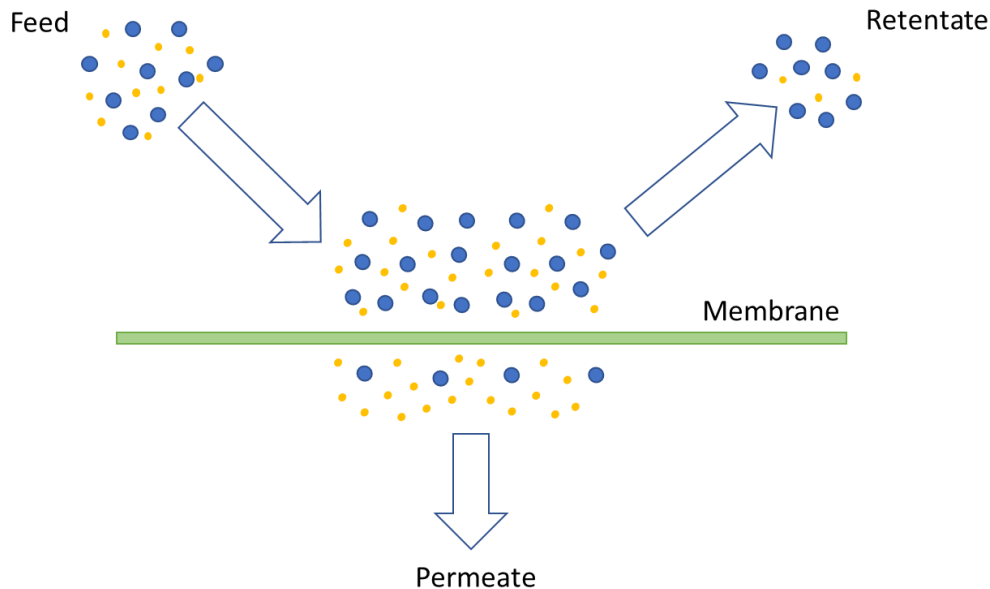
Figure 7. Membrane-based separation process. (Image: own work)

Membrane separation processes, such as microfiltration (MF), ultrafiltration (UF), nanofiltration (NF), reverse osmosis (RO) and gas separation, are well established processes with many industrial applications. NF, which can be seen as between RO and UF, is a removal process of solutes from aqueous feeds by applying a pressure gradient over a membrane.[25,26] The rejected solutes are typically divalent ions, sugars, dyes and organic compounds, which have molecular weight (MW) in the range of 200 to 1000 Daltons.[27] Selection of NF membranes is based on the molecular weight cut-off (MWCO) of the membrane. MWCO is defined as the molecular weight at which 90% solute rejection is obtained by interpolation from the MWCO curve, which is a plot of solute rejection against molecular weight.
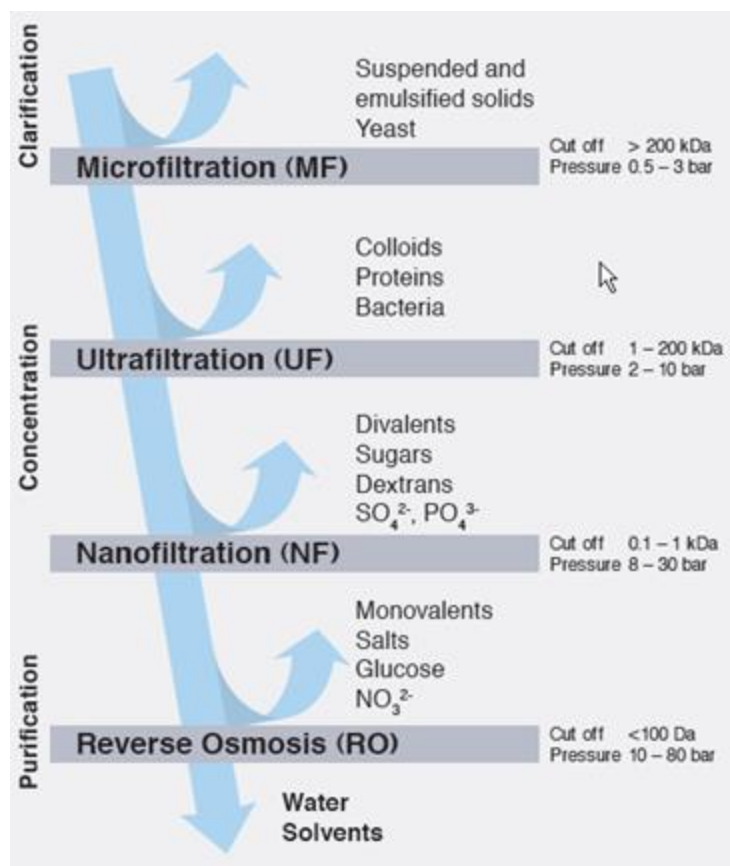
Figure 8. Membrane separation in aqueous environment.

Adapted from Membrane Separation in Aqueous Environment.[28]

1.5   Organic Solvent Nanofiltration (OSN)

A challenge for NF –and RO, to some extent– is to extend their application range from aqueous to organic feeds. Industries from oil refining to fine chemicals and pharmaceuticals could reap major benefits from reduced energy consumption and simplification of solvent-based processes, just as the desalination industry has benefitted from the introduction of reverse osmosis membranes.[29] Meeting this challenge requires solvent stable membranes that preserve their separation characteristics in a wide range of solvents. This emerging technology is termed organic solvent nanofiltration (OSN) which encompasses molecular separation and purification processes carried out in organic solvents, Figure 9, based on research efforts directed at fabrication of such solvent stable membranes.[29]

19
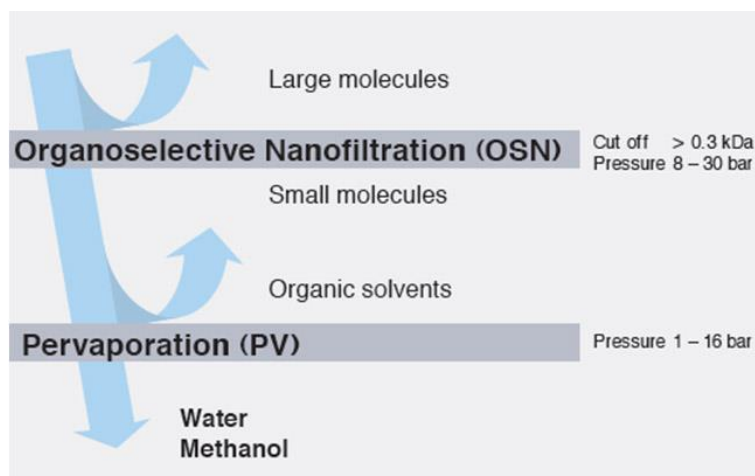
Figure 9. Organic Solvents Nanofiltration (OSN).

Adapted from Membrane Separation in Non-Aqueous Environment.[30]

A particularly difficult challenge for OSN is in certain demanding solvents like dipolar aprotic solvents such as DMF, *N*-methylpyrrolidinone (NMP), DMAc and DMSO, since most polymeric membranes would not be stable in these solvents.[31] This class of solvent is widely used in the synthesis of fine chemicals and pharmaceutical compounds as they dissolve both polar and less polar compounds, promote many types of reaction, have favourable vapour pressures and generally have high boiling points (allowing a wide range of temperatures to be employed to drive reactions without recourse to specialised high pressure equipment). Solute-solvent separations in industries that commonly use these dipolar aprotic solvents generally rely on conventional separation techniques such as distillations or extractions which consumes a lot of energy or produces wastes.[31] If OSN could be employed effectively in recovery of products from such solvents, then solvents purification and recycling processes can be made in a more efficient manner, reducing costs and energy consumption as well as improving the Process Mass Intensity (a measure widely used in the pharmaceutical industry to compare waste profiles of reactions).[32] Membrane separation process also has the advantage of potentially being able to be retrofitted to an existing separation process, turning it into a hybrid process.[33]

However, many current polymeric NF membranes are prepared from solutions of polymers in dipolar aprotic solvents producing membranes that exhibit poor stability to such solvents. It is clear that a key enabler of OSN is a membrane portfolio that combines chemical, mechanical and thermal stability with excellent rejections and high permeabilities.[34] This is where the opportunity

20

lies for cellulose nanofiltration membranes, as cellulose is known to be resistant to most organic solvents.[35] Therefore, a major expectation of the project was to be able to produce cellulose membranes that would be stable in organic solvent applications.

The term 'robust membranes' is used in the title as well as in the objectives of the thesis (Section 1.6 below) to mean that the membranes produced are hoped to be stable in organic solvent applications, both in sense of resistance to a wide range of organic solvents, including dipolar aprotic solvents family, as well as stable in the sense of durability of prolonged exposure to these solvents.

1.6   Hypothesis and Objectives

One of the main challenges for the development of cellulose membrane is the difficulty in getting high enough concentration of cellulose into solution to prepare cellulose membranes via solution casting method. The discovery of organic electrolyte solution (OES) gives opportunities in cellulose processing in general and cellulose membrane development in particular, hence studies and testing of cellulose dissolution by OESs formed the initial part of this thesis. Two hypotheses were developed during the initial phase of the project, the first was that the knowledge of cellulose dissolution in OESs would play an important role in the development of cellulose membranes, and the second was that testing and expected discovery of effective organic solvent as co-solvent in OESs could serve as an important enabler in the development of cellulose membranes for nanofiltration

The objectives of the project are therefore:

To investigate and gather data & knowledge of cellulose dissolution using various OESs as solvent systems, with emphasis on and discovery of efficient co-solvents.

To utilise the above findings to develop robust cellulose membranes via Non-solvent Induced Phase Separation (NIPS) methodology, particularly for organic solvent nanofiltration (OSN) applications.

To test and perform characterisation techniques on cellulose membranes produced for their permeation, rejection, as well as physical and mechanical properties.

Chapter 2 Experimental Section

2.1 Design of Experiments

To meet thesis objective 1: to investigate and gather data & knowledge of cellulose dissolution using various OESs as solvent systems, with emphasis on and discovery of efficient co-solvents, the following experiments and analyses were performed:

- Cellulose solubility testing in OESs
- Density and excess molar volume determination
- Analyses of solvent parameters and selection of co-solvents

To meet thesis objective 2: to utilise the findings from cellulose dissolution studies to develop cellulose membranes via Non-solvent Induced Phase Separation (NIPS) methodology, the following experiments were performed with their procedures recorded:

- Preparation of cellulose solution for casting
- Casting of membranes and Non-solvent Induced Phase Separation procedure
- Post treatment of membranes, including crosslinking

To meet thesis objective 3: to test and perform characterisation techniques on cellulose membranes produced for their permeation, rejection, as well as physical and mechanical properties, the following experiments were performed:

- Permeation tests
- Dye rejection tests
- Polystyrene rejection tests for molecular weight cut-off determination
- Degree of crosslinking measurements by HPLC
- Surface zeta potential measurements
- Captive bubble contact angle measurements
- Young's Modulus measurements
- DSC Thermoporometry measurements
- NMR Cryoporometry measurements
- Capillary Flow Porometry measurements
- Scanning Electron Microscopy

2.2 Solubility Testing

The cellulose used in this project was a microcrystalline cellulose powder with 20 μm particle size (purchased from Sigma-Aldrich). All solubility tests were done at 70 $^{\circ}$C to give the resultant solutions a workable viscosity range at high cellulose concentrations to enable some degree of mixing.

Cellulose powder is very hydrophilic, and water interferes with cellulose dissolution, hence the cellulose powder was dried in a Buchi glass oven at 90 $^{\circ}$C at near vacuum for at least 3 hours. 1-Ethyl-3-methylimidazolium acetate [EMIm][OAc] (>95% purity, produced by BASF, purchased from Sigma-Aldrich) was used. Water content was determined by Mettler Toledo DL37 Karl Fischer Coulometer.

For a given OES, molar fraction of ionic liquid (X_{IL}) and starting cellulose concentration was decided and quantities of [EMIm][OAc], the co-solvent and cellulose were determined. A low starting cellulose concentration was chosen such that all the cellulose would be dissolved by the given OES, i.e. that it was below the expected solubility.

The desired amount of cellulose was added to a 7 mL glass vial followed by the desired amount of the co-solvent. The cellulose-solvent mixture was stirred for 1 min. The dispersion of the cellulose in the solvent prevented the cellulose from coagulating. The required amount of [EMIm][OAc] was then added to the mixture. The vial was then capped and magnetically stirred under 70 $^{\circ}$C in a heating block. When complete dissolution was achieved (clear mixture), a small amount of cellulose was added to increase the cellulose concentration and the mixture vial was put back in the heating block until complete dissolution was achieved. This step was repeated until the mixture passed saturation point (solution becomes cloudy). Maximum time allowed to reach dissolution was set at 16 hours. When the solution becomes too viscous for the magnetic bar to turn, stirring was done manually using a thin stirring rod to ensure reasonable dispersion of cellulose in the mixture. Most of the solubility tests were done in triplicates with a small minority were done in duplicates.

2.3   Density and Excess Molar Volume Determination

<u>Theory and Principle</u>

Density and molar volume data for liquid mixtures are important from practical and theoretical points of view.

Molar volumes, V_M, were calculated using the measured densities of the mixture at different compositions. V_M is defined by Equation **1**, where M is molar mass and ρ is density.

$$V_M = \frac{M}{\rho}$$

Equation 1

Experimental measurements of these properties for binary mixtures have gained much importance in many chemical industries and engineering disciplines.[36] However, in this case, determination of density -and by extension, molar and excess molar volumes- of organic electrolyte solutions should be useful in revealing the nature of interaction(s) between the ionic liquid and the co-solvent.

For a binary mixture, in this case [EMIM] [OAc] and a co-solvent, V_M was determined by Equation 2 where ρ is the measured density of the mixture. The subscript 'IL' refers to the ionic liquid and 'solv' to the co-solvent.

$$V_M = \left[\frac{x_{IL}M_{IL} + x_{solv}M_{solv}}{\rho}\right]$$

Equation 2

Excess molar volume, V^E, which is the difference between molar volume in a real mixture and the sum of the components' molar volume in an ideal mixture was then calculated by Equation 3.

$$V^E = \left[\frac{x_{IL}M_{IL} + x_{solv}M_{solv}}{\rho}\right] - \left[\frac{x_{IL}M_{IL}}{\rho_{IL}} + \frac{x_{solv}M_{solv}}{\rho_{solv}}\right]$$

Equation 3

Experimental Procedures

Pycnometer bottles (10 mL) conforming to British Standard BS733 were used for density measurements of the ionic liquid/co-solvent binary mixtures. Each pycnometer bottle's exact volume was first ascertained by weighing each bottle filled with deionised water, density of which was taken as $1.00\,g.cm^{-3}$. Densities were measured for ionic liquid mole fractions (X_{IL}) ranging from 0 to 1. Measurements were done in triplicate. Molar volume, V_M, and excess molar volume, V^E, were then calculated for each X_{IL} using Equation 2 and Equation 3.

2.4 Preparation of Cellulose Membrane via Non-solvent Induced Phase Separation (NIPS) Method

2.4.1 Preparation of Cellulose Solution for Casting

The desired amount of dried microcrystalline cellulose (mc) was added to the co-solvent and mixed well to ensure the mc powder was well dispersed and pre-swelled. The ionic liquid was then added, and the mixture was mixed thoroughly. At cellulose concentration of around 10 %wt. or higher, the solution's viscosity would render magnetic stirring is ineffective and overhead stirrer is not recommended as it would trap air bubbles. The preferred dissolution method was therefore sonication at 60 °C in a closed bottle until solution became clear, typically overnight. The solution was then degassed using a vacuum oven at near vacuum at 60 °C until air bubbles were no longer seen (max. 30 mins).

2.4.2 Casting & Non-solvent Bath

The backing layer (Whatman 41 filter paper unless otherwise stated) was affixed to a glass plate and placed on the aluminium platen of **Elcometer 4340 Automatic Film Applicator** with Doctor Blade Reservoir (see **Error! Reference source not found.**). The degassed polymer solution was then poured to the reservoir. Casting speed was at set at '4' and the default blade opening **(casting thickness) was 0.8 mm**. Unless otherwise indicated, cast solution and the aluminium platen were at room temperature during casting. Unless otherwise indicated, a **30 seconds** wait was applied after casting before immersion in the non-solvent bath, this is defined as **standing time**. For 25 x 18 cm sized membrane sheet, 400 mL of non-solvent was used. The non-solvent was changed 4x in the next 24 hours to ensure maximum leaching of solvent from the polymer solution.

2.4.3 Post Treatment

After the nonsolvent bath, many of the membranes were then subjected to glycerol post-treatment, which was immersion in a 40:60 v/v glycerol : non-solvent for 2 hours. If a membrane is designated as never dried, it means that it was kept in this glycerol bath until it was ready to use. Drying method (for some of the membranes that were dried) was by fitting them onto embroidery hoops and leave for 24 hours at ambient laboratory atmosphere (18-20 °C and 40-50% RH). The hoop was used to keep even tension during drying and prevent uneven shrinkage.

2.5   Permeation Tests

Dead-end Cell

All permeation tests were conducted using a dead-end cell type from Sterlitech (HP4750 model), Figure 10. The cell has a maximum pressure rating of 1000 psig (69 bar) and is constructed from 316L stainless steel with chemically resistant components (PTFE-coated O-rings and seals). The cell assembly was connected to a high pressure N_2 gas cylinder (min. purity 99.9%, BOC) to pressurise the vessel. To maintain non-ambient temperatures the bottom part of the cell (where the membrane is placed) was immersed in a water bath heated with a hot plate with automatic temperature control. All permeation and rejection experiments were conducted at 22 °C in a Sterlitech dead-end cell (Figure 10) with stirring speed of 500 rpm, unless otherwise specified. Default volume of feed for permeation tests was 60 mL, and permeate volume was at least 30 mL and maximum of 50 mL. This range was to ensure that stable flux was obtained before terminating a test. When these volumes figures differed, these have been made clear when appropriate. Trans-membrane pressure was between 30 to 40 bar, unless otherwise specified.
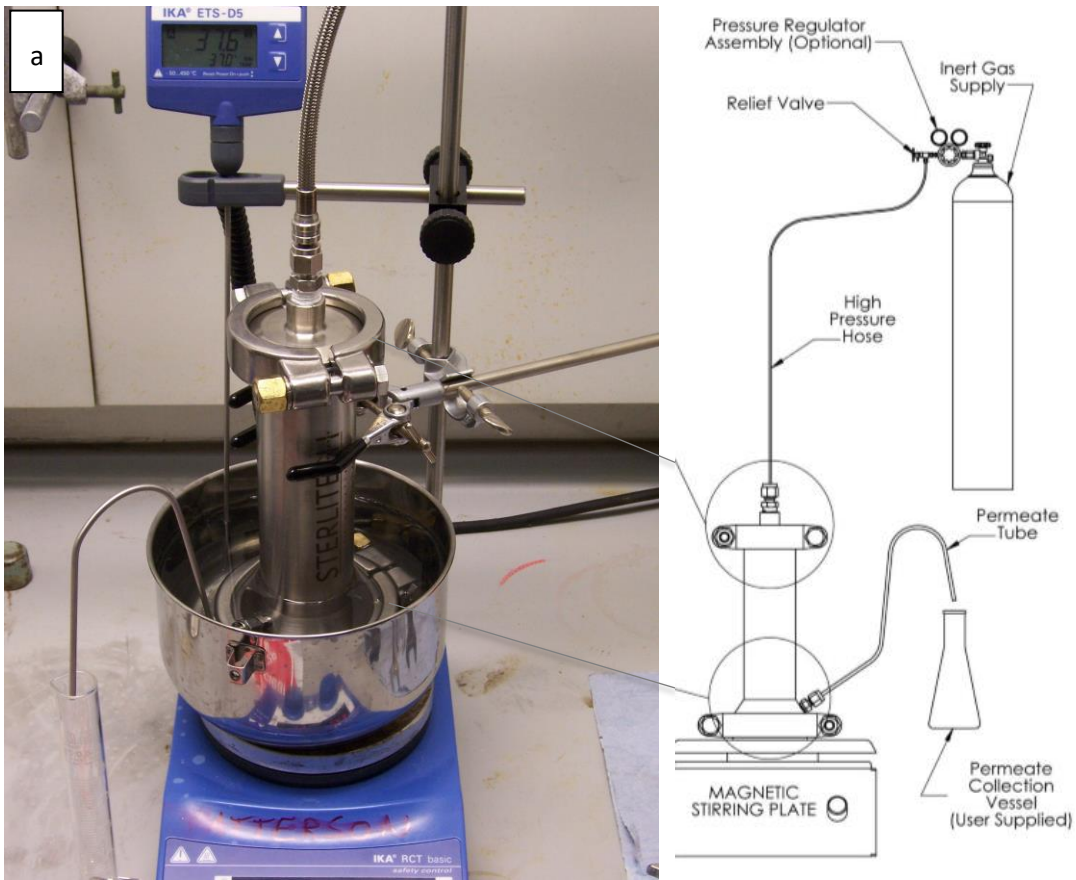
Figure 10. Sterlitech HP4750 membrane permeation cell assembly – a) The cell assembly during permeation test (image: own work).

2.6 Dye Rejection Tests Procedure

Materials

Rose Bengal (RB) and methylene blue (MB) were products of Sigma-Aldrich. Ethyl violet (EV) was purchased from Alfa Aesar. All organic solvents used were of HPLC grade, purchased either from Sigma-Aldrich, or Fisher, and used as received.

Method

All dye rejection tests were performed using the Sterlitech HP4750 dead-end cell. Feed volume was 60 mL and test is concluded when 30 mL permeate is obtained. Feed concentration values: 0.01 and 0.30 mM for RB in acetonitrile, 0.30 mM for RB in methanol, 0.13 mM for MB feed solutions, and 0.01 mM for EV feed solutions.

2.7 Polystyrene Rejection Tests for MWCO Determination

Materials

Polystyrene in powder form (MW of 1300, 2200, 3350, 4000, 5200 Da with polydispersity index between 1.06 to 1.1) was obtained from Alfa Aesar UK. THF (HPLC grade) was purchased from Fisher.

Method

Feed of 40 mL of PS solution in THF (0.40 g.L^{-1}) was used for each test. Test was completed when 20 mL of permeate has been collected. Both permeate and retentate were then analysed either by Cary 100 UV-Vis spectrophotometer at 260 nm wavelength.

2.8   Crosslinking of Cellulose Membranes

Chemicals. Glyoxal (>98%; 40% w/w) was purchased from Alfa Aesar. Methanol (HPLC Grade) was purchased from Alfa Aesar.

2.8.1   Crosslinking Procedure

Never dried membrane sample of typical size about 12 cm x 12 cm was washed with ca. 250 mL of methanol and then deionised water of approximately similar volume to remove the glycerol used from the post treatment. The sample was then added to 140 mL of 10% glyoxal solution bath in a heat-proof glass container for glyoxal impregnation for 15 minutes. About a dozen drops of 3M HCl was added to the glyoxal bath solution to obtain a pH of 2. The container was then placed in an oven for a reaction time of 1 hour at 75 °C (glyoxal concentration, reaction time and temperature were variables in the crosslinking optimisation study). The membrane sample was then washed with deionised water.

2.8.2   Degree of Crosslinking Measurements by HPLC

Hydrolysis

A glyoxal-crosslinked membrane sample was dried at 70°C vacuum oven at near vacuum for several hours until weight loss was no longer observed. About one gram of the dried membrane sample was cut and accurately weighed and placed in the reaction vessel. NaOH (40 mL; 4 M) were added. The reaction mixture was treated at 100 °C for 20 min. After hydrolysis, the extraction solution and the wash liquors were transferred to a 50-mL volumetric flask and allowed to cool. Finally, the volumetric flask was adjusted to the mark with 4M NaOH. Prior to the chromatographic analysis, the solution was filtered through a 20 micron PTFE disposable filter unit.

High Performance Liquid Chromatography (HPLC)

HPLC was performed on Shimadzu Class-VP with RID-10A UV/VIS detector, SIL-10ADvp Autoinjector and LC-10ADvp Pump. Separations were carried out using the strong cationic exchange 300 mm × 7.8 mm column Aminex HPX-87H (Bio-Rad Labs., Richmond, CA). The column was thermostated in a Shimadzu CTO-10AvpA column oven compartment. HPLC conditions were

as follows: mobile phase, H_2SO_4 (0.01 mol L^{-1}); flow rate, 0.7 mL min^{-1}; column oven temperature, 70 °C; UV detector wavelength, 210 nm.

2.9   Analytical and Characterisation Procedures

Viscosity Measurements

Viscosity measurements were conducted with Bohlin C-VOR 200 Rheometer equipped with plate-plate geometry with shear rates varied between 0.01 to 1000 s^{-1}. The top plate was raised to allow liquid sample to be administered to the bottom plate using a pipette before it was lowered again to the pre-set gap. The instrument was then run, and initial visual check was conducted as to ensure the correct quantity of the liquid sample.

Surface Zeta Potential Measurements

Instrument used was Zetasizer nano series model ZS from Malvern, with surface zeta potential cell kit.

Captive Bubble Contact Angle Measurements

Instrument used was Dataphysics Optical Contact Angle (OCA). A clear perspex container was custom made to hold the water for the sample to float in during measurements. A syringe needle was bent to a 'J' shape to accurately administer the air bubble.

Dynamic Mechanical Analysis

The mechanical analyser used for Youngs' Moduli measurements was DMA1 from Mettler Toledo, with the program STARe to acquire and process the data. Specimens were films with a size of 25 to 50 mm × 5 mm.

Thermogravimetric Analysis (TGA)

The thermogravimetric analyser was a *Setsys Evolution TGA 16/18* from Setaram. The program *Calisto* is employed to collect and process the data. The sample was loaded into a 170 µL alumina crucible.

2.10 Porometry

2.10.1 General Theories and Principles of Thermoporometry

Thermoporometry is a calorimetric method that determines pore size based on the melting or crystallization point depression of a liquid confined in a pore.[37] The basic principle is the fact that water contained within pores is at an elevated pressure compared to free water and therefore has a depressed melting temperature. The physical basis for the melting point depression is that the equilibrium temperature for a solid–liquid phase transition is determined by the radius of curvature of the interface between the solid and liquid phases, and this radius of curvature is closely related to the pore size.[37]

In the typical thermoporometry experiment, the probe liquid used is one that can completely wet the pores, thereby filling all accessible voids by capillary action. When excess of liquid is added, overfilling the pores, the gas phase no longer needs to be considered. This situation is depicted in Figure 11 where water is shown as the pore-filling liquid.
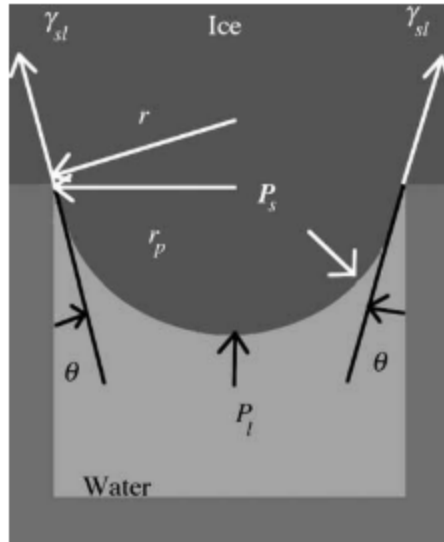
Figure 11. Excess water added to porous material in a typical thermoporometry experiment. The pore is small enough (highly curved surface) so that only liquid water exists within the pore, and free water outside the pores exists as solid water (ice). Symbols: P = pressure, γ = surface tension, θ = contact angle, r = radius of curvature. (From Landry, 2005)[37]

The relationship between the temperature depression ΔT and the pore radius r_p is given by the following,

$$\Delta T \cong \frac{2 T_0 \gamma_{sl}}{\rho_l \Delta H_f} \frac{\cos \theta}{r_p}$$

<div align="right">Equation 4</div>

which is analogous to the Gibbs-Thomson equation (Equation 5)[38], from which a representative pore diameter (D) was obtained, where V is the specific volume of ice, σ_{ls} is the surface energy at the ice–water interface, H_m is the specific melting enthalpy of water, and T_o is the melting point of water at 1 atmosphere pressure.

$$D = \frac{-4 V \sigma_{ls}}{\bar{H}_m \ln(T_m / T_0)}$$

<div align="right">Equation 5</div>

2.10.2 DSC Thermoporometry

Theories and Principles

A differential scanning calorimeter (DSC) is a suitable instrument for thermoporometry experiments due to its capability to precisely measure of small temperature shifts caused by exothermic freezing and endothermic melting transitions. Water is a common probe liquid with advantages such as: suitable for hydrophilic materials and considerably large heat of fusion, ΔH_f = 334 J/g, which is up to an order of magnitude larger than most organic liquids. The large ΔH_f of water enhances the sensitivity of the DSC technique to small volumes of adsorbed liquid.[37]

The principle of the isothermal melting technique is to raise the temperature in a frozen sample to slightly above 0°C where it is then held constant until the melting transition is completed. The heat absorbed at each temperature is measured by integrating the endotherm. The melting heat should correlate directly with the amount of melted water, and, consequently, the pore size distribution (PSD) is calculated from the melting temperature depression of the imbibed water.

Experimental Procedures

Instrument used was Setaram microSC. Thermal profile was cooling down to -25°C at 1K/min, followed by a heating ramp at 0.05K/min from− 25°C to 1°C. Sample was soaked in purified water in excess before loading in the cell. Mass of sample was around 50 mg. Sample holder was the standard 1 mL Hastelloy cells and the measurement cell contains the sample whilst the reference cell was empty. Sample was collected after DSC experiment and then dried at 60°C at reduced pressure to obtain the dry weight of the sample. The results from the DSC (heat flow vs temperature data) were then processed as described in the subsequent section.

The DSC profile (heat flow vs temperature) is transformed into pore size distribution, by first converting the temperature T into pore radius or diameter as described previously. Secondly, the heat flow from the melting is transformed into a differential pore volume by using the following equation[37]:

$$\frac{dV_p}{dr_p} = \frac{dQ}{dt} \frac{dt}{d(\Delta T)} \frac{d(\Delta T)}{dr_p} \frac{1}{m \Delta H_f(T)\rho(T)}$$

Equation 6

where $d(\Delta T)/dt$ is the scanning rate of the DSC experiment, m the mass of dry sample, and $\Delta H_f(T)$ and $\rho(T)$ the temperature-dependent heat of fusion and density of water, respectively. The quantity $d(\Delta T)/dr_p$ is derived numerically from Gibbs-Thomson equation.

2.10.3 NMR Cryoporometry

Theories and Principles

Using the general principle of thermoporometry, namely depression of melting point of liquid in confined spaces, Nuclear magnetic resonance (NMR) can be used as a measuring instrument by detecting the solid–liquid transition by exploiting NMR's sensitivity to molecular motion. NMR cryoporometry (NMRC) measures the difference between solid and liquid relaxation times. More specifically, it detects the emergence/disappearance of the liquid signal upon increasing/decreasing temperature by applying a spin-echo-type detection.[39] When the probe liquid used is water, 1H NMR is used to measure the quantity of water that has melted, as a function of temperature, making use of the fact that the transverse (spin–spin) relaxation times, T2, of hydrogen nuclei in solid ice is usually much shorter than that in liquid water.

The general procedure for NMRC is similar to DSC thermoporometry, namely a liquid is imbibed into the porous solid sample, the sample is cooled until all the liquid is frozen, and then warmed slowly, while measuring the quantity of the liquid that is liquid. The Gibbs–Thomson equation (Equation 2) is used relate the melting point depression to pore size.

Pore size distribution can be obtained by calculating the ratio of the NMR signal amplitude at a particular pore diameter to the amplitude when all the liquid (of known mass) is melted. NMRC is suitable for measuring pore diameters in the range 1 nm to about 10 μm.

Experimental Procedures

A membrane sample without any backing layer was washed several times in pure water (HPLC grade, Fisher UK) and then submerged in in water in a close vial overnight to ensure complete wetting. The wet membrane sample is then placed to the bottom of an NMR tube and water was pipetted slowly onto the wall of tube to prevent creation of air bubbles. The sample height was restricted to approximately 15mm to ensure that all sample was located within the transmitter/receiver coil, and thus was homogenously irradiated.

^{1}H NMR cryoporometry measurements were carried out on a Bruker AV-300 Spectrometer Each sample test was performed over a temperature range of 220–275K using a Bruker BVT-3000 temperature control unit. Two different temperature protocols were programmed: coarse temperature step (1 to 10K steps) between 220 to 262 K range, and fine temperature step (0.2 K) between 262 to 275K, with 5 minutes of equilibration time in each temperature step before T2 was acquired for 1 minute.

Results Processing

Measurements were performed using a spin-echo pulse sequence and the height of the echo is directly dependent on the volume of liquid in the sample.[40] In this project, the spin-echo amplitude is measured with a time interval τ of 1s (shorter than T2 of liquid water and longer than that of solid ice) to ensure that the signal is entirely from the water present. Therefore, this signal amplitude is measured as a function of temperature and should be proportional to the volume of liquid confined within pores of the membrane sample when T is below the melting point of water. The numerical raw data obtained from NMRC experiments comprised of two main value series: temperature and the corresponding signal intensity (obtained by curve integration).

To transform the above data to pore size distribution curve, the derivative of signal intensity was calculated with respect to temperature and these derivative values were then plotted to against inverse of temperature. The resultant plot (see Figure 47) showed peaks with each peak represent a certain range of pore sized present in the membrane sample. The range of temperatures upon which these main peaks occurred were then converted to pore radius by using equation derived

by Petrov and Furo,[39] which is based on Gibbs-Thomson equation. At the end, the peaks could then be assigned to the approximate pore sizes.

2.10.4 Capillary Flow Porometry

General Theory and Principle

The capillary flow (also known as bubble point) porometry method depends upon the capillary rise created by surface tension. A wetted capillary or pore immersed in a liquid draws liquid up the capillary until equilibrium with the force of gravity is obtained, Figure 12.
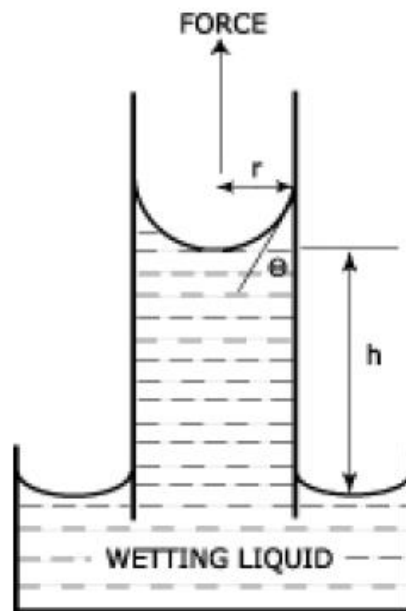
Figure 12. Principle of capillary flow porometry. From Yuan and Lee, 2013.[41]

The equilibrium conditions can be expressed as:

$$2\pi r \gamma \cos \theta = r^2 \pi h \rho g \qquad\qquad \textbf{Equation 7}$$

where:

r= radius of the capillary (or pore)

D= diameter of the capillary (or pore)

h= height of column of liquid

γ= surface tension of liquid

ρ= density of liquid

θ= contact angle between the liquid and capillary wall

g= acceleration due to gravity

The above equation can be further developed to the below equation, also known as Young-Laplace equation[41], where P is pressure and D is pore diameter.

$$P = 4 \, \gamma \cos \theta \, / \, D \qquad \qquad \textbf{Equation 8}$$

In theory, many different wetting liquids can be used. In order to obtain a good wetting of the sample, the wetting liquid should have the following physical properties: complete wettability to the material, low surface tension and low vapor pressure. The wetting liquid should also be chemically inert and should not cause swelling of the sample.

When a good wetting liquid is used and complete wettability is achieved, the contact angle is zero, hence Equation 8 becomes:

$$P = 4 \, \gamma \, / \, D \qquad \qquad \textbf{Equation 9}$$

The experiment involves wetting the sample with a liquid of low surface tension and low vapour pressure, consequently all pores are filled with the liquid. Wetted sample is subjected to increasing pressure using an inert gas and when the gas pressure is higher than the surface tension of the liquid in the largest pores, the liquid is pushed out and this instance is called bubble point. Increasing the gas pressure further causes the gas to flow through smaller and smaller pores until all the pores are emptied.

An inert gas is used to displace wetting liquid from pores and the gas flow rate achieved at a certain pressure is measured using flowmeter. This technique is generally considered valid for pore size range of between around 300µm to 15nm.[42]

Experimental Procedure

Instrument used was Porolux 1000 from Porometer NV. Wetting liquid was Porefil™ (a fluorocarbon compound) and nitrogen gas was used to pressurise the sample chamber and to displace wetting liquid from the pores. A computer running Porolux 1000 software was connected to the instrument to control, record and process measurement data.

Membrane sample was cut in circular shape of 2.5 cm diameter to fit the sample chamber. Since most of the membrane was post-treated with glycerol, a thorough wash was performed with methanol to remove any glycerol from the sample. To prevent hornification of cellulose and preserve the pore structure, the membrane sample was then transferred to Porefil liquid bath to keep it wet until it was ready to be placed in the sample chamber. A couple more drops of Porefil was added on top of the membrane before the sample chamber was closed and gas pressure line was connected.

Pressure step/stability with measured first bubble point (FBP) protocol was chosen as the experiment protocol which meant that the pressure inside the sample chamber was gradually increased from zero to typically 20-25 bar (user input). A data point is recorded when the defined stability algorithm is met for both pressure and flow. The porometer detects when a pore empties at a certain pressure and waits until all pores of the same diameter have been completely emptied before accepting a data point.

Results Processing

The instrument records gas flow rate and pressure and in when the two variables are plotted against each other, wet or dry curves can be produced. A wet curve is gas pressure and flow rate values produced during a wet run, i.e. when the wetting liquid is being expelled from the pores, whilst a dry curve is gas flow rate & pressure values during a dry run, when the gas flows through the sample without liquid in its pores. Typical measurement is done with the wetting liquid in the sample pores, hence wet curve is produced (blue line in Figure 13). First bubble point is identified as the point of departure from linearity in the initial wet curve regime, as illustrated in Figure 13 and it represents the largest dominant pore sizes. When a dry curve is produced, the point where a wet curve joins its dry curve, it represents the smallest pore sizes (Figure 13). A half dry curve

can be produced by the software (by dividing the flow of the dry curve by two) and the pressure at which the wet curve intersects its half dry curve is the mean flow pore diameter.
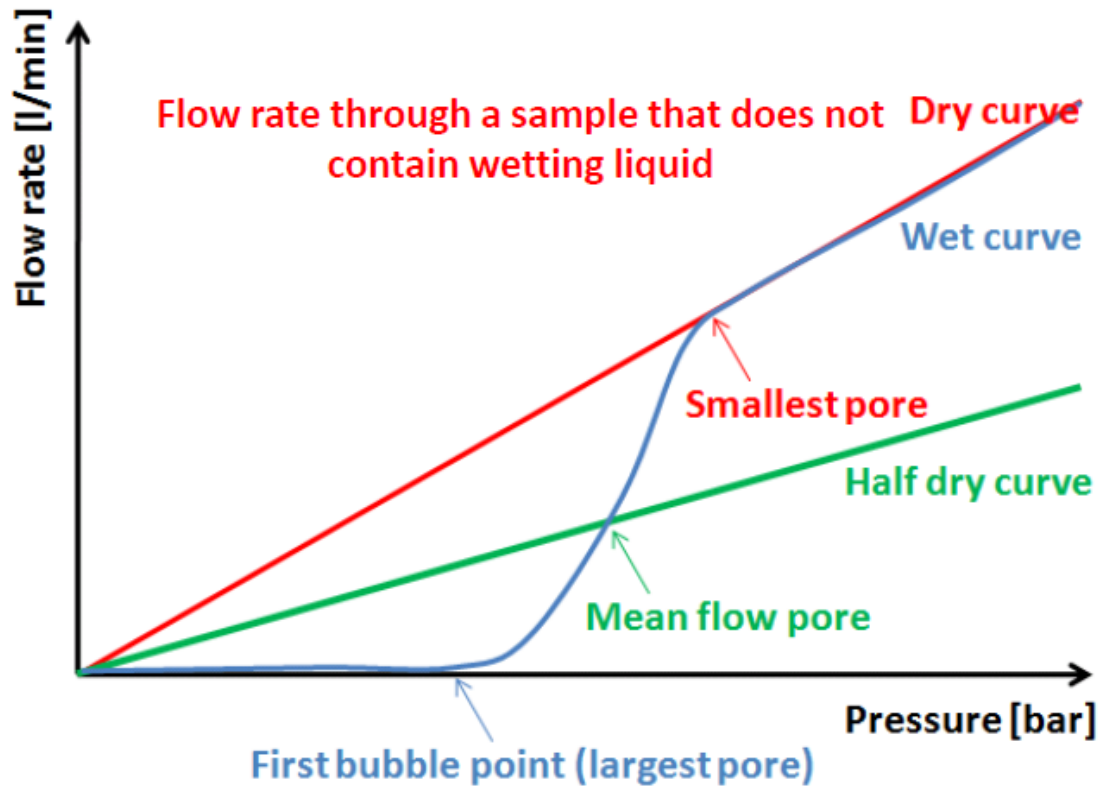
Figure 13. Typical gas flow rate and pressure responses from capillary flow porometer. (Image: own work)

Scanning Electron Microscopy (SEM)

SEM images was produced by JEOL Field Emission Scanning Electron Microscope 6301F. Samples were dried and degassed overnight under reduced pressure and sputter coated with chromium.

Chapter 3 Cellulose Dissolution in Organic Electrolyte Solutions

3.1   Introduction

Investigation of organic electrolyte solutions (OESs) for cellulose dissolution, specifically measurement of dissolution capacities and selection of organic solvents as co-solvents, formed the early part of this project, as efficient cellulose solvents are seen as important enablers for the development of cellulose membrane via solution casting method. The ionic liquid (IL) chosen for this project is 1-ethyl-3-methylimidazolium acetate ([EMIm][OAc]) due to its reasonably high cellulose dissolution capability and relative affordability and availability.

It is clear from the literature, much of which were reviewed in Chapter 1, that the addition of certain organic solvents (primarily dipolar aprotic solvents) to [EMIm][OAc] enhanced cellulose dissolution. Although several ILs and OESs have been demonstrated to dissolve cellulose, only a limited number of ILs are known, at present, to be effective solvents; and the link between ion structure, role of the solvent (in OES) and cellulose dissolution has yet to be completely understood. Such information is crucial for selecting solvent systems that would have suitable properties (i.e., thermal stability, minimum use of IL, ease of separation & recycling of IL, ease of product recovery, low toxicity, manageable cellulose solution viscosity, etc.).

3.2   Dissolution Capacities and Co-solvent Choices

Microcrystalline cellulose (MC) was selected as the test substrate as its relatively low average degree of polymerization of 150–300 provides solutions of reasonable viscosity.[43] The elevated temperature used (70 $^{\circ}$C) was selected as readily accessible using a wide range of cosolvents of variable boiling points, while remaining below the temperatures at which cellulose degradation has been shown to be significant.[44] The structures of all solvents tested as OES components with [EMIm][OAc] are presented in Figure 14 and included the following: 1-methylimidazole (1-MI); dimethyl sulfoxide (DMSO); dimethylformamide (DMF); dimethylimidazolidin-2-one (DMI); dimethylacetamide (DMAc); sulfolane; γ-valerolactone (γ-val); γ-butyrolactone (γ- but); propylene carbonate (PC); tetramethylurea (TMU); and methylpyrrolidinone (NMP).
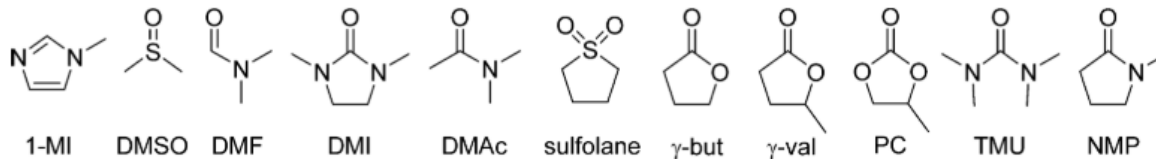
Figure 14. Co-solvents Tested in Organic Electrolyte Solutions with the Ionic Liquid [EMIm][OAc]. (Images: own work)

Dissolution capacities of an OES were determined at various mole fraction of IL, XIL. As XIL increased, the quantity of MC dissolved tended to the value soluble in pure [EMIm][OAc]. The best OESs can dissolve >70% of the maximum amount of MC soluble in pure IL at XIL as low as 0.3 (Figure 15).
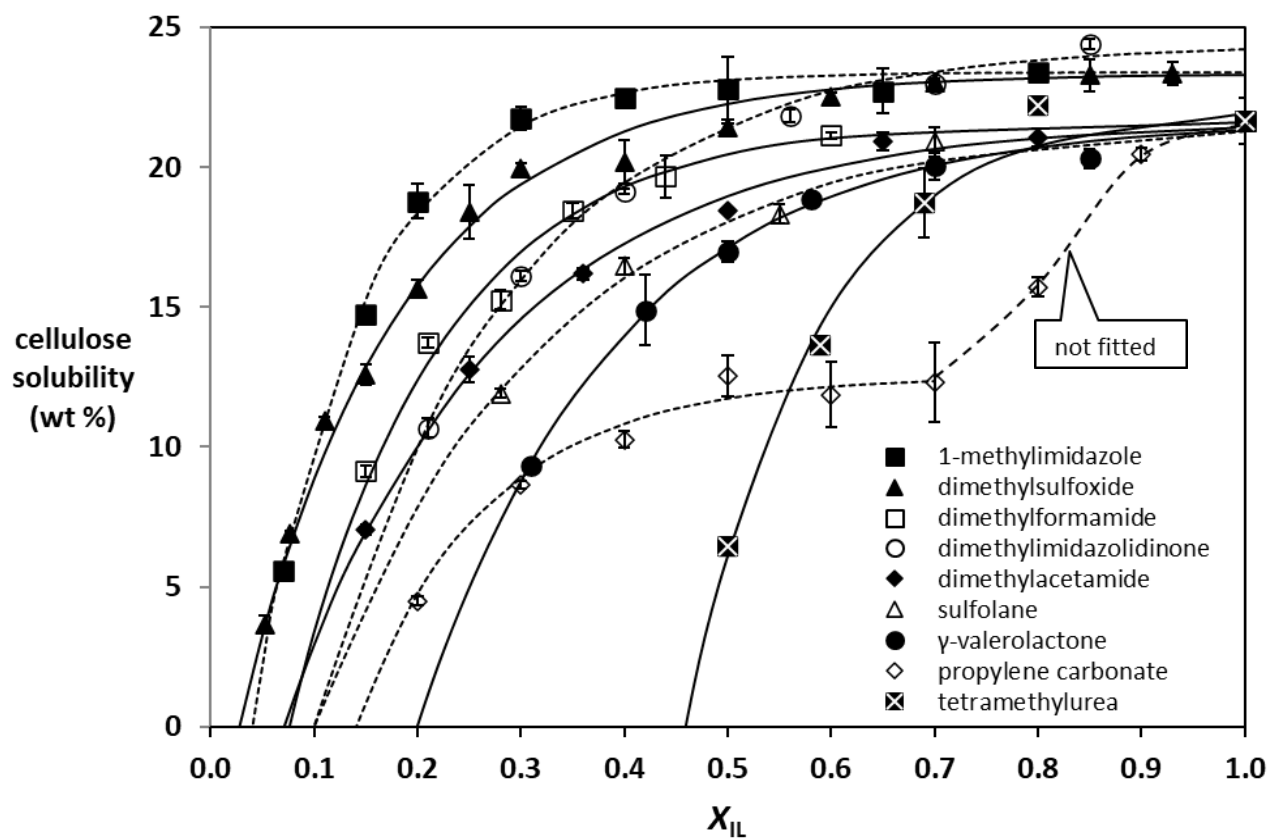
Figure 15. Weight percent of cellulose dissolved in OESs versus mole fraction of ionic liquid, X_{IL} (dissolved cellulose reaches a maximum of 22−23 wt %) at 70°C. Full solubility data table appear in the appendix. (Image: own work)

Comparison of the OESs based on mole fraction IL required to effect dissolution of a given quantity of cellulose suggests that some solvents, notably 1-MI, DMSO, DMF, etc., are "good" co-solvents, while others, such as TMU, are significantly less effective. These results significantly expand the findings by Olsson et al.[45] and Rinaldi[16] where they discovered several of these dipolar aprotic solvents are efficient cellulose co-solvents when paired with [EMIm][OAc].

In general, the IL will be the costliest (and often the least 'green') component of the OES, therefore we created a measure of the efficiency of IL use in cellulose dissolution, defined as grams of cellulose dissolved per gram of IL, and these efficiency measure values were plotted against the mole fraction of IL, Figure 16. Differences between the relative efficacies of the solvents are clearly seen, with 1-MI yielding the greatest mass of cellulose dissolved per unit mass of IL.
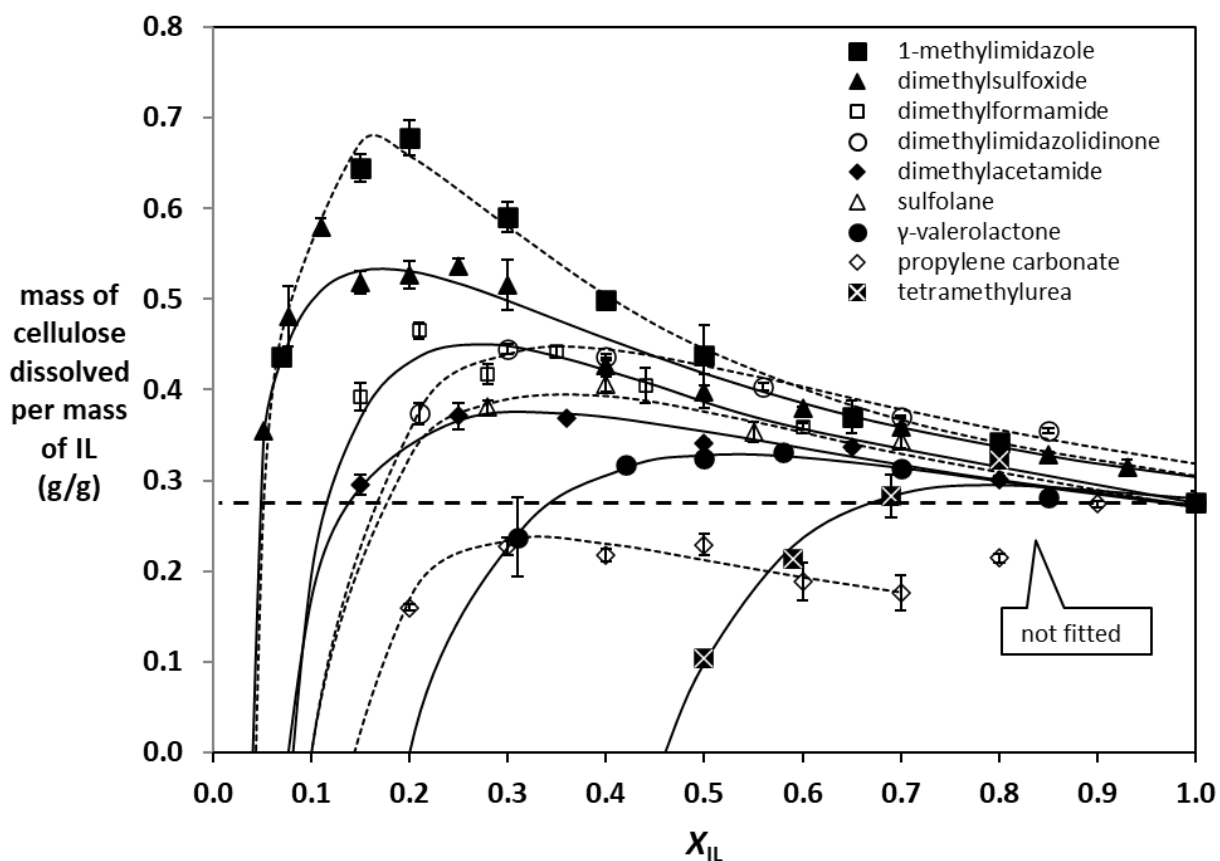
Figure 16. Dissolution efficiency expressed as grams of cellulose dissolved per gram of IL versus mole fraction of ionic liquid, X_{IL}. The horizontal dashed line indicates the dissolution efficiency of pure [EMIm][OAc]. (Image: own work)

In order to rank the co-solvents in terms of microcrystalline cellulose (MC) dissolution performance in their respective OESs, several quantities were evaluated, and they are:

Minimum X_{IL} required to initiate cellulose dissolution. The lower this number, the better the OES in minimising the use of the IL.

- X_{IL} required to achieve maximum efficiency (refer to the efficiency curves, Figure 16**).** The lower this number, the better the OES in minimising the use of the IL and maximising the dissolution performance.

- Maximum efficiency measure, in gram IL per gram of MC (refer to the efficiency curves, Figure 16). The higher this value, the more efficient the OES is.

These 3 quantities are listed in Table 3.

Table 3. Minimum X_{IL} values of [EMIm][OAc] required to produce an OES capable of dissolving microcrystalline cellulose (MC) and measure of the efficiency of the OES. (Data: own work)

Co-solvent	Minimum X_{IL} required to initiate dissolution	X_{IL} required for maximum efficiency	Maximum Efficiency Measure (g IL/g MC) (Neat IL = 0.27 g/g)
1-MI	0.05	0.17	0.66
DMSO	0.02	0.16	0.56
DMF	0.06	0.28	0.45
DMI	0.10	0.33	0.44
DMAc	0.06	0.35	0.36
Sulfolane	0.12	0.40	0.39
γ-Val	0.18	0.61	0.33
TMU	0.45	0.75	0.32

In order to compare the OESs, or more specifically the co-solvents, against each other, we can use the three quantities in Table 3 as metrics. A co-solvent can be considered a 'good' if the first two metrics (the X_{IL} values) are low and the efficiency measure is high. From these metrics, combined with comparing the dissolution curves in Figure 15 and Figure 16, it can be concluded that 1-MI is the clear winner, with DMSO follows in second place, while DMF, DMI, DMAc, NMP and sulfolane are of similar performance. γ-Val has lesser performance than this group. The bottom performers are TMU and PC.

TMU, despite its significant structural similarity to DMI, shows very poor efficiency measures. Interestingly, the most efficient IL co-solvent, 1-MI, is not the solvent with the lowest minimum X_{IL} required to effect dissolution of MC. Indeed, there are clues that 1-MI might be distinct from the other solvents as the shape of the curve reflecting quantity of cellulose dissolved versus IL concentration does not match that of all other solvents tested, possibly pointing to some mechanistic peculiarity. It is notable that this is the only co-solvent in the group with a nitrogen atom hydrogen bond acceptor (all others are oxygen atom acceptors); nonetheless, as our focus was on efficient and green cosolvents, this was not explored further.

3.3   Molar Volume of Co-Solvent and Excess Molar Volume of OESs

During the evaluation of solution properties in an attempt to explain the differing performances of the OESs, attention was paid to the molar volume of the OESs, which are caused by the differences in molar volume of the individual co-solvents, as well as the specific molecular interaction between [EMIm][OAc] and the individual co-solvent. Low molar volume of a pure liquid means its molecule is less bulky and has better packing efficiency. Table 4 lists the molar volume of the individual co-solvents.

Table 4. Co-solvent molar volume

(Superscript number after each value denotes the reference it was taken from, OT = own test)

Co-solvent	Molar volume, V_m (mL.mol^{-1})
1-Methylimidazole (1-MI)	79.71[OT]
Dimethyl sulfoxide (DMSO)	71.00[6]
Dimethylformamide (DMF)	77.10[5]
1,3-Dimethyl-2-imidazolidinone (DMI)	108.10[5]
Dimethylacetamide (DMAc)	92.98[5]
Sulfolane	95.30[5]
γ-Valerolactone (γ-val)	95.67[OT]
Tetramethylurea (TMU)	120.00[5]

It becomes clear, however, that the fact the co-solvents have differing molar volumes does not fully account for the differences in cellulose dissolution capacity (in gram/gram) of the OESs. This is because the dissolution curves were plotted from a mixture of [EMIm][OAc] + a co-solvent at differing compositions (X_{IL}), and molar volume of a mixture cannot simply be determined from the molar volumes of the mixture's components, due to specific interaction between the different chemical moieties in a mixture. Instead, they must be determined experimentally. To this end,

46

molar volumes of a mixture, V_M, were calculated using the measured densities of the mixture at different compositions using pycnometer. Refer to Chapter 2 Experimental Section for the measurement procedure and calculation method.

Table 5. Comparison of density values measured and obtained from literature.

Reference temperature is 20°C unless otherwise stated.

Discrepancy of measured vs reported density of EMIM AcO is 0.1%.

Pure Liquid	Density from experiment (g mL^{-1})	Density from literature (g mL^{-1})
EMIM AcO	1.1004	1.1015[a]
DMSO	1.1016	1.100[b] (@25 °C)

[a] Obtained from [46]

[b] Obtained from [47]

Densities, molar volumes, and excess molar volumes of 5 [EMIm][OAc]-based OESs were measured experimentally, and their results are shown in Figure 17, Figure 18, and Figure 19.
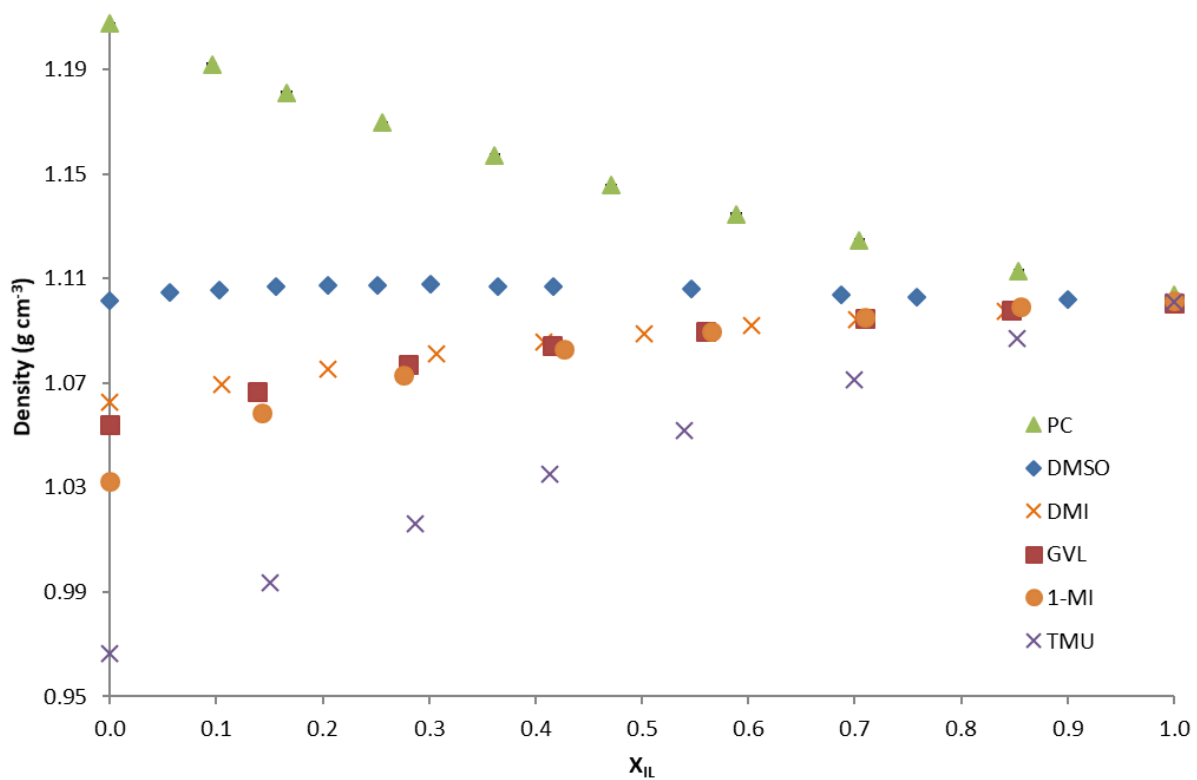
Figure 17. Densities of [EMIm][OAc] + solvent binary systems at 20°C.

Measurements errors were <0.1%. Full data can be found in the appendix.
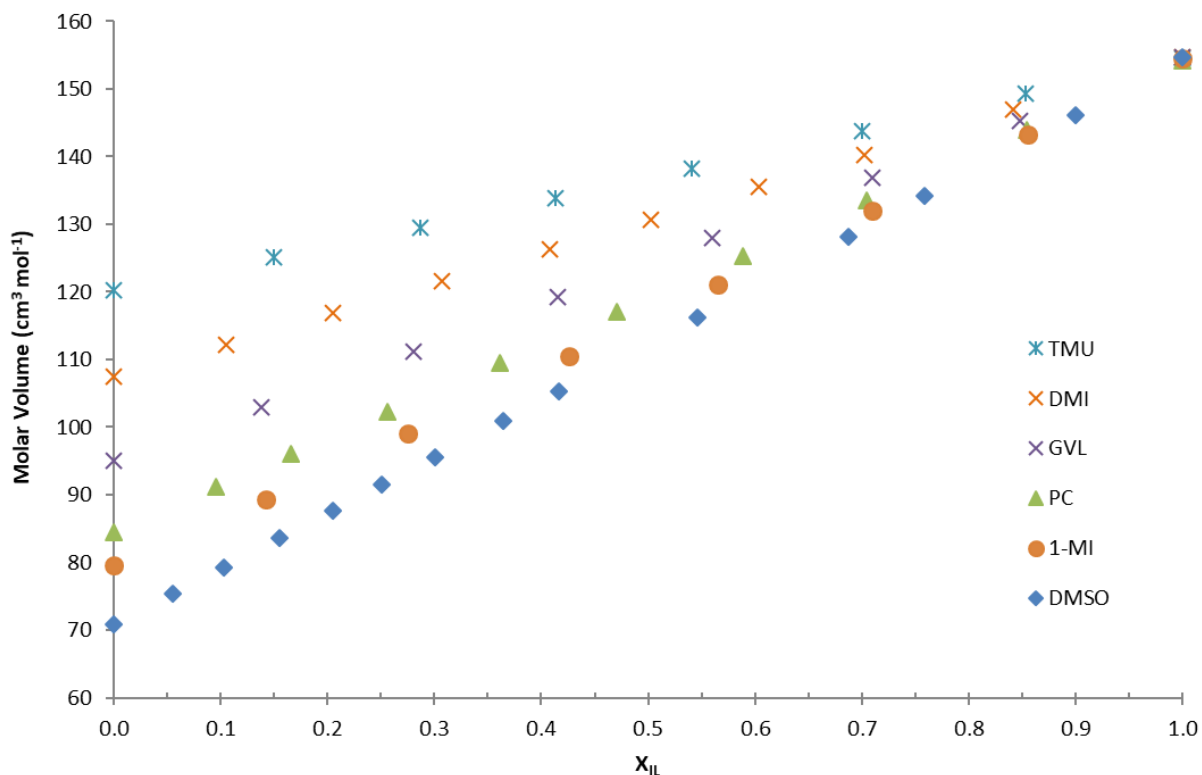
Figure 18. Molar volumes of [EMIm][OAc] + solvent binary systems at 20°C.

Measurements errors were <0.1%. Full data can be found in the appendix.

The densities of the OESs had a slight downward concave (mountain) shape, except for [EMIm][OAc]/PC (Figure 17), whilst the excess molar volumes (V^E) curves had a 'valley' shape, which is as expected (inverse of the density), Figure 19. This 'valley' shape is a typical shape of V^E of two miscible liquids mixtures, which means that the V^E of the mixture at different compositions is negative, due to efficient packing of the two liquids at the molecular level.

The V^E curve for [EMIm][OAc] + 1-MI was significantly lower (values were more negative) than that of the 4 other OESs, and as pointed out previously, 1-MI was singled out as the 'superior' co-solvent, in terms of enhancing cellulose dissolution, amongst those tested. However, it interesting to see that V^E curves of DMI, γ-val, TMU, and DMSO were close to each other whilst it was established previously from cellulose dissolution curves that TMU and γ-val were inferior co-solvents compared to DMI and DMSO, both in g/g and mol/mol basis.

49
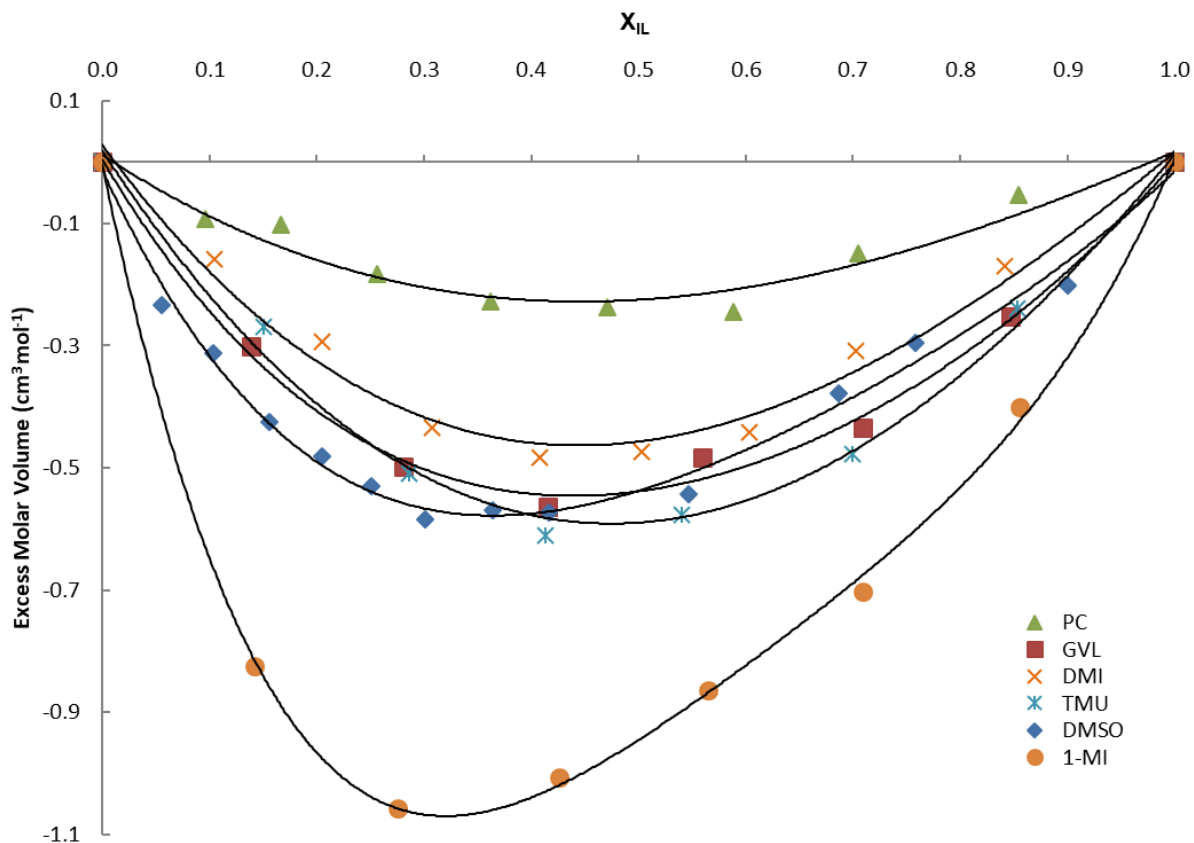
Figure 19. Excess molar volume of [EMIm][OAc] + solvent binary systems at 20°C. Measurements errors were <0.1%.

Cellulose swelling in organic solvent studies by Fidale *et al.* concluded that molar volume (V_M) of the solvent is one of three factors found to correlate well with swelling, with negative relationship, i.e. low molar volume correlates to higher degree of swelling.[48] The other two factors were hydrogen bond acceptor or basicity (β) and polarisability (π*). It was asserted that cellulose swelling and dissolution have a common feature, namely, the disruption of its supramolecular structure, hence both are controlled by the same solvent-biopolymer interactions.[48,49] Having relatively small molecules (low V_M of 71 mL mol^{-1}), it enhances the efficiency of DMSO in providing such disruption, leads to its exceptional swelling.[48] Indeed, DMSO has also been shown as an exceptional cellulose co-solvent in this study, quite possibly by the same mechanism. Our experimental data on excess molar volumes of the OES (ionic liquid + co-solvent) showed that low excess molar volume (V^E) of an OES is probably one factor that, all the other qualifying factors being equal, contributes to enhancement of cellulose dissolution, as shown in the case with

[EMIm][OAc] + 1-MI. It is obvious that there are other parameters that need to be satisfied to make an OES a good cellulose solvent, with some authors have reported in their studies.[16,19–21,50,51]

It is widely believed that cellulose dissolution occurs when the solvent is able to disrupt cellulose's intra and intermolecular hydrogen bonds[4,35,52,53]. It is then hypothesised that if OES provides such ability, then the more efficiently packed (lower V^E) it is, the more able the co-solvent and the ionic liquid to act synergistically provide such hydrogen bonds disruption, thereby enhancing dissolution.

Full explanation of our findings on excess molar volumes of cellulose-dissolving OESs can only be revealed when we fully understand the specific interactions between [EMIm][OAc], co-solvent, and cellulose. Molecular dynamic simulations could offer valuable insights in this regard. One important input to perform these simulations is the molar volume of the OESs involved at different compositions (X_{IL}), some of which were measured experimentally in this project, as outlined above. Collaborative efforts with our external research partners was initiated to investigate this issue using our experimental data of densities and molar volumes of OESs at different X_{IL}.

3.4 Solvent parameters and selection

Having established that some dipolar aprotic solvents are indeed good cellulose co-solvents when paired with [EMIm][OAc], further analysis on solvent parameters to compare and indeed, to select cellulose co-solvents that are fit for purpose. Rinaldi and others used Kamlett−Taft parameters as the basis for comparison of solvents, but here we use the recently compiled databases of Catalán[54] and Laurence and co-workers[55] providing solvent parameters for 160 and more than 300 solvents, respectively. Catalán defines four empirically derived parameters: **solvent polarizability (SP); solvent dipolarity (SdP); solvent acidity (SA); and solvent basicity (SB)**. The so-called nonspecific solvent/solute interactions are described by two parameters (polarizability and dipolarity), thus avoiding confounding these two different effects.[54] Laurence *et al*. define **dispersion induction (DI); electrostatic (ES); solute Lewis base/solvent Lewis acid (α1); and solute hydrogen bond donor/solvent hydrogen bond acceptor (β1)** as parameters to describe solute/solvent interactions.[55] Many of solvent parameters are derived from each other and it is clear that these scales and parameters are not dissimilar, but we thought that it would be useful to select a single set of parameters to describe solvent/solute interactions and ultimately to use such solvent parameters as tools for solvent selection. Specifically in this project, choosing an efficient and "greener" solvents for use in OESs for dissolution of cellulose could facilitate cellulose membrane production via solution casting method.

Since only a single ionic liquid was being used throughout the project, namely [EMIm][OAc], the only variable to be considered is the co-solvent used to form the OES. Using the six solvents confirmed to form effective OESs for dissolution of cellulose when paired with [EMIm][OAc] and which also appear in both Catalan and Laurence databases (DMSO, DMF, 1-MI, sulfolane, NMP, DMAc), ranges for each of the four parameters described by Catalán and Laurence can be determined, Table 6. These ranges are represented graphically in Figure 20, and the parameters describing these solvents fall into narrow bands.

Table 6. Solvent Parameters from the works of Catalán[54] and Laurence[55] for the six solvents selected as effective cosolvents in OESs with [EMIm][OAc], γ-but, and two solvents with structural similarities (TMU and PC).

(Solvent parameters data obtained from [54] and [55], other values are from own work)

	Catalán				Laurence			
	SP	SdP	SA	SB	DI	ES	α_1	β_1
DMSO	0.830	1.000	0.072	0.647	0.84	1.00	0.00	0.71
DMF	0.759	0.977	0.031	0.613	0.78	0.87	0.00	0.69
1-MI	0.834	0.959	0.069	0.658	0.86	0.97	0.00	0.70
sulfolane	0.830	0.896	0.052	0.365	0.85	0.93	0.00	0.34
NMP	0.812	0.959	0.024	0.613	0.83	0.80	0.00	0.76
DMAc	0.763	0.987	0.028	0.650	0.79	0.85	0.00	0.75
max[a]	0.834	1.000	0.072	0.658	0.86	1.00	0.00	0.76
min[a]	0.759	0.896	0.024	0.365	0.78	0.80	0.00	0.34
range[a]	0.075	0.104	0.048	0.293	0.08	0.20	0.00	0.42
percent of total range[a]	7.5	9.5	4.5	29.3	7.0	17.5	0.0	33.5
γ-but[b]	0.775	0.945	0.057	0.399	0.79	0.94	0.00	0.45
TMU[c]	0.778	0.878	0.000	0.624	0.81	0.71	0.00	0.75
PC[d]	0.746	0.942	0.106	0.341	0.77	1.07	0.00	0.40

[a] The minimum and maximum values of the six selected solvents were used to search the databases, and the percentage range over the parameter is included as a measure of specificity.

[b] New greener cellulose dissolving OES identified in this analysis.

[c] A poor cosolvent not included in the range analysis but tested due to structural similarity with DMI.

[d] Bears a superficial structural similarity to γ-but and γ-val.
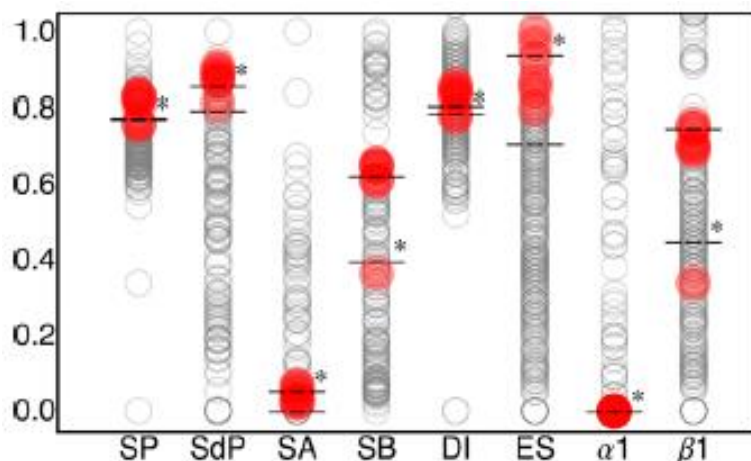
Figure 20. Catalán and Laurence parameters presented as ranges defined in each database. The values for the six 'good' co-solvents are represented in red. Parameters describing the newly identified greener co-solvent, γ-but, are indicated as ---* and those for TMU (a rather poor solvent) as ---. (Solvent parameters data obtained from [54] and [55], other values images are from own work)

The fact that the six 'good' cellulose co-solvents fell within narrow ranges of the Catalán[54] and Laurence[55] databases, led us to search new solvent(s) that are within or close to these ranges. Upon interrogation of both databases for such solvents falling within ±5% of the defined ranges yielded one solvent candidate: γ-butyrolactone (γ-but). Full sorted solvent parameters in both databases are included in the Appendix. Testing [EMIm][OAc]/γ-but showed that it does, indeed, form an efficient cellulose dissolving OES, with a solubility curve falling well within the group 'good' OESs (Figure 15.) and with efficiency closely matching that of DMF and other dipolar aprotic solvents (Table 3).

This finding led to consideration of using this selection criteria to select cellulose co-solvents that might provide greener credential for cellulose membrane preparation, especially since many of the dipolar aprotic solvents that are within the defined ranges are associated with potential reproductive toxicity, such as DMAc, DMF, NMP, and some others. While γ-butyrolactone is not identified as having such hazards, there is significant concern about the ease of its conversion into γ-hydroxybutyrate (GHB), a compound listed in Schedule II of the 1971 UN Convention on

Psychotropic Substances or simply ingested directly as an intoxicant (γ-but is metabolized to GHB).[56]

Thus, γ-butyrolactone is a controlled substance in some countries, including UK. In an effort avoid the above-mentioned risk and restriction on γ-but, a similarly structured solvent, γ-valerolactone (γ-val), was tested and it proved to form a reasonably effective OES for cellulose dissolution when combined with [EMIm][OAc]. γ-Val can be produced from biomass[57] and has a 'green' solvent credential.[58]. Furthermore, its physical properties are suited for solution casting of cellulose membrane, such as low vapor pressure and immiscibility with water, which would aid in its recovery post phase inversion in water, the process frequently used to prepare polymeric membrane via solution casting.

3.5   Conclusion

A range of OESs composed from binary mixtures of [EMIm][OAc] and various dipolar aprotic solvents have been studied for their capacities to dissolve microcrystalline cellulose (MC) and most were found to have very similar efficacy when compared using the basis of mole fractions of solutes and solvents. In this case, 1-MI, DMSO, DMF, DMAc, NMP, DMI, and sulfolane all provide OESs that are effective cellulose solvents at low mole fraction of added ionic liquid.

Having said that, if the objectives are to maximise the quantity of MC dissolved whilst minimising the composition of the IL (for cost and viscosity minimisations), then the solubility curves expressed in gram of MC per gram of OES are useful to identify the most appropriate co-solvents to use. Indeed, for cellulose membrane preparation via solution casting and phase inversion method, the above-mentioned objectives are very relevant. In this case the best co-solvent seems to be 1-MI. DMSO is probably the next in line in terms of dissolution capacity, but not considered a good co-solvent to use for solution casting due to its high viscosity and difficulty (low mobility in its separation during the phase inversion. DMF, DMAc, NMP, DMI, and sulfolane could also satisfy this role although DMF, DMAc, NMP are decidedly 'non-green' due to their toxicity and other hazards, particularly potential reproductive hazard.

Analysis of solvent parameters from the works of Catalán and Laurence and co-workers yielded with two potential co-solvents not associated with some of the hazards associated with many dipolar aprotic solvents. Because of the regulation surrounding the purchase of γ-butyrolactone due its psychotropic nature, γ-valerolactone seems to be a suitable potential candidate for use as cosolvent for formation of cellulose dissolving OESs with [EMIm][OAc]. Whilst this project primarily concerned in preparation of cellulose membranes for nanofiltration applications, this finding could offer significant improvements, with regards to safety profiles and sourcing of solvents from renewable sources, for large processing of cellulose to form more sustainable materials.

The findings from the extensive cellulose dissolution tests combined with the discovery of γ-butyrolactone and γ-valerolactone as effective cellulose co-solvents met the 1st objective of this thesis as outlined in Section 1.6.

Chapter 4 Development of Cellulose Membranes

4.1 Introduction

As there has been increased interest in the application of organic solvent nanofiltration (OSN) to many areas including the pharmaceutical, fine chemical and petrochemical industries,[59] efforts in finding solvent stable NF membranes is accelerating. The lack of commercially viable membranes that are stable in a broad range of organic solvents including polar aprotic solvents is a challenge and gave rise to the rationale for this project. This section offers a brief review the current state of organic solvent nanofiltration (OSN) membranes and focuses on cellulose-based membranes reported in literature.

4.1.1 Organic Solvent Nanofiltration (OSN) Membranes

Many of the current commercial OSN membranes are either composites comprising a polydimethylsiloxane (PDMS) separating layer on a polyacrylonitrile (PAN) support, or integrally skinned asymmetric membranes made of polyimides (PI).[34,60] Although PAN shows good solvent resistance, the PDMS separating layer swells appreciably in many solvents resulting in limited solvent stability.[34] Commercial PI OSN membranes have been shown to give good performances in several organic solvents, but polyimides have generally poor stability and performance in polar aprotic solvents. Inorganic membranes have been developed which offer good stability in organic solvents, but they are often more expensive and difficult to handle.[34]

See-Toh *et al*. described a method to improve the chemical stability of integrally skinned asymmetric polyimide (PI) membranes through chemical crosslinking of a preformed membrane.[59] The crosslinked PI membranes showed good performance in a range of organic solvents, including difficult solvents such as THF, NMP and DMF with almost total exclusion of species (rejection>99.9%) beyond 300 Da.[59] However, possible re-imidisation and loss of crosslinking at elevated temperatures limits their range of application to temperatures <100 °C. Crosslinking of polymeric membranes has been shown to increase their chemical and thermal stability, however, this is often at the expense of a decrease in permeability.[34]

There are a limited number of OSN membranes that have been commercialised, some of them are: Koch and Starmem™ membrane series, SolSep membranes, DuraMem™ membrane series, and Inopor series of ceramic membranes.[27]

Koch Membrane Systems (USA) was the first company to enter the OSN market with three different membranes designed for solvent applications.[27] However, two of these are no longer manufactured and according to the company, the membranes are only stable in mostly non-polar solvents and have limited stability in dipolar aprotic solvents.[27]

The Starmem™ membranes series consist of hydrophobic integrally skinned asymmetric OSN membranes with active surfaces manufactured from PIs. The membranes are claimed to be stable in alcohols, alkanes, aromatics, ethers, ketones and others such as butyl acetate and ethyl acetate.[27] Starmem™ membranes are the only OSN membranes applied at a large scale, in the refining industry for solvent recovery from lube oil.[27]

SolSep membranes offers five NF membranes with different stabilities and nominal MWCO values between 300 and 750 Da. According to the manufacturer, the membranes are stable in alcohols, esters, and ketones, and some of them are also stable in aromatics and chlorinated solvents.[27] They are believed to be thin film composite (TFC) type and some of them having a silicone top layer.[27] There is relatively limited information for the performance of these membranes in the literature, but low solvent permeability was reported[27] and there is no report on permeation data on dipolar aprotic solvents.

DuraMem™ OSN membranes are manufactured by Evonik MET and are of integral asymmetric type based on cross-linked PI. These membranes are available with different MWCO curves (180–1200 Da) and possess excellent stability in a range of solvents, including dipolar aprotic solvents such as DMF and NMP. The membranes have a sponge-like structure and are stable in most OSs, including toluene, methanol, DCM, THF, DMF, and NMP.[27] The membranes showed stable fluxes and good separation performances, with DMF permeability in the range of 1 to 8 L m^{-2} h^{-1} bar^{-1}.[27]

While there are report of progress made in the development of solvent-resistant ceramic membranes,[25] the intrinsic hydrophilicity of the oxide pore surfaces of ceramic NF membranes results in low fluxes of non-polar solvents through these membranes. Another major challenge to make ceramic membranes suitable for NF range is to reduce the pore size to nanometer range, to

get MWCO values to below 1000 Da. Modification of the pore surface, such as the silylation technique patented by HITK (Germany) has claimed MWCO as low as 660 Da.[25]

4.1.2 The Need for Truly Resistant OSN Membranes

From the current portfolio of commercial OSN membranes, it is clear that robust, solvent stable NF membranes, stable particularly in dipolar aprotic solvents, are highly desired. This is a particularly difficult challenge for OSN membranes since these popular 'aggressive' dipolar aprotic solvents such as DMF, NMP, DMAc and DMSO, render most polymeric membranes unstable.[31] Indeed, these solvents are often the ones employed to dissolve the polymer to make polymers solutions used to cast the membranes. There are only a handful commercial OSN membranes that claim to be stable in these solvents.

DuraMem™ membrane series from Evonik claimed to be stable in dipolar aprotics, but tests indicate that membrane performance deteriorates quickly in these environments.[61] SolSep BV, a renowned membrane manufacturer, offers only 1 membrane product -out of their many offerings- that is suitable for use in DMF, NMP and DMSO.[62]

It is clear that a key enabler of OSN is a membrane portfolio that combines chemical, mechanical and thermal stability with excellent rejections and high permeabilities.[34]

4.1.3 Cellulose Membranes

In the literature, cellulose-based membranes (or simply cellulose membranes) often include membranes that are made from derivatised or underivatised cellulose. A common example of the former is cellulose acetate membranes. To be technically accurate, the term cellulose membrane(s) used in this thesis is reserved for membranes that have underivatised cellulose as the active layer.

There is not a large body of work on cellulose membranes fabricated by direct cellulose dissolution and solution casting in the literature. This is primarily due to the difficulty in employing an efficient cellulose solvent to prepare sufficiently high concentration of cellulose solution for membrane casting by phase inversion (regeneration) technique. Cellulose membranes prepared using this phase inversion method are often called regenerated cellulose (RC) membranes. One of the earliest reports of RC membrane is by Yang *et al.* in 1999 where they reported preparation of

microporous RC membranes by coagulating mixture solution of cellulose cuoxam and polyethylene glycol (PEG).[63] Different molecular weights (MW) of PEG are used to tune the morphology, structure and pore size of the microporous cellulose membranes, however, neither permeation nor rejection tests were done on this study to assess the applicability of the membranes for separation purposes.

In 2005, Xiong et al. reported a pH-sensitive RC membrane using NaOH/thiourea aqueous solution as the cellulose solvent, and chitosan acetic acid solution as the anti-solvent.[64] Although they are calling the membrane as cellulose/chitosan hybrid, the chitosan content was determined to be very low. In an aqueous application test, they found that the membrane exhibited a high rejection of Cu^{2+} at pH = 5 due to the amino groups in the impregnated chitosan molecules.[64] The rejection mechanism was considered to be a combination of nanofiltration and complexation of Cu^{2+} with amino groups. No application test in organic solvent environment was conducted.

Benavante and co-workers studied a commercial regenerated cellulose (RC) dialysis membrane with 2000 Da cut-off to characterise the transport of NaCl solutions (ionic and diffusive transport).[65] Their results showed the significance of electrostatic interactions at low concentrations (up to 0.05 M) but diffusive effects are predominant at higher NaCl concentrations.

Karim et al. reported composite membranes for water purification in 2014 that were fabricated with cellulose nanocrystals (CNCs) as functional entities in chitosan matrix via freeze-drying process followed by compaction.[66] Their membranes successfully removed 98%, 84% and 70% respectively of positively charged dyes like Victoria Blue 2B, Methyl Violet 2B and Rhodamine 6G, after a contact time of 24 h. The removal of dyes was expected to be driven by the electrostatic attraction between negatively charged CNCs and the positively charged dyes. A mediocre water flux (64 $L.m^{-2}.h^{-1}$) was reported, and no flux test was conducted with organic solvent.

Thin-film composite membranes were prepared by Chu and co-workers from cellulose fibres fabricated from wood pulp using 2,2,6,6-tetramethylpiperidin-1-yl)oxy (TEMPO)-mediated oxidation.[67] An ultrafiltration (UF) thin-film nanofibrous composite membrane was subsequently prepared by using the oxidised cellulose nanofibers as the top barrier layer, polyacrylonitrile (PAN) electrospun scaffold as the mid-layer and polyethylene terephthalate (PET) non-woven as supporting substrate. The maximum pore size of the cellulose nanofibrous top layer was ~55 nm as estimated by the molecular weight cut-off (MWCO) method. The permeate flux of the

membrane was found to be about 5-times higher than that of commercial UF membranes (e.g. PAN10) produced with the same polymer components without the cellulose nanofiber barrier layer.[67] Due to the existence of the PAN and PET layers, the membranes were not resistant to organic solvents, hence are not appropriate for OSN applications.

Using TEMPO-oxidised cellulose nanofibrils similar to the above, Bismarck and co-workers prepared nanopapers using papermaking process for OSN purposes.[68] The nanopapers are suitable for NF of organic solvents and water. By using differently sized cellulose nanofibrils, they were able to tune the MWCO values of their membranes, which were ranging from 6 to 25 kDa (using polyethylene glycols), which placed the membranes at the upper end of the NF range. Flux measurements of 3 solvents showed increases in the following order: water < THF < n-hexane.[69]

As discussed briefly earlier in this thesis, the development of multilayer membranes for nanofiltration and ultrafiltration, with thin selective layers of naturally available cellulose has been hampered by the availability of efficient cellulose solvents. Nunes and co-workers proposed the manufacture of cellulose membranes based on two approaches: (i) cellulose silylation and regeneration by acid treatment and (ii) casting from solution in 1-ethyl-3-methylimidazolum acetate [EMIm] [OAc] followed by phase inversion in water.[70] With these methods, they were able to coat porous supports with semi-crystalline cellulose. Their regenerated cellulose membranes prepared by silylation led to MWCO as low as 5 kDa (measured using polyethylene glycol) with 8.1 L.m^{-2}.h^{-1}.bar^{-1} water permeance and only 3% NaCl rejection. Membranes prepared from [EMIm] [OAc] - cellulose solution had MWCO as low as 3 kDa and 13.8 L.m^{-2}.h^{-1}.bar^{-1} water permeance. Self standing cellullose membranes were also prepared without any support and confirmed to be insoluble in water, tetrahydrofuran (THF), hexane, dimethylformamide (DMF), methyl-2-pyrrolidinone (NMP) and dimethylacetamide (DMAc). They concluded that cellulosic membranes are therefore potentially suitable also for application in solvent medium.

In 2015, Peinemann and co-workers reported a new route of fabricating regenerated cellulose nanofiltration membranes.[71] Their membranes are composite membranes with a thin selective layer of cellulose, which was prepared by regeneration of trimethylsilyl cellulose (a hydrophobic cellulose derivative) film followed by crosslinking. Filtration experiments using mixtures of sugar and sodium chloride showed that solutes above 300 Da were highly rejected whereas practically no rejection was observed for NaCl. They claimed that this rejection profile is a big advantage as existing commercial nanofiltration membranes typically exhibit NaCl rejection in the range of 30–

60% and that membranes with zero NaCl rejection are required for recovery and purification applications in food, chemical and pharmaceutical industry.[71]

In 2019, Wang and co-workers utilised a proprietary 'green' solvent to develop ultrafiltration (UF) and nanofiltration (NF) membranes with conventional polymers, including polysulfone (PSF), polyethersulfone (PES), and cellulose acetate (CA).[72] The prepared cellulose acetate membrane demonstrated water permeability of 1.5 ± 0.25 L m^{-2}h^{-1}bar^{-1} with NaCl and MgCl$_2$ rejection of 85.1 $\pm$ 5.7% and 93.2 $\pm$ 4.7%, respectively.[72] However, their membranes were not tested with organic solvents as they focused on water desalination and reclamation purposes.

Li and co-workers (2021) developed a bamboo cellulose-based nanofiltration membrane using a combination of layer-by-layer assembly and spraying methods.[73] The nanofiltration performance of the composite membrane was evaluated using 500 ppm NaCl solutions under 0.3 MPa pressure and as found that to have a rejection rate of about 36.11 % against a 500 ppm NaCl solution and membrane flux of about 12.08 L/(m^{2}h) was reached.[73] Although the combined layer-by-layer assembly and spraying provides a scalable and convenient fabrication technique, they did not test the membrane for organic solvent nanofiltration applications.

4.1.4   Nonsolvent Induced Phase Separation (NIPS) Membrane Preparation Technique

Many of the OSN membranes developed to date are integrally skinned asymmetric (ISA) membranes prepared by phase inversion method developed by Loeb and Sourirajan.[74] The method, which involves precipitation of a casting solution by immersion in a non-solvent (or antisolvent) bath, is often termed Non-Solvent Induced Phase Separation (NIPS) method.

The nonsolvent-solvent-polymer membrane-forming system can be represented by a ternary phase diagram (Figure 21). The corners of the triangle are the neat nonsolvent (1), solvent (2) and polymer (3). The binodal curve (also called cloud point curve), represents the limit of the miscibility of the mixture. The area inside the binodal curve is called the miscibility gap. Any mixture whose composition lies inside this gap separates spontaneously into two phases which are in equilibrium with each other. The area inside the spinodal curve is highly unstable while that between the spinodal and binodal curves is metastable. For example, in Figure 21, if the points A and A' represent two phases in equilibrium with each other, the line AA' represents a tie-line

across these two points. Any mixture whose composition falls along the tie-line, demixes spontaneously into two phases with compositions A and A'.
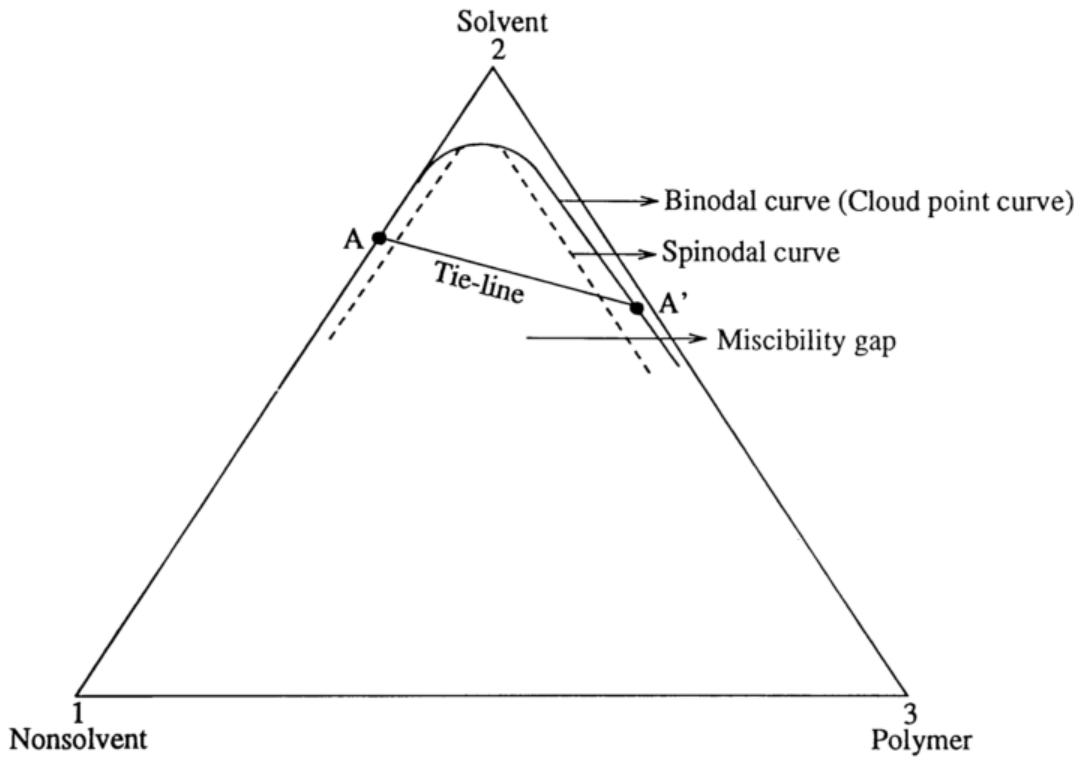
Figure 21. Ternary phase diagram in membrane casting system. Adapted from Burra, 1993.[75]

Achieving high polymer concentration in the casting solution is important in order to achieve NF separation performance (generally MWCO < 1000 Da). Polysulfone-based OSN membranes prepared by Holda *et al* used polymer concentration of up to 29 wt.% with NMP/THF mixture as the solvent,[76] whilst Darvishmanesh *et al* prepared NF flat sheet membranes based on polyphenylsulfone (PPSU) with PPSU concentrations between 17 to 25 wt.% in dipolar aprotic solvents DMAc, NMP, or DMF.[77] Hendrix *et al* prepared poly(ether ether ketone)-based NF membranes with polymer concentrations of 15-23 wt% in NMP in the casting solutions.[78]

Membranes prepared from NIPS method typically possess a skin-layer on top of a more porous sublayer with the same chemical composition, Figure 22.
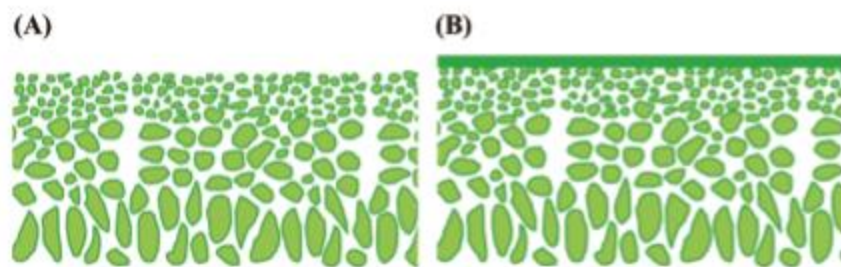
Figure 22. Schematic representation of polymeric membranes: (A) Integrally skinned asymmetric (ISA) membrane; (B) thin film composite (TFC) membrane. Adapted from Szekely et al, 2014.[79]

Broens *et al.*[80] described the membrane formation mechanism based on theoretical and experimental knowledge of phase separation phenomena in concentrated polymer solutions of cellulose acetate (CA), polysulfone (PSf), polyacrylonitrlie (PAN) and polydimethylphenyleneoxide (PDPO). They demonstrated that different types of phase separation phenomena, such as liquid-liquid demixing and gelation of the concentrated polymer phase, are responsible for the build-up of the dense skin layer and the supporting porous sublayer in asymmetric membranes. From the ternary phase diagrams of CA-dioxane-water and PSf-dimethylformamide (DMF)-water systems, they concluded that the factors which favour the formation of a dense skin (i.e. nanofiltration membranes) are: (a) a higher initial polymer concentration in the casting solution, which increases supersaturation of the polymer in the top layer of the membrane during the coagulation step; (b) a lower tendency of the nonsolvent to penetrate the top layer of the cast membrane; and (c) a lower coagulation bath temperature which, once again, increases the supersaturation of the polymer in the top layer. On the other hand, factors favouring the formation of ultrafiltration type of membranes are lower polymer concentrations in the initial casting solution and addition of nonsolvent to the polymer casting solutíon.

These integrally skinned asymmetric (ISA) membranes generally suffer from limitations in terms of flux for some organic solvents, and tight membranes (MW cut-off = 150–300 Da) have poor fluxes in dipolar aprotic solvents, including THF and acetone.[29] This limitation might be overcome by carefully controlling the formation of the separation layer (the skin), but it is not usually a straight forward procedure.[29]

Thin film composite (TFC) membranes were developed to achieve higher fluxes than ISA membranes, without sacrificing selectivity, but to date there are very few reported TFC OSN membranes which can give satisfactory performance in dipolar aprotic solvents.[29]

It is obvious that despite some reports of the excellent solvent resistance of cellulose membranes, there is not that many works exploiting this desired characteristic for OSN applications. Efficient cellulose solvent, or rather, the lack of it, continues to be the main issue. Having done in-depth study of cellulose dissolution in electrolyte organic solutions, we are in a good position to develop cellulose membranes by using NIPS method.

4.2 Results and Discussions

Table 7 below outlines cellulose membranes and their designated membrane identification (ID) numbers along with their preparation conditions.

Table 7. Membranes ID and their preparation conditions

Membrane ID	Cast solution $(cc/X_{IL}/cs)^a$	Hot casting?[b]	Non-solvent	Notes
60	13/0.17/1-MI	No	MeOH	Backing layer[c] was viscose
62	13/0.17/1-MI	No	Water	Backing layer[c] was viscose
64	13/0.17/1-MI	No	MeOH	
68-1	16/0.23/1-MI	No	MeOH	0.5 mm casting thickness[d]
68-2	16/0.23/1-MI	No	100% humidity + MeOH	0.5 mm casting thickness[d]
70-1	16/0.23/1-MI	No	Acetone	
70-2	16/0.23/1-MI	No	100% humidity + acetone	
76	13/0.17/1-MI	No	MeOH	
80	13/0.17/1-MI	No	MeOH	Standing time[e] = 10 min
81	13/0.17/1-MI	No	MeOH	Standing time = 20 min
79	13/0.17/1-MI	No	Acetone	
6	16/0.5/GVL	No	MeOH	
25	20/0.31/1-MI	Yes	MeOH	
27-1	20/0.31/1-MI	Yes	MeCN	Standing time = 10 min
27-2	20/0.31/1-MI	Yes	MeOH	Standing time = 10 min
32	20/0.57/GBL	Yes	MeCN	Standing time = 10 min

Notes:
[a] cc = cellulose concentration, in % wt ; X_{IL} = IL mole fraction ; cs = co-solvent
[b] Hot casting: both solution and aluminium platen were pre-heated to 65 °C
[c] Only these 2 membranes used viscose as backing layer, the rest used Whatman 41 filter paper
[d] Only these 2 membranes were cast at 0.5 mm, the rest were cast at 0.8 mm.
[e] Standing time = wait period after casting and before immersion in anti-solvent bath. Default was 30 sec. When hot casting, membrane was removed from heat during this standing time.

4.2.1　Membrane Preparation

Backing Layer

When choosing the type of backing or support layer for our cellulose membranes, two technical requirements became obvious. Firstly, the material must have good resistance to wide range of organic solvents, particularly to those from dipolar aprotic family for reasons discussed previously. Secondly, the material must be able to bind well to the cellulose. These requirements quickly exclude some of the commonly used membrane support materials such as polyacrylonitrile (PAN), polyethylene terephthalate (PET) and cellulose acetate (CA).

Viscose fabric (45 g/m^2) was as a candidate as it is generally considered as 100% cellulose. Tests showed that although solvent resistance and binding strength were excellent, its surface heterogeneity caused operational issues during casting, resulting in high variability in final membrane thicknesses, impacting membrane reproducibility adversely. The final choice was Whatman 41 filter paper, chosen for the very low ash content (ashless grade), meeting the two technical requirements above, as well as better surface homogeneity than viscose fabric (as long as it is kept crease and fold free).

Casting Solution Composition: Cellulose Concentration and Co-Solvent

In polymeric NF membranes preparation, high polymer concentration (ca. 20 wt.%) in the casting solution is generally required to produce dense membranes capable of NF separation performances (generally MWCO < 1000 Da). Dissolving more than several weight % of microcrystalline cellulose (MCC) was not considered achievable before certain ionic liquids (such as [EMIm][OAc]) were discovered to be highly efficient cellulose solvents. MCC was chosen because of its relatively low degree of polymerisation (typically around 300 to 400), to maximise the cellulose content in the casting solution. The maximum [EMIm][OAc] dissolving capacity of MCC was found to be 22-23 wt. %.

For cellulose membrane casting, using an OES with high organic solvent composition, whilst still offering sufficient cellulose dissolution capacity, becomes important to minimise the use of the ionic liquid (IL), as well as to lower the viscosity of the resultant solution. [EMIm][OAc] is highly viscous with viscosity of 141.8 mPa.s at 25 °C,[81] compared to γ-valerolactone, as an example of a co-solvent, with viscosity of 2.2 mPa.s at 25 °C.[82] Based on the study of [EMIm][OAc]–based

organic electrolyte solutions (OESs) with different co-solvents in chapter 3, four organic solvents were shortlisted to be used as co-solvents in Table 8.

Table 8. Solvent shortlist as co-solvent for membrane casting solutions (own work)

Solvent	Reason & Comments
Dimethyl sulfoxide (DMSO)	One of the most efficient co-solvents*, but has high viscosity.
1-Methylimidazole (1-MI)	One of the most efficient co-solvents*
γ-Valerolactone (GVL)	'Green solvent' credential
γ-Butyrolactone (GBL)	Recently discovered as a cellulose co-solvent.[82]

Notes: * with regards to cellulose dissolution

Table 9 outlines the viscosity values of the four casting solutions used to prepare cellulose membranes in the project. Due to its high viscosity, solution 20/0.31/1-MI was pre-heated to 65 °C and the aluminium platen on the casting machine was also turned on to the same temperature, to allow more viscous solutions (higher cellulose concentrations) to be cast.

Table 9. Dynamic viscosity values of membranes casting solutions at 25 °C (own work)

Cast solution (cc/X_{IL}/cs)[a]	Viscosity (Pa.S)
13/0.17/1-MI	10.1
16/0.23/1-MI	95.7
16/0.5/GVL	178
20/0.31/1-MI	346

Notes: [a] cc = cellulose concentration, in % wt ;
X_{IL} = IL mole fraction ; cs = co-solvent

To investigate the effect of co-solvent in membrane performance, membrane 27-1 is compared to membrane 32. Both membranes were cast using the same MCC concentration solution with the same casting and post-treatment conditions. The differences were the co-solvent used (1-MI for 27-1 ; GBL for 32) and IL mole fraction, as IL mole fraction needed to be adjusted according to the co-solvent used to be able to dissolve 20% mcc. As GBL is a less efficient cellulose co-solvent, the IL mole fraction needed to be higher.

Table 10. Membrane performance comparison due to co-solvent effect (own work)

Membrane ID	Cast solution (cc/X_{IL}/cs)[a]	MeCN permeance (L.m^{-2}.h^{-1}.bar^{-1})	Zeta surface potential (mV)	Rejection of polystyrene 3350 (%)
27-1	20/0.31/1-MI	0.6 ± 0.2	-21 ± 7	35
32	20/0.57/GBL	1.7 ± 0.3	-4 ± 6	24

Notes: [a] cc = cellulose concentration, in % wt ;

X_{IL} = IL mole fraction ; cs = co-solvent

Table 10 compares the performance of these two membranes. Although membrane 27-1 shows that it has 65% lower MeCN permeance than membrane 32, polystyrene 3350 rejection values for both membranes are low for NF standard. In other words, these membranes do not seem to have a dense, nonporous skin. Phase inversion theory states that the higher the mutual affinity (or miscibility) between the solvent and antisolvent is, the higher the rate of demixing is likely to be, and more porous membrane will be obtained.[26] In the case of low mutual affinity, an asymmetric membrane with a dense nonporous top layer is likely obtained. Although other parameters influence membrane structure, the choice of solvent- nonsolvent is crucial.[26]

Acetonitrile (MeCN), as the nonsolvent used in the above two membranes, is miscible with [EMIm][OAc], GBL, and 1-MI. This solvent/nonsolvent miscibility seems to have produced the formation of porous membranes, hence the low rejection values of polystyrene 3350.

Nonsolvent

When the casting solution was cast onto a glass plate, the plate was then immersed in a non-solvent bath. The solvent, i.e. [EMIm][OAc] and the co-solvent demixed from the polymer solution and mixed with non-solvent, resulting in liquid to solid phase inversion.

As mentioned in the introduction section, the choice of the nonsolvent for phase inversion purpose for cellulose solution in [EMIm][OAc] is limited. There are two non-solvents that are commonly used in the literature with this polymer solution system, namely water and methanol. As the choice of non-solvent is crucial in determining membrane structure, four organic solvents

were tested in this project for membrane production, namely water, methanol, acetone, and acetonitrile

Using **water** and **acetone** as non-solvents for membrane formation was found to produce membranes with insufficient strength in the never-dried state. The cellulose layer was found to be lacking toughness and flexibility and prone to cracking and fissures formation when the membranes were put under flux tests.

Methanol was found to be a good nonsolvent in this regard, producing cellulose layer with sufficient flexibility and toughness to withstand handling and testing in the dead-end cell. Towards the later stage of the project, **acetonitrile** was also found to be a feasible nonsolvent, and was used in formation of two membranes.

4.2.2   Effect of Standing Time on Membrane Performance

Standing time is defined as the waiting time after casting and before immersion in the non-solvent bath. Three standing times of 30 sec, 10 mins, and 20 mins were used in preparation of membranes 76, 80, and 81, respectively, with methanol as the non-solvent. The idea behind this was during the wait time was that interaction between the cast polymer solution and the water vapour in ambient atmosphere (i.e. humidity) could be used to effect structural differences in the membrane.

However, flux test results of the above three membranes showed that the effect of standing time seemed to be minimal, at least in terms of permeance, as shown in Figure 23. The effect of using a different non-solvent, though, in this case methanol vs. acetone, was pronounced, with membrane that was produced using acetone as non-solvent, showed lower permeance. The use of acetone as non-solvent was not investigated further, however, due to reasons mentioned previously.
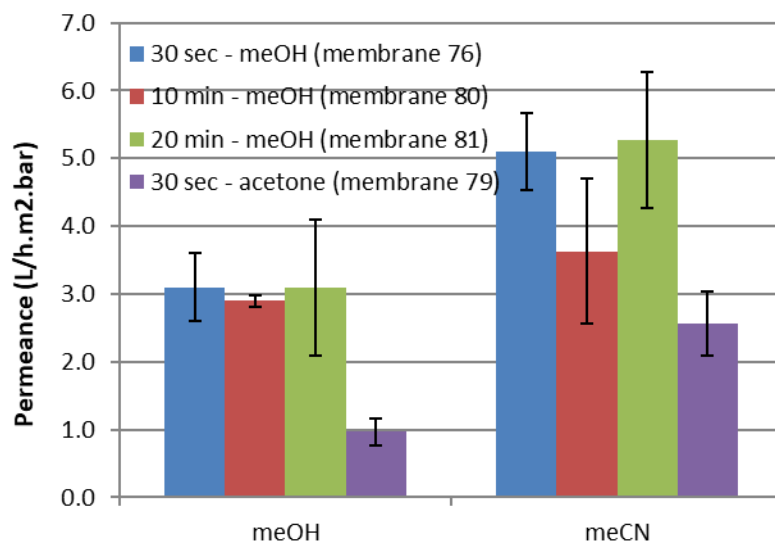
Figure 23. Flux test results comparing membranes prepared with varying standing times and MeOH vs acetone as non-solvent. Labels indicate the standing time and non-solvent used and membrane ID. Tests done in duplicates with membranes of the same batch, except for membrane 80 and 81, which were from different batches. For summary table of membrane IDs, refer to Table 7, Section 4.2.

4.2.3   Glycerol Post Treatment and Drying

Removing membranes from antisolvent bath starts the evaporation process of the non-solvent i.e. membrane drying. Cellulose membranes exhibit significant shrinkage upon drying, and with low boiling point antisolvent such as methanol, the membranes start drying and shrinking within minutes of removal from antisolvent bath. Flux tests with dried membranes yielded zero flux, which indicate that the drying process eliminated any internal porous structure of the cellulose membranes, rendering them impermeable to liquids. With drying occurred especially quickly when the membranes were kept in volatile non-solvent such as methanol, a wetting agent was needed to keep the membrane from drying out during handling and testing. To this end, a glycerol post treatment (refer to Chapter 2 Experimental Section) was performed to all membranes by default except when indicated otherwise.

To measure the effectiveness of this glycerol treatment against drying, membrane 76B and 76C-D were prepared for flux test, where the only difference was that 76B was glycerol-treated and kept never-dried, i.e. kept immersed in glycerol/MeOH mixture, whilst 76C-D was glycerol-treated and then dried in ambient condition (21 $^{\circ}$C and 45 % RH) for 24 hours. The results of the flux test showed that the permeance values of three solvents (MeOH, MeCN, and THF) were similar in both membranes (Figure 24), suggesting that the glycerol treatment worked to prevent hornification of the cellulose active membrane layer due to drying. Flux values of untreated cellulose membranes subjected to the same drying protocol were found to be practically zero (no flow after 2 hours under 40 bar).
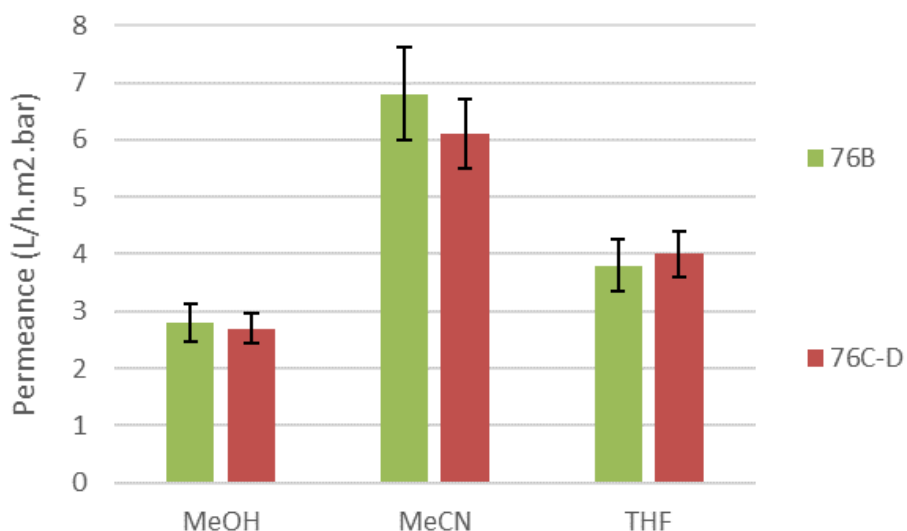
Figure 24. Flux test results comparing same batch membranes with different post-treatments (76B: glycerol-treated & never-dried; 76C-D: glycerol-treated & ambient-dried). Tests done in duplicates with membranes of the same batch. For summary table of membrane IDs, refer to Table 7, Section 4.2.

4.2.4 Reproducibility

Reproducibility in membrane preparation, assessed from the results of various tests and characterisation methods, is important as it gives an indication on the validity and consistency of

the membrane preparation protocols employed. Permeation test results provide good opportunities to assess the issue as repeat tests are more easily performed on different test membrane pieces compared to some other tests, and that permeance values reflect the surface as well as structural properties of the membrane test pieces.

To discuss reproducibility, the uncertainty of permeance values from the repeat tests of membrane test pieces needs to be quantified. The uncertainty is calculated using the half range method, (half range divided by average), and this method chosen so that a relative uncertainty can be calculated from the error bar of repeat permeance test results (expressed in percentage) and compared it other relative uncertainties obtained from repeat permeance tests of different membranes.

From the numerous permeance test results that have been reported in this chapter, the relative uncertainties obtained range from 3.4% to 32%. A note, though, that the 32% relative uncertainty was from permeance tests performed on the same membrane ID (i.e. prepared under the same conditions) but from different batches. The range of relative uncertainties from repeat permeance tests of membranes of the same batch was 3.4% to 17%. These figures indicates that reproducibility or consistency of membrane prepared from the same batch is somewhat within reasonable expectations, but reproducibility of inter-batch membranes could be improved, and should be a part of future work of the project.

4.2.5   Solvent Resistance

There is a lot of effort to develop robust membranes that are resistant to more and more organic solvents, as advances in this area will open up many potential OSN applications, typically in, but not limited to, pharmaceutical and fine chemical industries. However, as outlined in the literature review on this chapter, NF membranes that are resistant to aggressive solvents, specifically dipolar aprotic solvents, are exceptions rather than the norm. The solvent resistance of cellulose membranes developed in this project is therefore, of a great interest.

Cellulose is known to be resistant to most known organic solvents and regenerated cellulose sheet developed using the same NIPS method (i.e. cellulose layer without any backing layer) was indeed

found to be stable (i.e. no weight loss) when immersed in these four dipolar aprotic solvents: DMSO, DMF, DMI and DMAc, for overnight under room temperature. In addition to this, the solvents listed in Table 11 had been used for permeation tests of cellulose membranes in a dead-end cell set up at 21 °C and trans-membrane pressure of up to 50 bar with no visible deterioration on the membrane integrity.

Table 11. List of solvents that had been used in flux measurements (own work)

Solvent	Solvent Class
Dimethylsulfoxide (DMSO)	Dipolar aprotic
Tetrahydrofuran (THF)	Dipolar aprotic
Acetonitrile (MeCN)	Dipolar aprotic
Ethyl acetate (EtOAc)	Dipolar aprotic
Methanol (MeOH)	Dipolar protic
Water	Dipolar protic
Toluene	Non-polar
Hexane	Non-polar

Further discussions on flux values and solvent-membrane interaction for these solvents are presented in chapter 5, however the main point here is that cellulose membranes were resistant to wide-ranging organic solvents. DMSO and water yielded much lower flux values than the other solvents due their relatively high viscosities, but none of the solvents used caused the membrane test pieces any apparent degradation.

4.3   Conclusion

This chapter serves to provide introduction to cellulose membrane and its place within the membrane separation technologies. Cellulose membrane preparation by solution casting and non-solvent induced phase separation (NIPS) techniques were described and the reasoning behind some of the variables and choices during membrane development stage was explained.

Results and discussions on membrane performances and characterisations are presented in subsequent chapters.

It is evident from the literature review that cellulose membranes are not common, due to difficulty in processing (dissolving) underivatised cellulose. Our approach in cellulose membrane development, i.e. using [EMIm][OAc]-based organic electrolyte solutions (OESs) as cellulose solvents and then employing the NIPS (non-solvent induced phase separation) to produce the membranes is a novel way to produce cellulose membranes for nanofiltration/ultrafiltration purposes. Finding an efficient cellulose solvent capable of dissolving high amount of underivatized cellulose (> ca. 5 % wt.) whilst still yielding a workable viscosity has been a big challenge. Our investigation of co-solvents in forming [EMIm][OAc]-based OESs as efficient cellulose solvent systems yielded important findings to make this project feasible. One of the [EMIm][OAc]-based OESs that was used for membrane casting solution had an IL content of 0.31 mole fraction, with 1-methylimidazole as the co-solvent, and was able to dissolve 20 % wt. of microcrystalline cellulose resulting in viscosity of 346 Pa.s at 20 $^\circ$C. Such a high content of cellulose solution with a moderate viscosity value was not known to be possible until now, and these highly efficient cellulose solvent systems are important enablers to prepare cellulose membranes by solution casting method.

In terms of membrane component, Whatman 41 filter paper (ashless, quantitative grade) served as a satisfactory backing layer, providing excellent adhesion and solvent resistance, owing to high purity of cellulose. Hornification of cellulose, which would destroy any internal porosity in the active layer upon drying, was avoided by employing glycerol post-casting treatment. Resistance to different classes of organic solvent was excellent, as expected from cellulose. Organic solvent nanofiltration (OSN) membranes that are resistant to dipolar aprotic solvents in particular, are highly desirable –especially in pharmaceutical industry, where the use of such solvents is widespread– but are not common, because of the polymeric nature of NF membranes. Therefore, cellulose membranes have the potential to play an important role in such applications.

The method developed to produce cellulose membranes, along with the materials and solvent systems used, met the 2nd objective of this thesis as outlined in Section 1.6.

Chapter 5 Membrane Permeation Studies

5.1 Introduction

5.1.1 Trans-membrane Flow in OSN Membranes

Flux or permeation rate or trans-membrane flow is the volume of liquid flowing through the membrane per unit area and per unit time and is considered one of the important parameters in membrane separation unit operation as it determines the commercial feasibility of the system.[26] It is generally expressed in terms of $L.m^{-2}h^{-1}$ and the permeability or permeance by $L.m^{-2}h^{-1}bar^{-1}$. OSN membranes, with high solvent fluxes and high retention of organic solutes, are highly sought after for various commercial applications. Flux or permeance values of common organic solvents through some commercial membranes are reported in Table 12 as well as elsewhere in the literature.[25,27,60]

5.1.1.1 Transport Mechanisms: Pore-Flow and Solution-Diffusion Models

Transport mechanisms are relatively well understood for aqueous nanofiltration (NF) systems. However, fundamental transport mechanisms of organic solvent/OSN membrane systems are not very well developed[83], and due to the added complication of solvent-membrane interaction, results from work in this area are usually only applicable to membranes made from the same materials.

Researchers have studied and modelled the transport behaviour of organic solvents in polymeric membranes. Flory pioneered the studies of polymer–solvent interactions in 1950s.[84] Two distinct processes have been reported for different membranes and operating regimes. The transport processes for high-pressure liquid systems in all areas from microfiltration (MF) to reverse osmosis (RO) are pressure-driven physical mechanisms, whereas membrane separation involving dense membranes and vapours or gases, such as pervaporation, gas separation and vapour permeation are considered to be governed by chemical transport processes such as adsorption and diffusion.[83]

Hydraulic transport of fluids through any kinds of physical pores (membranes and other media), in the absence of chemical interactions between the fluid and the pore wall, i.e. purely physical

transport, is pressure-driven and governed by Darcy's Law. For liquids, the flux behaviour can be described by the Hagen–Poiseuille equation for viscous flow[85]:

$$J = \left(\frac{\varepsilon r^2}{8L\tau}\right)\left(\frac{\Delta P}{\mu}\right)$$

Equation 10

where J is the solvent flux, ε the porosity, r the average pore radius, ΔP the differential pressure across the membrane, μ the liquid viscosity, L the membrane thickness, and τ the pore tortuosity factor. In many cases, the pore geometry and geometry distribution are unknown, so the tortuosity factor reduces to an adjustable parameter. This physical, pressure-driven liquid transport mechanism is known as **pore–flow model**.

In contrast, chemical transport mechanisms are considered predominant in pervaporation, gas separation and vapour permeation with dense membranes. One of the widely held model is the **solution–diffusion model** first proposed by Lonsdale *et al.*[84] This model explains molecule transport by a substance dissolving in the membrane and diffusing through it. Solubility and diffusivity differences, therefore, determine the separation potential of the membrane.[86]

To provide desired molecular weight cut-off below 1000 Da, the selective layer of polymeric OSN membranes is non-porous or possesses micropores at the range of several nanometers.[87] The asymmetric nature of polymeric OSN membrane's selective layer, typical in membrane prepared from non-solvent induced phase separation (NIPS) technique, means that the top part of the selective layer (skin) is considered dense or possessing micropores with larger pores beyond the skin. Solvent transport through the dense part of the selective layer typically results in meaningful polymer–solvent interaction.[88] This generally means that transport phenomena within OSN membranes are governed by both pore–flow model solution–diffusion model to a varying degree of domination.[89]

Interactions between the solvent and polymeric membranes have led to the development of alternative transport equations. Machado *et al.*[90] proposed a resistance-in-series model to describe the flux of organic solvents through composite polymeric membranes. Three significant resistances to mass transport were identified as viscous flow in the membrane top layer, viscous flow in the porous support and hydrophilic/hydrophobic resistances. The resulting equation for solvent flux is:

$$J = \frac{\Delta P}{\phi[(\Delta\gamma + f_1\mu) + f_2\mu]}$$

<div align="right">**Equation 11**</div>

where ɸ is a single parameter incorporating the membrane characteristics (porosity, tortuosity, thickness), Δγ is the surface energy difference between the membrane and solvent, f1 and f2 are constants incorporating the individual mass transfer coefficients and pore radii, and μ is the viscosity of the fluid.

The model predicts that hydrophobicity plays an important role in solvent flux; polar solvents (generally possessing high surface tension) are expected to have a low flux through hydrophobic membranes, and a high flux through hydrophilic membranes.

5.1.1.2   *Compaction Effect and Solvent Fluxes in Commercial OSN Membranes*

Initial flux decrease is found to be a common phenomenon in commercial membranes, usually attributed to membrane compaction, with the variation between initial and steady-state fluxes depending upon membrane and solvent.[91] Membrane compaction is a phenomenon that occurs in pressure driven membrane processes, where pressure tests the mechanical strength of the polymeric membrane. The flux response to pressure during membrane compaction is illustrated in the drawing below. If no membrane compaction occurred, flux would have a linear correlation with pressure. The deformation caused by membrane compaction is often irreversible.
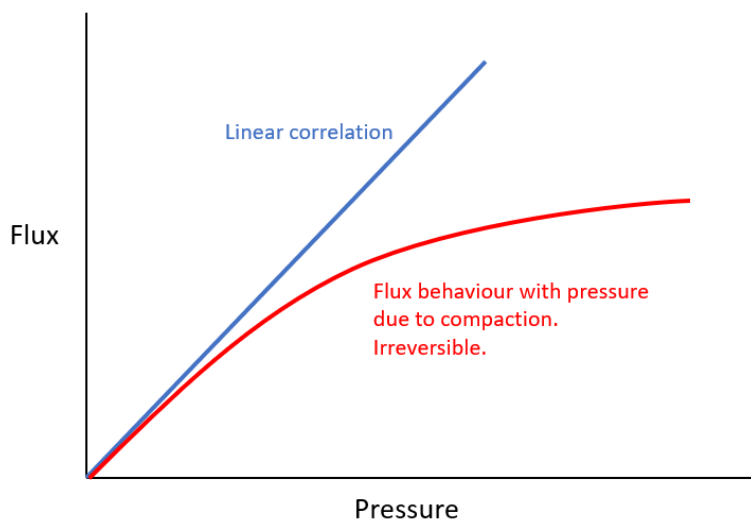
Figure 25. Pressure vs. flux behaviour with regards to membrane compaction effect. Adapted from Strathmann *et al.*[91]

Solvent flux through the membrane also increases with rise in temperature driven by reductions in viscosity of solvents, increase in solvent diffusion coefficients,[83] or by increases in polymer chain mobility.[92] The nature of the membrane (hydrophilic or hydrophobic), physical properties of solvents, such as dipole moment, dielectric constant, and solubility parameter, affect membrane–solvent interaction, which in turn affects solvent flux.[93]

As discussed above, the Machado's model predicts that polarity and hydrophobicity of solvents play an important role in solvent flux. Bhanushali *et al*. suggested that solvent viscosity and surface tension are dominant factors controlling solvent transport through NF membranes.[94] Whereas Zwijnenberg *et al*. also report the importance of the surface energy difference in a study of polar and non-polar solvents with hydrophilic membranes.[95] Permeation through the membrane pores is only possible when the difference in surface energy can be overcome by the applied pressure.

Table 12. Solvent permeance values of some commercial OSN membranes
(Data is from own work unless otherwise indicated in Ref. column)

Membrane	Ref.	Solvent	Permeance L/(h.m^2.bar)
PV 1070 (Sulzer Chemtech)	[96]	Ethanol	5.2[a]
MPF 50 (Koch)	[96]	Ethanol	1.2
	[97]	Methanol	2.5
	[89]	Toluene	2.9
	[97]	Hexane	18.0
MPF 44 (Koch)	[97]	Methanol	1.9
	[97]	Ethyl acetate	0.2
Desal 5 DK (Osmonics)	[97]	Methanol	0.5
	[97]	Hexane	6.0
HITK T1	[97]	Methanol	0.4
		Ethyl acetate	0.2
STARMEM 120 (W.R. Grace)	[98]	Methanol	5.7
STARMEM 122	[89]	Methanol	3.3
	[89]	Toluene	0.9
STARMEM 240	OT	Acetonitrile	4.1
		Methanol	1.4
		Toluene	1.3
Solsep 010206	OT	Acetonitrile	4.6
		Methanol	1.4
		Toluene	0.8
PuraMem 280 (Evonik)	OT	Acetonitrile	4.9
		Methanol	4.3
		Toluene	1.9
DuraMem 200 T1 (Evonik)	OT	Acetonitrile	2.9
		Methanol	1.0
		DMSO	0.5
GMT-oNF-2	OT	Acetonitrile	0.2
		Toluene	1.5

Conditions, unless indicated, are: T = 20-25 ^{o}C and P = 30-40 bar. [a] P = 7 bar. OT = own test

5.1.2   Rejection of Dyes and Molecular Weight Cut-Off (MWCO) in OSN Membranes

Rejection (R) of an NF membrane against particular solute can be calculated by

$$R\,(\%) = \left(1 - \frac{C_p}{C_f}\right) \times 100$$

Equation 12

where C_p and C_f are the concentration of the solute in the permeate and the feed, respectively.

The separation performance of OSN membranes can also be expressed in terms of MWCO, obtained by plotting the percentage rejection of solutes versus their MW (typically 200–1000 Da) and interpolating the data to find the MW corresponding to 90% rejection.

Rejection of Dyes

Although standard MWCO characterisations have been developed for aqueous NF systems using test solutes such as PEG, alcohol, and sugar, a standard method for OSN systems has yet to be established.[95] This is because mainly because of the combination of two factors: dissolution issues of these organic solutes in organic solvents and the complication of determining these solutes concentration in organic solvents.[99] An example of the latter is the inability of using Total Organic Carbon (TOC) analyser –a widely used instrument for measuring solute concentration in aqueous NF studies– as both the solute and solvent contain carbon. Therefore, many rejection studies of OSN membranes are performed using dyes as the test solutes and many reports these dye rejection result as the MWCO of the membrane (Table 13), although many question the validity of reporting MWCO this way.[100]

The advantages of using dye(s) in evaluating rejection or determining MWCO in OSN membranes are: it is generally a quick and cost-effective method, and its facile determination of dye concentration in permeate/retentate, e.g. by a UV–Vis spectrophotometer. However, the complex nature of solute–solvent–membrane interactions mean dye rejection result can be highly specific to a particular solute–solvent system and the membrane's MWCO can be expected to change in a different solute–solvent systems.[95]

Typically, solvents affect the separation performances in two ways: solvent–membrane interaction and solvent–solute interaction.[25] It has been asserted that membrane–solvent interaction generally has more impact on the solute rejection compared to the solvent–solute

interaction.[101] Sani *et al*. studied the rejection profile of an OSN membrane as a function of dye MW in three different alcohol-based solvents (methanol, ethanol, and isopropanol) and found the separation efficiency of the dye decreased in the order of isopropanol–ethanol–methanol.[102] They suggested that this was caused by the different degree of polymer (membrane) swelling by the different solvents, causing a change in membrane pore dimensions.[102]

Effect of Swelling on Rejection

It is generally known that the degree of membrane swelling can be determined by the difference between solubility parameters of the solvent and the polymer (membrane). The higher the difference in the solubility parameters of the two, the smaller the degree of membrane swelling usually is. However, researchers reported conflicting results on the effect of membrane swelling on membrane pores. For example, according to Ebert and Cuperus, when a porous membrane swells, the pores become narrower and result in higher rejection,[101] while other researchers reported that the effect of solvent-induced swelling on polymeric NF/RO membranes caused pore dilation, decreasing rejection performance.[77] [103]

Molecular Weight Cut-Off (MWCO) of a Membrane

Oligomeric forms of polyisobutylene,[27] polyethylene glycol (PEG),[99] polystyrene,[104] linear and branched alkanes,[105] and dyes have been used as solutes to estimate MWCO of OSN membranes. The properties of solutes and solvents, such as structure, size, charge, and concentration, are found to affect the performance of OSN membranes.[59] Figure 26 shows MWCO curves for Starmem™ 122 in different solvents using polystyrene oligomers. MWCO of some of the commercially available membranes are reported in Table 13.
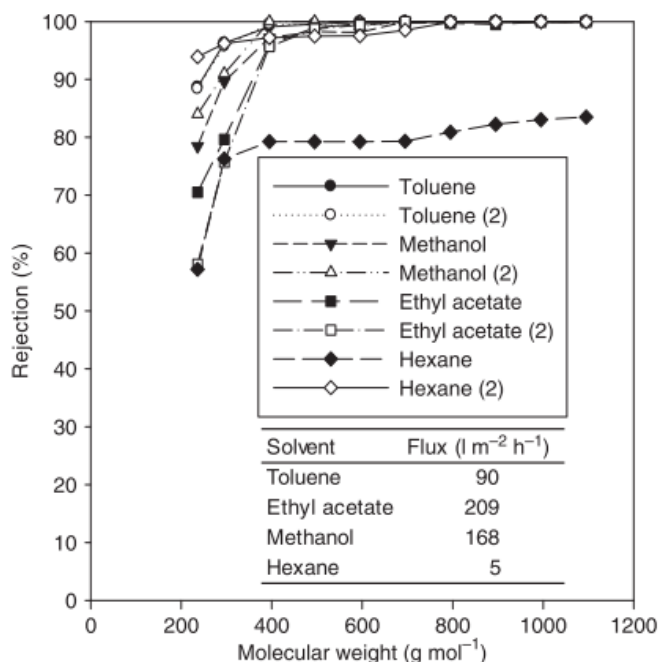
Figure 26. Molecular weight cut-off curves for Starmem™ 122 using polystyrene oligomers in different solvent systems at 30 bar. From See-Toh et al, 2007.[104]

Table 13. MWCO and solute rejection for some commercial OSN membranes. From Peeva et al, 2010.[27]

	MWCO ($g\,mol^{-1}$)	Reported rejection (%) of solute	Solute (molecular weight, $g\,mol^{-1}$)	Solvent	Nature
MPF-60	400		Sudan IV (384)	Acetone	Hydrophobic
MPF-50	700		Sudan IV (384)	Ethyl acetate	Hydrophobic
MPF-44	250		Glucose (180)	Water	Hydrophilic
MPF-U20S	2000		-	-	-
Starmem™ 120	200		n-Alkanes	Toluene	Hydrophobic
Starmem™ 122	220		n-Alkanes	Toluene	Hydrophobic
Starmem™ 228	280		n-Alkanes	Toluene	Hydrophobic
Starmem™ 240	400		n-Alkanes	Toluene	Hydrophobic
NF030505	-	-	-	-	-
SolSep-169	880	91	Erythrosine B (880)	Acetone	-
		65	Victoria blue (506)	Ethyl acetate	-
SolSep-3360	880	92	Erythrosine B	Ethanol	-
HITK-T1	220	99	Victoria blue (506)	Methanol	-
	220	97	Erythrosine B (880)	Acetone	-
Desal-5	-	99	Sucrose (342)	-	-
Desal-5-DK	-	99	Sucrose (342)	-	-
Membrane YK		43	Sudan IV (384)	Hexane	-
		86	Sudan IV (384)	Methanol	-
DuraMem™	250–1200 (tunable)		Polystyrene oligomers	DMF	Hydrophobic

The selection of membranes for OSN applications depends upon the MWCO specified by the manufacturer. In aqueous solutions, a number of methods have been developed to determine the MWCO of a NF membrane.[61] However, these methods cannot be directly applied for use in

84

organic solvent systems due to various issues such as solute solubility and compatibility in organic solvents, as well as the numerous and complex solute-solvent- membrane interactions present. Suitable techniques for determining the concentration of the probe molecule in the permeate is also problematic when applied across a range of solvents. Several relatively new methods using different solute molecule types have been developed specifically for OSN systems, as summarised in Table 14.

Table 14. Comparison of common MWCO determination methods in OSN

Important attributes	Solute used			
	Alkanes	Polystyrenes (PS)	Polyethylene glycols (PEG)	Polypropylene glycols (PPG)
Detection method **Can investigate the effect of these on rejection**	Gas chromatography MW and structure of solute	Detection by UV MW of solute only	Use of ELSD* MW of solute only	Use of ELSD* MW of solute only
MW of repeating unit	Not constant	104 Da	44 Da	58 Da
Solvent applicability	Limited solubility in polar solvents	Solvent swap required for some solvents that obscure chromatogram (e.g. toluene, hexane, ethyl acetate)	Insoluble in most non-polar solvents Molecule conformation issues in some organic solvents[106]	Soluble in non-polar solvents, but solvent swap required for some solvents to improve detection
Concentration determination	Can determine conc. for each MW	Difficult to determine conc. of each oligomer	Difficult to determine conc. of each oligomer	Difficult to determine conc. of each oligomer
Solutes cost and availability	Lack of pure commercial samples >400 Da	Expensive for narrow MW samples	Cheap and wide range of available oligomers	Less widely available than PEG, but cheaper than PS.

*ELSD: Evaporative Light Scattering Detector, an HPLC detector.

5.2 Results & Discussions

General Comments

As a characteristic of a membrane, the terms flux, permeance and permeability are often used interchangeably to mean trans-membrane flow or permeation rate, however, when looking at the values, one should always be aware that flux is trans-membrane volumetric flowrate per surface area of the membrane, whilst permeance (or permeability) is flux divided by the applied trans-membrane pressure.

Flux is an important characteristic in a membrane, as it will eventually determine the economic feasibility of the membrane application. Consequently, membranes with high flux are desired. Obviously, apart from flux, sensible discussion of membranes and their applications should also include their other vital characteristics, most notably selectivity or rejection performances. However, for organisational purpose, discussions on flux and selectivity in this chapter will be separated.

5.2.1 Membrane Compaction and Solvent Permeation Studies

Compaction generally occurs in reverse osmosis and nanofiltration membranes since the applied pressures are relatively high.[88,98] However, membrane compaction in cellulose membranes prepared in this project can be considered negligible, as shown in Figure 27 that flux values are generally stable right from beginning and Figure 28 confirms the linear relationship between flux and applied pressure.
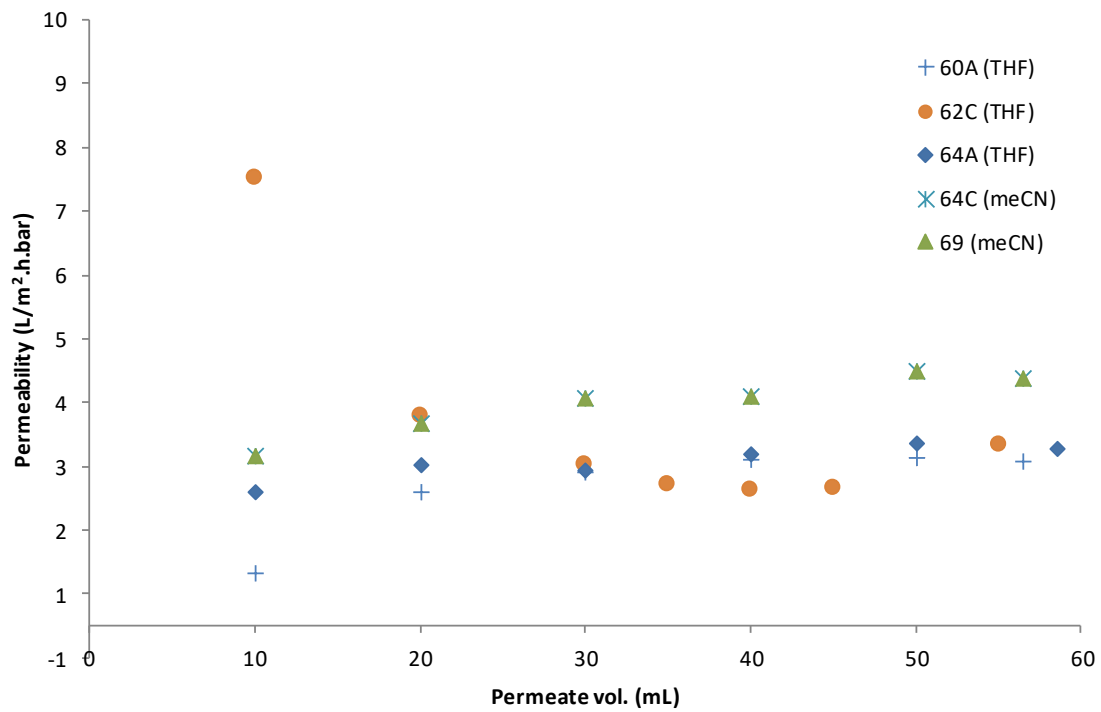
Figure 27. Typical flux profiles of cellulose membranes.
Legend denotes membrane ID number and the solvent used for permeation
(refer to section 4.2 for more details of these ID numbers).
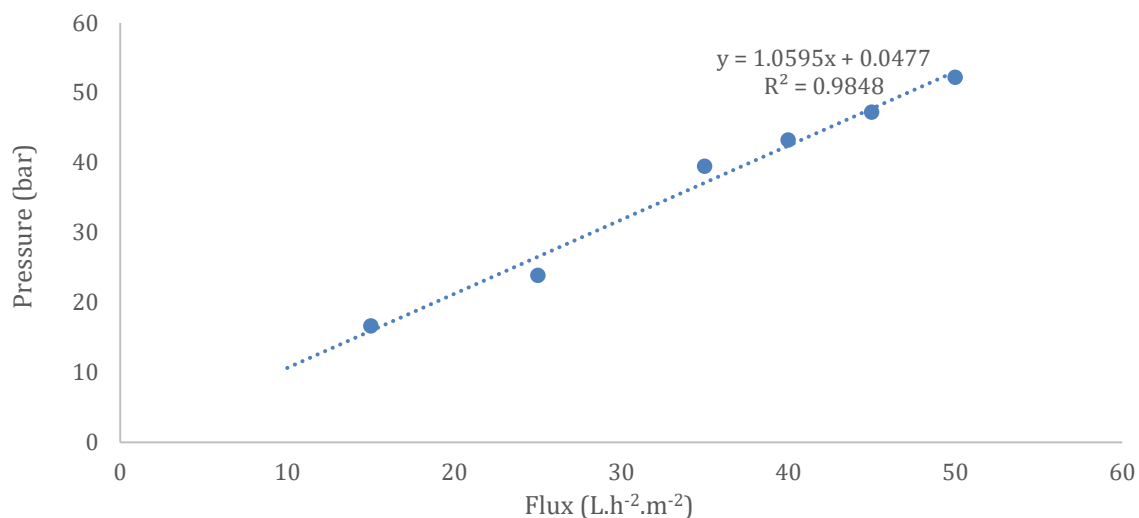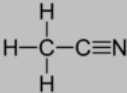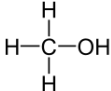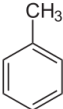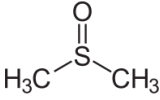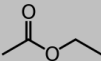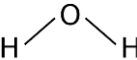
Figure 28. Linear relationship (R^2=0.985) between applied pressure to acetonitrile flux of membrane 32X.

As previously discussed, a distinct advantage of cellulose as a polymer is its resistance to most known organic solvents. With the underivatised cellulose dissolution in organic electrolyte solution (OES) and the subsequent membrane preparation utilising non-solvent induced phase separation (NIPS) method, the final product (regenerated cellulose membrane) retains the solvent-resistant property of cellulose. This characteristic, obviously, lends itself very well to organic solvent nanofiltration (OSN) application. To this end, numerous solvents were tested for flux measurements, and the rationale for using these solvents are outlined in Table 15.

Table 15. Solvents used in permeation studies

(Images are used under Wiki Commons licence, other data are own work)

Solvent (abbreviation)	Structure	Comments and reason for use
Acetonitrile (MeCN)		Dissolves a wide range of polar and non-polar compounds, used as dipolar aprotic solvent in organic synthesis.
Methanol (MeOH)		Popular solvent in laboratory and organic synthesis, important chemical feedstock. A representative from alcohol/protic class of solvents.
Tetrahydrofuran (THF)		Versatile solvent due to its moderate polarity and water miscibility. Important role in modern chemical reactions.
Toluene		A popular solvent from a hydrocarbon (non-polar) solvent class.
Hexane		Widely used solvent from hydrocarbon (non-polar) solvent class, more hydrophobic (higher log P) than toluene.
Dimethyl sulfoxide (DMSO)		Important dipolar aprotic solvent, less toxic than other dipolar aprotics such as DMF, DMAc, NMP. Not extensively tested in this project as it swells cellulose.
Ethyl acetate (EtOAc)		Popular laboratory solvent, low cost, low toxicity. Not extensively tested in this project.
Water (H_2O)		Although this project concerns with OSN, nanofiltration operations in aqueous systems are important. Not extensively tested in this project as it swells cellulose.

Amongst the various solvents that were utilised to perform permeation experiments in this project (see Table 15), three in particular were tested most frequently: acetonitrile (MeCN), methanol (MeOH), and tetrahydrofuran (THF). The flux values of other solvents such as toluene, hexane and ethyl acetate were also measured, albeit only on limited occasions. DMSO and water flux values, although tested, are not part of the discussion in this section due to the heavy swelling the two solvents caused on cellulose membranes, rendering their permeance values incomparable to the other non or less swelling-inducing solvents.

Table 16. Selected properties of solvents. Adapted from Fidale *et al.*[48] [107]

Solvent	Viscosity[108] (cP) @20 °C	Dielectric Constant	Surface Tension (dyn/cm) @25 °C	Octanol-Water Partition Coefficient[109]	Cellulose Swelling Propensity* (nSw)
Acetonitrile	0.36	37.5	28.7	-0.33	0.71
Ethyl acetate	0.45	6.0	23.2	0.73	0.14
Tetrahydrofuran	0.55	7.6	26.7	0.46	0.36
Methanol	0.59	32.7	22.1	-0.69	1.05
Toluene	0.59	2.4	27.9	2.73	-
Hexane	0.31	1.9	17.9	3.90	-

* This measure of cellulose swelling is from the work of Fidale *et al.*[48] [107] The unit nSw is moles of solvent/anhydroglucose unit. To give a sense of the scale, two solvents that cause the highest swelling amongst 36 tested are water and DMSO, with nSw of 4.82 and 1.98, respectively, and lowest recorded swelling is 0.12 nSw (2-methyl-2-propanol).

To compare the flux of different solvents, flux (or permeance) data of 9 different membranes were compiled and for each set, the permeance values of the different solvents tested were normalised to that of MeCN's. This normalisation allows solvents permeance values of one membrane to be compared to that of a different membrane, discounting the variability due to different membrane properties, and to allow us to focus solely on the solvent effect.

Based on permeation tests results of 6 solvents (MeCN, EtOAc, THF, MeOH, toluene, and hexane) from 9 different membranes prepared in this project (membrane IDs 76X, 80X, 25, 25X, 27-1, 27-2, 27-1X, 32 and 32X, where X denotes crosslinked membrane), the order of the average permeance values, in decreasing order, is MeCN > EtOAc > THF > MeOH. Figure 29 plots these permeance averages along with inverse of solvent's viscosity to show that the flux trend of MeCN, THF, MeOH, and EtOAc correlates well in their inverse viscosities (the curves tracked each other) showing that the higher the solvent viscosity, the lower the flux. The average permeance values are normalised to that of MeCN's, which allows direct comparison of permeance values of different solvents between different membranes.
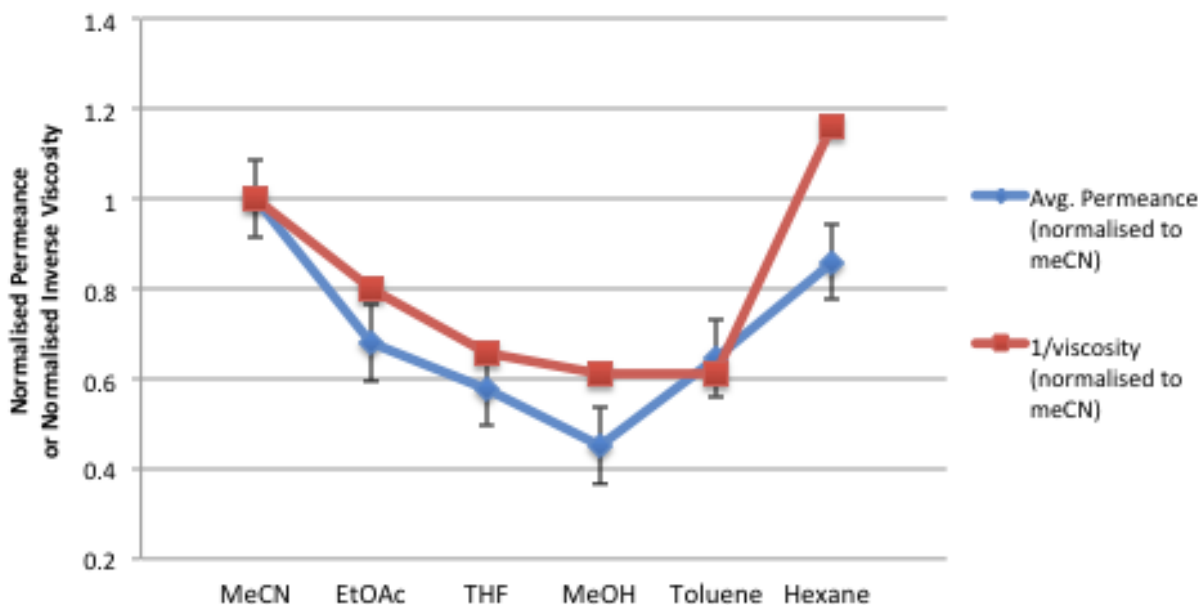
Figure 29. Blue: Average permeance of 6 solvents, normalised to MeCN value for each membrane. **Red**: Inverse viscosity, normalised to MeCN value. Number of permeance data points for MeCN, EtOAc, THF, MeOH, toluene and hexane are 9, 3, 7, 8, 4 and 3 respectively, tested on membrane 76X, 80X, 25, 25X, 27-1, 27-2, 27-1X, 32 and 32X. For summary table of membrane IDs, refer to Table 7, Section 4.2.
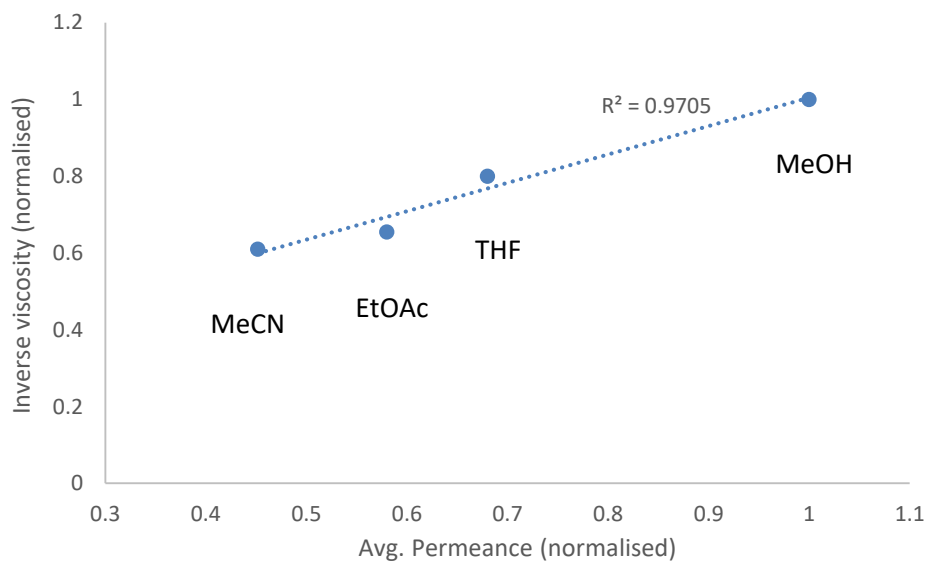
Figure 30. Average permeance values (normalised) vs. inverse viscosity (normalised) of 4 solvents, tested on membrane 76X, 80X, 25, 25X, 27-1, 27-2, 27-1X, 32 and 32X. For summary table of membrane IDs, refer to Table 7, Section 4.2.

The importance of viscosity on membrane flux is known,[27, 83] and indeed the viscosity term, μ, is on the bottom of Hagen–Poiseuille equation for viscous flow, indicating the inverse relationship between flux and viscosity.

The near zero intercept on the linear regression of flux vs. trans-membrane pressure data (Figure 28) suggests that there was one dominant transport mechanism. With Figure 30 demonstrating linear correlation between flux and viscosity, it suggests that pore–flow model is the dominant transport model at least for the 4 solvents involved. This means that these solvents transported through the membrane largely via a single mechanism and that any structural changes in the membrane layers had a negligible effect on flux levels.[84] Indeed, many studies in OSN have shown similar, single mechanism model of solvent permeation, notably in polydimethylsiloxane (PDMS) membranes,[83] however, to the author's knowledge, this is the first time that such result has been reported in solvent permeation in a regenerated cellulose membrane.

This single transport model, however, is only valid for similar liquids. In this case it is the polar solvent class with low interaction with cellulose. It is well known that certain solvents interact highly with certain polymer; causing the polymer to swell. It is then relevant to identify cellulose swelling solvents and the solvent parameters that govern this interaction. Due to the complex nature of the interaction and different types of cellulose, multiple parameters are likely to be involved. Fidale *et al*. studied cellulose swelling in numerous solvents, and their findings are that microcrystalline cellulose swelling correlates with the following solvent parameters (in order of importance): [48,107]

- for aprotic solvents: molar volume, basicity (β) and polarity/polarisability (π*)
- for protic solvents: acidity (*p*Ka or α), β, π* and molar volume

where α, β and π* are the solvent's solvatochromic parameters.[110 111]

The extent of cellulose swelling was low for MeCN, EtOAc and THF, and slightly higher for MeOH (see Table 16 and its notes) which indicated that the interactions of those solvents with cellulose were low. This could support the case for a single transport mechanism for these solvents and explained the linear correlation of their fluxes with their viscosities (Figure 30).

As the results in Figure 29 show, toluene and hexane permeance values did not correlate with the viscosity trend to the degree of the other 4 solvents (MeCN, THF, MeOH, EtOAc) did. This could be explained by the fact that toluene and hexane are quite different from the other 4 solvents,

particularly in terms of the two being hydrophobic solvents, as indicated by their log Kow values in Table 16.

It is interesting to point out the flux values for **hexane**. Hexane has the lowest viscosity amongst the six solvents and the only one with viscosity lower than MeCN. Despite the hydrophobic effect of **hexane**, which should be acting to lower its flux on the hydrophilic cellulose membrane, the (low) viscosity effect appeared to be powerful enough to overcome this by yielding a higher flux compared to those of more viscous but hydrophilic solvents such as EtOAc, THF, and MeOH (Figure 29).

The two most swelling solvents amongst the 36 solvents tested by Fidale *et al.*, are water (nSw=4.82) and DMSO (nSw=1.98),[48][107] and the permeance of these two solvents are compared with other non or less swelling solvents in Figure 31.
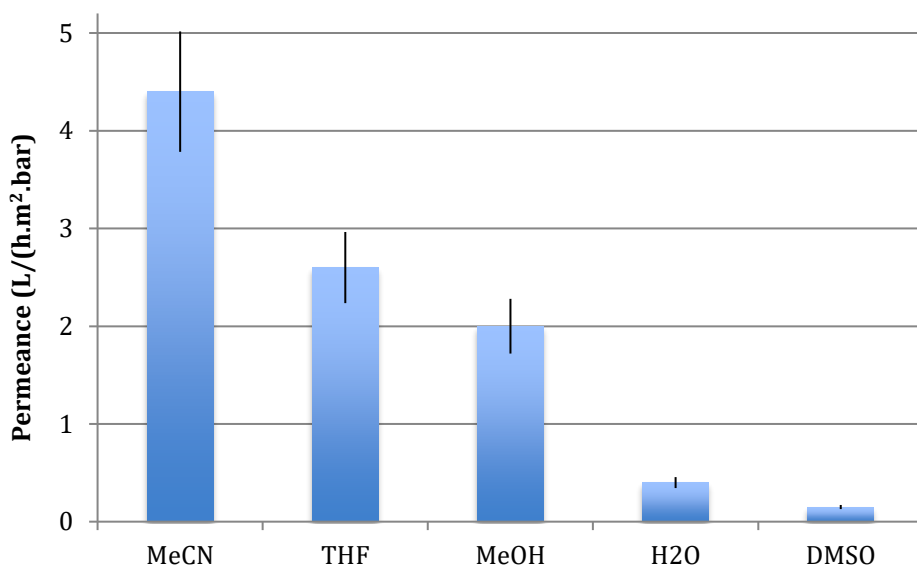
Figure 31. Solvent permeance values of membrane 6X.

Tests done in duplicates from membranes of the same batch.

The effect of solvent-induced swelling on polymeric NF/RO membranes is generally understood (and observed) to cause an increase in flux, with some workers ascribed this due to pore dilation,[77] [103] whilst others attributed it to the increase in the diffusion coefficient due to increased mobility of the swollen polymer chains.[112] [113] While the flux values of water and DMSO were much lower compared to those of non/less swelling solvents in our case (Figure 31), this does not necessarily suggest an exception, considering the viscosity effect (both water and DMSO's viscosities are

higher than the other 3 solvents). Figure 32 plots the same permeance data from Figure 31 against viscosity of the solvents in order to examine the effect of viscosity (especially that of water and DMSO) on flux. The rate of permeance decrease of the first 3 solvents (MeCN, THF and MeOH) as their viscosities increase is roughly constant, a linearity seen earlier, but then the rate of decrease slows down in the case of water and DMSO, suggesting that the flux values of high swelling solvents might indeed be higher than low swelling ones, provided that their viscosities are equal.
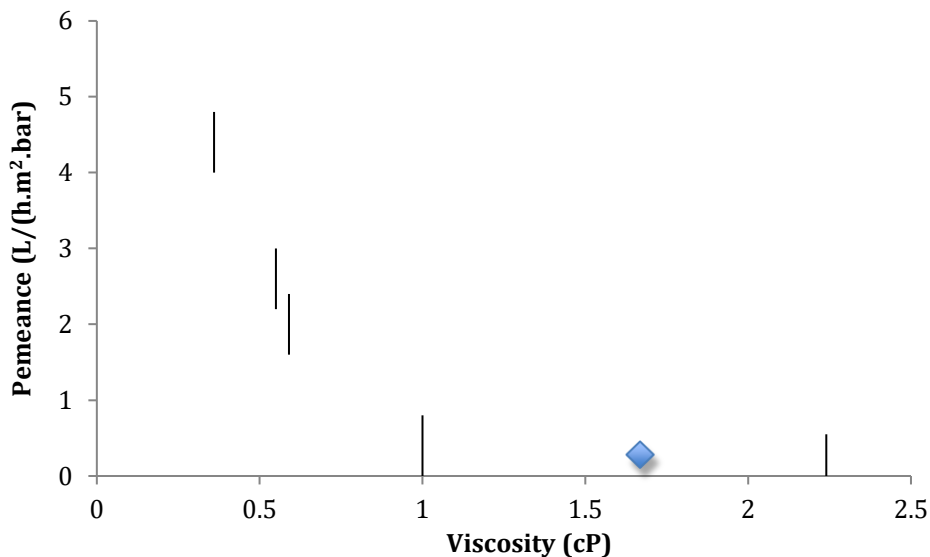
Figure 32. Viscosity vs. permeance of 5 solvents from membrane 6X.
From L-R: MeCN, THF, MeOH, water, DMSO.
Tests done in duplicates from membranes of the same batch.

As flux is a very important characteristic in OSN, comparison of solvent permeance values of cellulose membranes is reported in the table below, alongside two commercial OSN membranes.

Table 17. Comparison of solvent permeance values (in $L.h^{-1}.m^{-2}.bar^{-1}$) between cellulose membranes and two commercial OSN membranes

Solvent	Cellulose membranes*	PuraMem 280 (Evonik)	DuraMem 200 T1 (Evonik)
MeCN	3.2 (0.9)	4.9	2.9
THF	2.5 (0.8)	NC	NT
MeOH	1.5 (0.7)	4.3	1.0
Toluene	0.7 (0.3)	1.9	NT

* Average permeance values from 4 cellulose membranes (membrane IDs: 25, 27-1, 27-2, 32)
NC: Not compatible ; NT: Not tested

Solvent permeance comparison to two prominent commercial OSN membranes (Table 17), shows that cellulose membranes generally have comparable flux performances, but with an advantage of wider solvent resistance, especially to aggressive dipolar aprotic solvents such as THF.

5.2.2 Rejection of Rose Bengal, Methylene Blue and Ethyl Violet

Three dye compounds, as outlined in Table 18, were used in this project. Rose Bengal (RB) is commonly used as a rejection test molecule in NF/UF membranes due to its MW (in the upper range of NF threshold), its excellent solubility in water and many organic solvents, and its facile concentration determination by UV-Vis detection, the latter is true for using dyes in general.[114] [76] [115] The disodium salt form is the one that is most commonly used, hence it is an anionic dye. Methylene blue (MB) was chosen as a second test molecule, representing cationic dye class. MB is also a quite commonly used test molecule in NF due its good solubility in water and other polar solvents.[116] Ethyl violet (EV) was chosen as a third test molecule due its solubility in the organic solvents intended for use in these tests.

Table 18. Dye compounds used for rejection studies
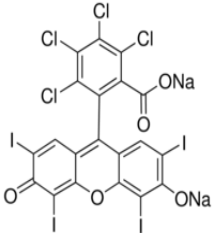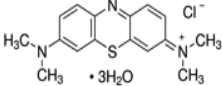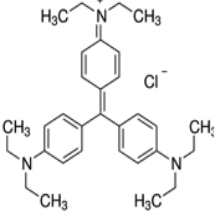
	Rose Bengal (RB)	Methylene blue (MB)	Ethyl violet (EV)
MW (g/mol)	1018	320	492
Structure			
Type	Anionic	Cationic	Cationic
Tested in	DMSO, THF, MeCN, MeOH,	MeCN, MeOH	MeCN, MeOH

Table 19. Dye compounds rejection values of cellulose membranes
in acetonitrile (MeCN) and methanol (MeOH)

	Rose Bengal (RB)	Methylene blue (MB)	Ethyl violet (EV)
	Rose Bengal	Methylene blue	Ethyl violet
Rejection in MeCN	>95%	>95%	>95%
Rejection in THF	>95%	N/A	N/A
Rejection in MeOH	<10%	<10%	<10%
Rejection in DMSO	Low*	N/A	N/A

All rejection values (except *) were obtained from membranes 64, 76, 79, 80, 81, 6, 27-2, 32 and 32 crosslinked, in duplicates. * RB permeation test in DMSO was performed on a cellulose membrane that was prepared in the early stage of the project. The rejection was 21%, but since the membrane is not considered comparable with the later variant used in subsequent rejection tests, 'Low' label was chosen to represent the value. Images are from Wikimedia Common license.

The summary of rejection results from the 3 dyes is outlined in Table 19. Rejection of RB in MeCN and THF is very high, whilst the same compound demonstrated low rejection in MeOH and, most likely, in DMSO, too. As mentioned briefly in the footnote of Table 19, an RB rejection test in DMSO was performed early in the project with a preliminary variant of cellulose membrane that was not considered comparable with the later variants. This 'early' variant membrane that was used for RB in DMSO rejection test was cast using a pour-casting method onto a petri dish with a

much higher membrane thickness -about 2.5x thicker- compared to the membranes used in the other 3 solvents (MeCN, THF, MeOH). Therefore, the 21% RB rejection that was obtained in DMSO is not comparable to that of the other solvents. It is reasonable to assert that the RB rejection in DMSO would have been considerably lower than 21% had it been done on the same, much thinner membrane.

As discussed earlier, MeCN and THF are low-swelling cellulose solvents (low interaction) whereas MeOH is mildly interacting and DMSO is highly interacting. Therefore, the variable rejection of RB in different solvents can be explained by the extent of solvent-membrane interaction: in low interacting solvents, the solvent's affinity towards the membrane polymer is low, hence the solute molecules are the preferentially adhere to the sorption sites in polymer chains, yielding high rejection, whereas when there's a considerable solvent-polymer affinity, the solvent molecules compete with the solutes' to interact with the polymer chains, resulting in low rejection of the solute.

Considering that these cellulose membranes tend to have a negative charge (membrane properties will be discussed in Chapter 6), electrostatic repulsion, i.e. Donnan exclusion effect, could be attributed to the very high RB rejection (in low interacting solvents), as the dye is negatively charged. However, the fact that RB is heavily sorbed by the membrane, based on physical observation of the membrane post-permeation (intense red colour) and the fact that the permeate is RB-free (complete RB rejection), suggested that solute-membrane adsorptive interaction was probably the dominant rejection mechanism.

The fraction of dye adsorbed onto the membrane can be estimated by performing RB mass balance of the system, i.e. mass of RB in the feed subtracted by mass in permeate & retentate,. For RB in MeCN, a typical value for the fraction adsorbed was 0.4 - 0.5 of the total dye mass in feed.

To confirm and examine the RB adsorptive rejection mechanism, an extended RB permeation/rejection test was performed (Figure 33 and Figure 34).
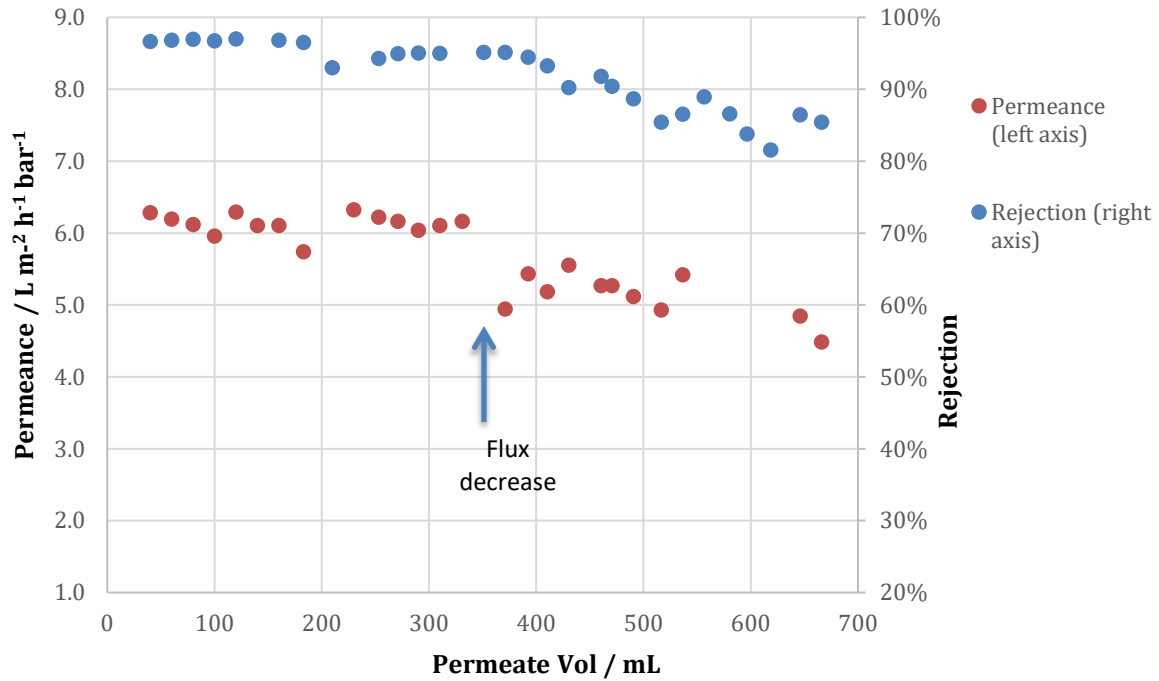
Figure 33. Extended RB permeation/rejection test on membrane 27-2

A breakthrough point (a point where RB concentration in permeate stream starts to increase steadily) is identified at around 350 mL permeate volume (Figure 34). This is accompanied by the onset of steady flux decrease from the initial constant flux profile (Figure 33).
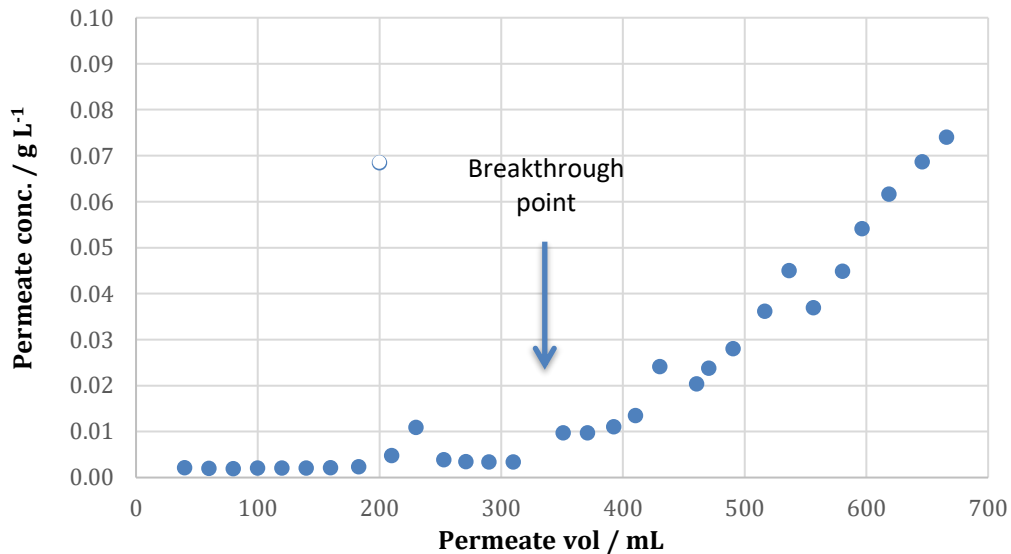
Figure 34. Extended RB permeation test, showing RB concentration profile in permeate stream, tested on membrane 27-2.

These behaviours reinforce the assertion that the RB rejection mechanism in this case is by adsorption to the membrane surface, as opposed to size exclusion (physical sieving) or Donnan exclusion mechanisms. In sorption mechanism, a breakthrough point occurs when all the sorption sites on the membrane surface area are fully occupied, thus subsequent solute molecules flow through the membrane, 'breaking through' to the permeate side. Adherence of solute molecules to these 'sites' causes the membrane to eventually foul, reducing the trans-membrane flow, as seen in Figure 33. Another tell-tale of this adsorption saturation event is the fact that the fraction of RB adsorbed onto the membrane drops off after a breakthrough point has been reached, as shown in Figure 35.
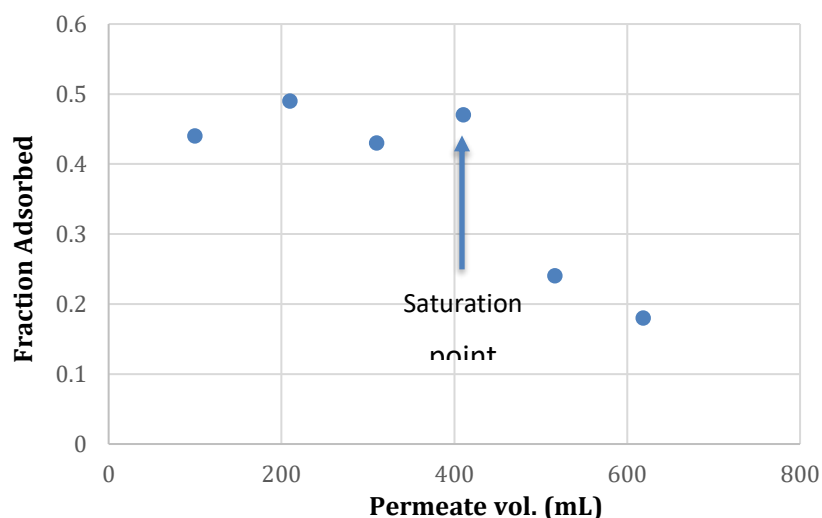
Figure 35. Fraction of RB adsorbed to the membrane (g of RB adsorbed/g of RB in feed), as calculated by mass balance around the membrane, in the extended RB permeation test on membrane 27-2.

The contrasting rejection values of both methylene blue (MB) and ethyl violet (EV) in MeCN (high rejection) and MeOH (low rejection) can be explained using the same rationale. Despite the difference in the ionic nature of RB (anionic) and MB & EV (cationic), all three compounds were similarly very highly rejected (>95%) in MeCN tests. An intense blue colour (or violet for EV) of the membrane after permeation test indicated that MB and EV were readily sorbed to the cellulose membrane. This pointed out, as in the case with RB, that MB and EV rejections were predominantly due to solute-membrane adsorptive interaction. It was also found that by permeating MeOH on the used membrane test pieces post dye rejection tests, desorption of these 3 dyes were able to be carried out quite effectively. After the extended RB permeation test, RB

desorption by MeOH (by simply permeating MeOH through the test piece in the dead end cell) achieved >90% recovery, as confirmed by visual inspection as well (near absence of red tinge on the test piece). The same phenomenon was also observed when desorbing MB and EV with MeOH, which seemed to suggest that facile cleaning of cellulose membrane from adsorbed polar compounds can be achieved simply by MeOH wash or possibly by other solvents that have moderate or high interaction with cellulose.

The high adsorptive interaction between RB/MB/EV and cellulose could be due to the hydrogen bonding between the molecule and cellulose polymer chain. In their work of measuring the rejection of various polar compounds by porous cellulose acetate (CA) membranes in aqueous environment, Matsuura and Sourirajan theorised that polar compounds can sorb onto CA via hydrogen bonding.[117]

5.2.3   Permeation Studies on Swollen of Cellulose Membrane

One of the desired properties of any membrane separation system is robustness, and this includes tolerance when operating conditions drift outside optimum levels, for e.g., increased water content of a feed stream in an OSN separation unit. Cellulose membrane is found to swell heavily in water, which can be a major downside, as it would affect the flux and separation performances of the system. This section examines the extent of water swelling in cellulose membrane and the consequence on flux, flux recovery and polystyrene 1300 Da (PS 1300) rejection.

The initial THF permeance prior to the test was 4.1 $L.h^{-1}.m^2.bar^{-1}$ and permeance values of wet THF feeds of 2.8% and 6.9% v/v water content were 3.5 and 2.0 $L.h^{-1}.m^2.bar^{-1}$, respectively, tested on membrane 80X where X denotes crosslinked membrane. This means a reduction of permeance value of 15% and 51%, respectively (Figure 36). On the wettest THF test (23% v/v water content), the permeance was 0.55 $L.h^{-1}.m^2.bar^{-1}$, which translates to a drop of 87% over the original, neat THF permeance.

Rejection of PS 1300 was quite low in neat THF, i.e. 13%, but increased to 30% after the membrane was exposed to wet THF containing 12% water. Subsequent exposure to higher water content did not seem to significantly change the rejection of PS (Figure 36).
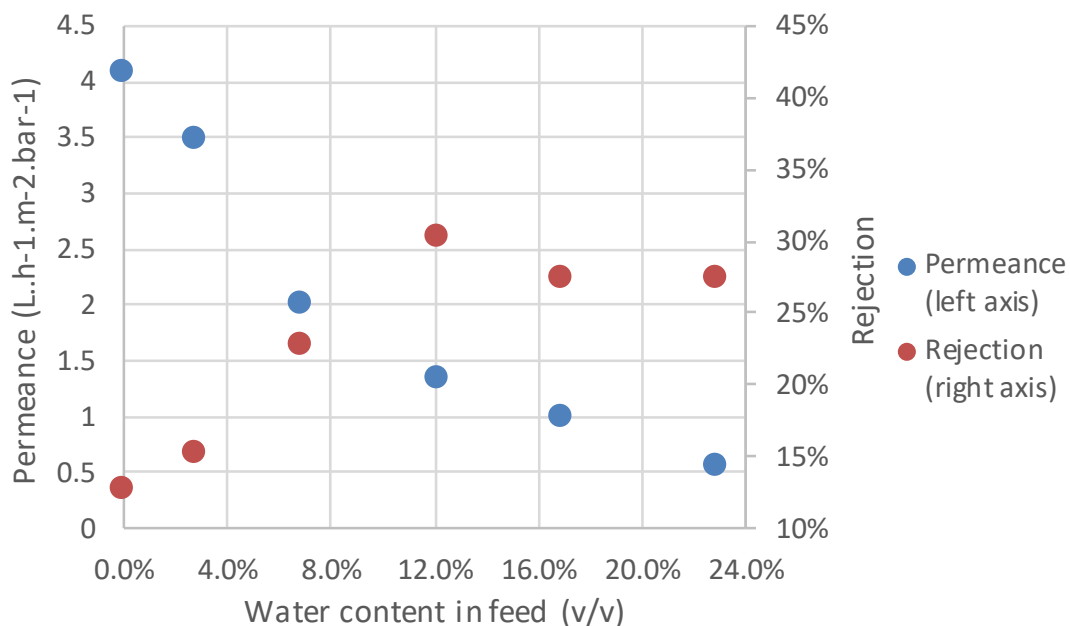
Figure 36. Six series of THF permeation (with increasing H_2O content) & PS 1300 rejection tests on membrane 80X. The PS 1300 rejection tests were performed in neat THF solution.

Many NF literatures reported a decrease in solute rejection in swollen membrane, primarily attributed due to pore enlargement,[77][103][113] although Ebert and Cuperus reported the opposite effect, i.e. narrowing of pores when a porous membrane swells, resulting in higher rejection[101]. The latter phenomenon could explain the fact that in the initial extent of swelling test (i.e. from 0 to 12% of water content in feed), rejection of PS 1300 increases (Figure 36). The rejection seemed to plateau after 12% water content, which could mean that the swelling had reached maximum. The low rejection of PS, compared to dyes with smaller MW, is due to lack of polystyrene-cellulose adsorptive interaction, discussed in more detail in the next section.

Flux recovery test was also performed to investigate whether swollen membrane can recover to its pre-swollen flux. Figure 37 plots the neat THF permeance values of a swollen membrane (wetted by 23:77 water:THF) and the values shows that flux remained low. This suggests that water-induced swelling in cellulose membrane cannot be easily reversed.
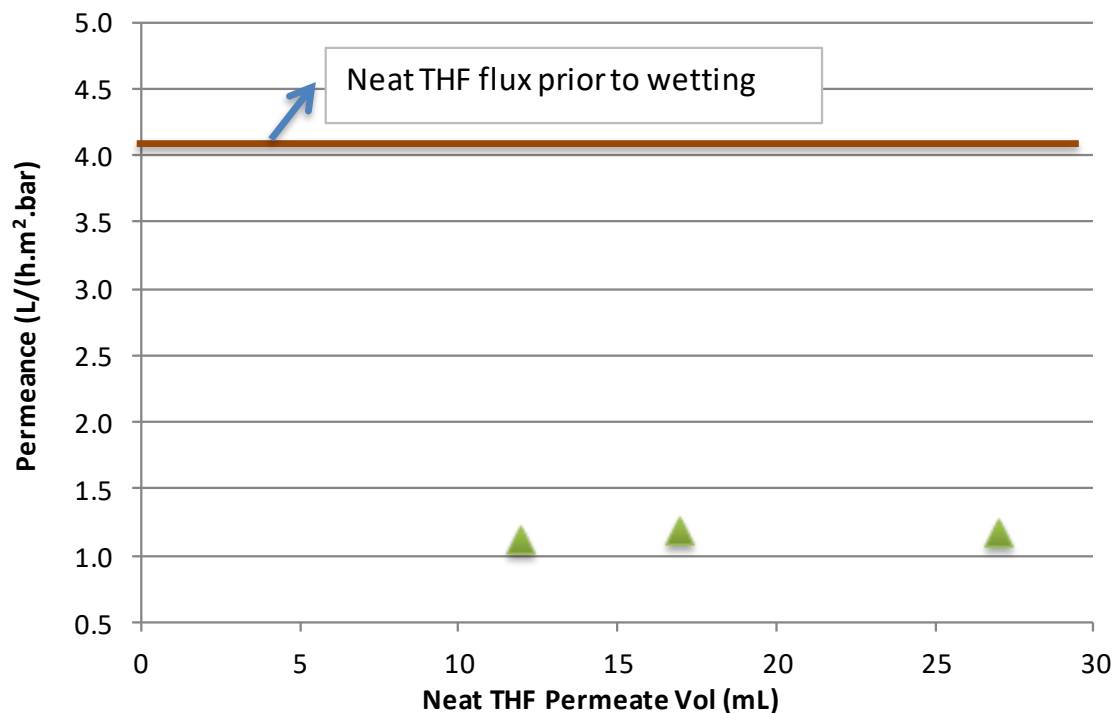
Figure 37. Flux recovery test with neat THF feed after exposure to 'wet' THF (up to 23% v/v water content) on membrane 80X. The red horizontal bar represents the original, neat THF permeance prior to membrane wetting and the green triangles are neat THF permeance values after membrane wetting.

5.2.4 Rejection and Molecular Weight Cut-Off (MWCO) by Polystyrene

Rejection measurement of NF membrane using neutral solute is important for determining membrane MWCO. Only neutral solutes are usually considered in MWCO determination as any charged solutes might influence the separation rate of NF membrane that due to membrane's surface charge. Commonly, these neutral solutes are selected from polymers having the same structural unit (i.e. homologous series). Polystyrene (PS) series were chosen in this project due its excellent solubility in organic solvents and its facile quantitative analysis by UV detection. The MWCO of a membrane is defined as the MW of the component that is rejected by greater than 90%.

Five PS series with the following MW were used for MWCO test: 1350, 2200, 3350, 4000, and 5200 Da. However, not all 5 of the PS series were used every time due to cost and time saving

reasons. Four membranes were tested with these PS solutions and the rejection curves are shown in the figure below.
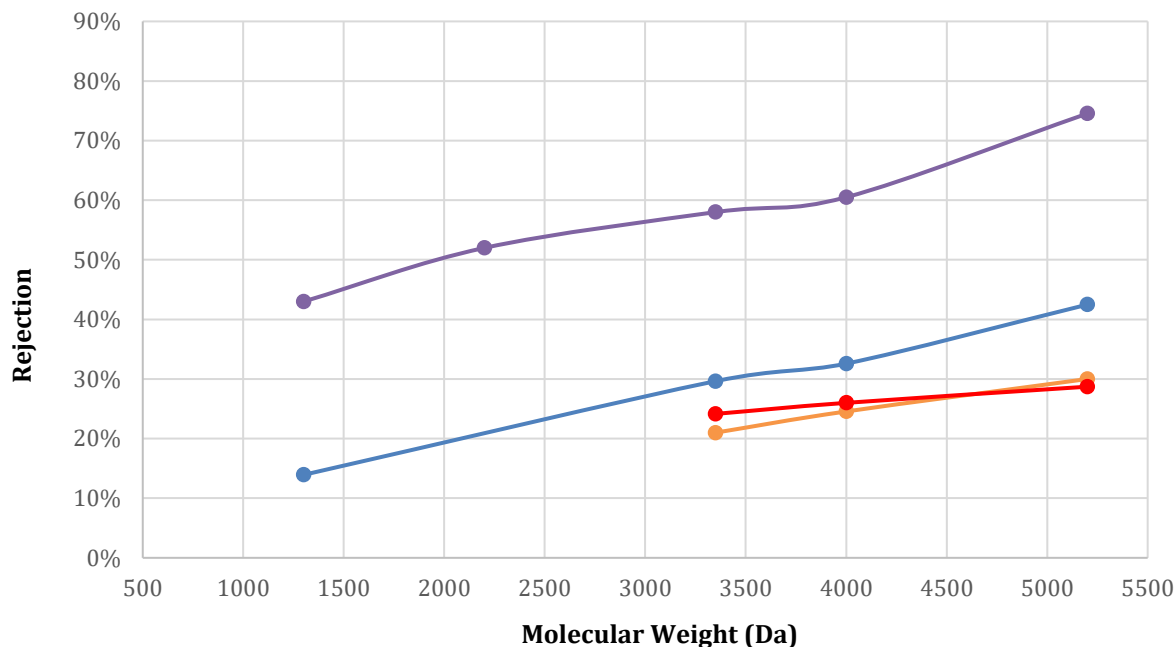
Figure 38. Rejection curves of PS from 4 cellulose membranes.
Membrane IDs: 27-1 (purple) – 27-2 (blue) – 32 (red) – 6 (orange)

As can be seen from the figure above, rejection values of PS oligomers are low, especially if compared with dyes rejection values discussed in the preceding section, even though the PS oligomers used are of much higher MW than those of the dyes. The rejection by adsorption mechanism, as shown in the case of dye rejection, can explain this low rejection. As PS is unable to form any hydrogen bonding with cellulose, the oligomers were not adsorbed but instead permeated through the membrane, causing low rejection.

Amongst the four membranes tested in the above figure, the 'tightest' membrane is membrane 27-1, which, if extrapolated to 90% rejection, would give a MWCO of around 6000 to 6500 Da. This MWCO would put the membrane in the upper range of NF to the lower range of UF spectrum. For discussions on the differences between these membranes, hence the tunability of their MWCO values, please refer to discussions in section 4.2.

5.3   Conclusion

Solvent permeation in cellulose membranes prepared in this project were shown to have negligible membrane compaction effect when tested with low interacting solvents, even at high trans membrane pressure (up to 50 bar). This is seen as an advantage as membrane conditioning would be quicker. The dominant transport mechanism seemed to be pore-flow model, at least for similar liquids with low cellulose interaction. This means that viscosity plays a significant role in determining flux. Two of the most swelling solvents for cellulose, i.e. water and DMSO, were shown to have lower fluxes compared to low/medium interacting solvents such as MeCN, THF and MeOH, however, whether the lower fluxes were caused by membrane swelling or by the fact that these 2 liquids have higher viscosity, requires further investigation. Hydrophobic solvents such as toluene and hexane were found to deviate from the linear correlation between flux and viscosity previously seen in the hydrophilic, low interacting solvents, but not by much. The results suggest that viscosity effect is more significant than hydrophobic/hydrophilic effect with regards to flux performance.

The effect of membrane swelling due to water content on flux was also measured, to simulate a scenario where an OSN process unit were to be contaminated by water. Exposure to wet THF feed (2.8 % v/v water content) resulted in 15% reduction in neat THF flux. This reduction in flux became 87% when the membrane was exposed to THF with 23 % v/v water content. Washing & permeation of the membrane with neat THF was not able to reverse the swelling. Modest increases in PS 1300 rejection with progressively swollen membranes suggest that the swelling caused narrowing of membrane pores, which is consistent with the reduction in flux.

Flux comparison to commercial OSN membranes indicated comparable performances. For example, for MeCN, the average permeance value was 3.9 $L.h^{-1}.m^{-2}.bar^{-1}$ compared to 4.9 $L.h^{-1}.m^{-2}.bar^{-1}$ of PuraMem 280 and 2.9 $L.h^{-1}.m^{-2}.bar^{-1}$ of DuraMem 200.

MWCO of the 4 variants of cellulose membranes tested by PS oligomers all show values of >6500 Da, indicating that these membranes can be considered as 'tight' UF membranes. However, their separation performances for polar compounds are very high, even for small solute with MW as low as 320 Da, provided that the solvent used is a low interacting (non swelling) one. The rejection mechanism was concluded to be solute-membrane adsorptive interaction, possibly by hydrogen bonding of the solute molecules to the hydroxyl groups of cellulose.

Although fouling is a concern especially when the main rejection mechanism is by solute adsorption, facile desorption was proved possible by washing or permeating with a solvent with moderate (or high) affinity towards cellulose, such as MeOH.

These characteristics, coupled with true solvent resistant nature, will likely give cellulose membranes an opportunity to be a very promising membrane portfolio in the world of OSN.

The results and findings gathered during these membrane permeation studies, combined with the results and findings from the characterisation tests in Chapter 6, met the 3rd objective of this thesis as outlined in Section 1.6.

Chapter 6 Crosslinking, Physical Properties and

Characterisation of Cellulose Membranes

6.1   Introduction

Following the development of cellulose membranes in Chapter 4 and permeation and rejection tests of the membranes in Chapter 5, this chapter deals with crosslinking as a modification method of cellulose membranes as well as characterisation techniques carried out and the results they provided.

6.1.1   Crosslinking Cellulose

Chemically modifying cotton fabric to impart durable-press properties (shrinkage resistance, crease recovery) is well-known in the textile world.[10] This is possible due to the presence of a large number of accessible hydroxyl groups along the cellulose back-bone structure. By using an appropriate chemical substance having at least two reactive groups that can react with hydroxyl groups, covalent bonds can be formed between cellulose polymer chains (see Figure 39), a mechanism known as crosslinking. Several chemical substances have been reported as crosslinking agents for cellulose; namely formaldehyde, polycarboxylic acids, epichlorohydrin, epoxides (e.g. 1,2,3,4-diepoxibutane), dichloroethane, or diisocyanate.[1]

Dimethylol-dihydroxyethyleneurea (DMDHEU) is the most widely used formaldehyde-based chemical crosslinking agent. However, cotton fabrics treated with DMDHEU tend to release formaldehyde during the curing process, storage, and consumer use.[119] Due to the fact that formaldehyde is regarded to have carcinogen potential and that many of these alternative crosslinking agents mentioned above are not environmentally friendly and can be toxic,[119] intensive investigations have been undertaken to find to develop crosslinking agents that are more benign, and one such agent is glyoxal (ethanedial).

Glyoxal has been investigated to be an effective durable-press agent.[119] Glyoxal is an almost fully biodegradable and low toxicity chemical (compared to formaldehyde) and can be obtained from

renewable resources by the oxidation of lipids and as a by-product of biological processes.[118] Eichhorn and co-workers demonstrated that bacterial cellulose (BC) networks can be cross-linked via glyoxalization.[118] The fracture surfaces of samples showed that, in the dry state, less delamination occurs for glyoxalised BC networks compared to unmodified BC networks, suggesting that covalent bond coupling between BC layers occurred during the glyoxalisation process. Although their mechanical tests showed that the stress and strain at failure were reduced after glyoxalisation, the wet mechanical properties of the BC networks are improved. They found that the stress-transfer efficiency of deformed dry and wet glyoxalised BC networks was significantly increased compared to unmodified material, and was attributed to the covalent coupling induced during crosslinking.[118]
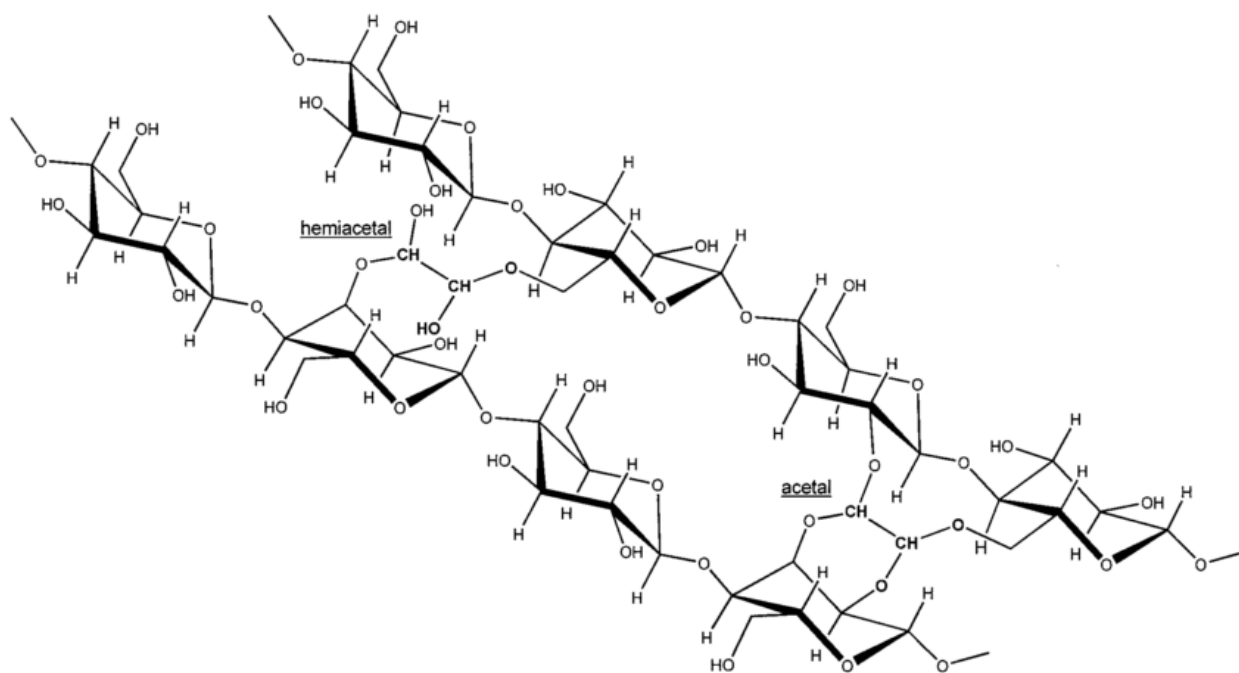
Figure 39. Acetal or hemiacetal linkages formed by reaction of glyoxal with the hydroxyl groups of the cellulose. From Quero *et al*.[118]

Peinemann and co-workers reported a new route of fabricating regenerated cellulose nanofiltration membranes.[71] Their membranes are composite membranes with a thin selective layer of cellulose, which was prepared by regeneration of trimethylsilyl cellulose (a hydrophobic

cellulose derivative) film followed by crosslinking using glutaraldehyde. Filtration experiments using mixtures of sugar and sodium chloride showed that solutes above 300 Da were highly rejected. No comparison studies were performed, however, on the benefit of crosslinking their membranes.[71] Apart from the work from this group, there seems to be no other reports on crosslinking cellulose-based membranes in the literature at the time when work in this chapter started.

6.1.2 Hornification of Cellulose

The term hornification is a technical term originated in wood pulp and paper research literature that refers to the stiffening of the polymer structure that takes place in lignocellulosic materials upon drying or water removal.[120] When wood pulp fibres are dried, the internal fibre volume shrinks and this shrinkage is irreversible, because of structural changes in wood pulp fibres[120],
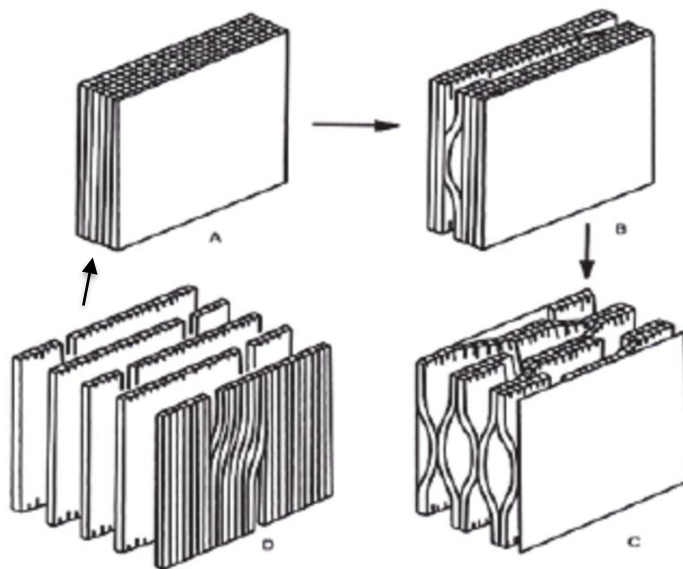
Figure 40. Diagram depicting collapse of internal structure in lignocellulosic fibre due to hornification. D: Wet virgin fibre → A: Dry fibre → B: Re-wetting process → C: Wet hornified fibre. From Östlund *et al*.
[121]

Hornification of cellulose fibres has been attributed to the irreversible change of cell wall structure due to the collapse of pores[122] Ostlund and co-worker reported that regenerated cellulose shows

a similar behaviour as native cellulose when subjected to drying.[121] In cellulose membrane separation applications, hornification refers to collapse in the pore structures of the membrane due to drying, which usually renders irreversible change in the membrane's properties.

6.2 Results and Discussion

6.2.1 Crosslinking of Cellulose Membrane

As initial tests on dried crosslinked cellulose membranes showed non-zero flux values (compared with the negligible flux on dried non-crosslinked cellulose membranes, refer to Chapter 5 Membrane Permeation Studies), development of crosslinked cellulose membranes was initiated with an investigation to find the optimum crosslinking reaction conditions. Optimum in this context is defined as reaction conditions that will offer the highest degree of crosslinking.

Crosslinking Optimisation Study

Optimisation study of crosslinking by glyoxal was performed, investigating three variables:

- Glyoxal solution concentration (10% and 20% v/v)
- Reaction temperature (75 and 105 °C)
- Reaction time (1, 2 and 3 hours)

Measuring degree of crosslinking accurately is problematic due to the inability to differentiate intra- and inter-chain linkage during crosslinking process. However, a quantification method of the portion of glyoxal that has reacted with cellulose is still useful as an indication of how much intra- or inter-chain links had formed. For the purpose of quantification, in this thesis this measure is termed 'apparent degree of crosslinking'. To this end, an analysis method developed by Schramm and Rinderer[119] was employed. Bound glyoxal was released from the crosslinked test piece using sodium hydroxide solution, and at the same time, glyoxal was converted into the sodium salt of glycolic acid (hydroxyacetic acid). Subsequently, the glycolate thus formed was measured by means of HPLC. The degree of crosslinking in this report was then defined as mol of glycolic acid per mol of anhydroglucose unit (AGU). The mole of AGU was calculated from the dry weight of the test piece. The results from this optimisation study are outlined in Table 20. From the results, the optimum crosslinking reaction condition was 20% glyoxal concentration, 105 °C

and 1 hour reaction time. These conditions were then adopted as the default condition preparation of crosslinked cellulose membranes in this work.

Table 20. Results from crosslinking optimisation study,

by order of apparent decreasing degree of crosslinking

Run No.	Glyoxal conc. (%)	T (^{o}C)	Time (h)	Apparent Degree of Crosslinking*	Error (+/-)
5	20	105	1	0.99	0.03
4	20	75	2	0.74	0.04
6	20	105	2	0.73	0.04
8	20	105	3	0.73	0.04
7	10	105	2	0.60	0.04
2	10	75	2	0.60	0.04
9	10	105	3	0.51	0.03
3	10	75	1	0.45	0.04
1	20	75	1	0.33	0.04

*Apparent Degree of crosslinking = mol of glycolic acid per mol of anhydro-glucose unit

One interesting trend can be observed from the results of this crosslinking optimisation study: that at 105 ^{o}C, increase in crosslinking reaction time resulted in a reduction of the apparent degree of crosslinking (run numbers 5 vs 6). This result seemed to suggest that at 105 ^{o}C, exposure over 1 hour duration caused thermal degradation of the acetal or hemiacetal linkages formed by reaction of glyoxal. Increasing reaction time at 75 ^{o}C from 1h to 3h did result in increased in apparent degree of crosslinking (run numbers 4, 8, and 1) which suggested that 75 ^{o}C was well within the thermal degradation limit.

Crosslinking to Minimise the Hornification Effect of Cellulose

As outlined earlier, hornification of cellulose upon drying poses problems, and especially so in development of cellulose membranes. Flux values of untreated cellulose membranes which were subjected to overnight ambient drying, were found to be practically zero (no flow after 2 hours under 40 bar of transmembrane pressure). Glycerol treatment proved effective to overcome this problem (see Chapter 4), but this adds another layer of complexity in the membrane preparation procedure.

Results from flux tests of crosslinked cellulose membranes showed that crosslinked membranes seemed to resist hornification upon drying, Figure 41.
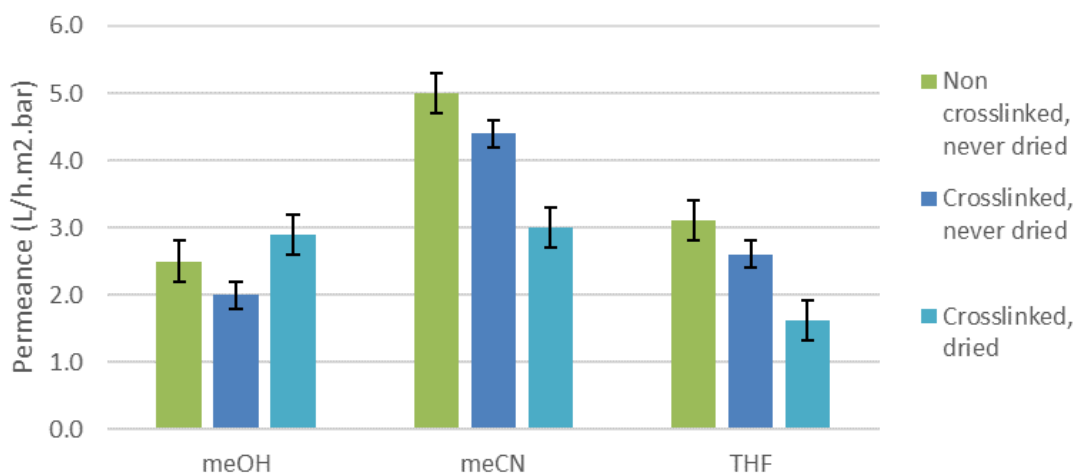
Figure 41. Permeance values comparison of non-crosslinked and crosslinked membrane.

(Membrane ID: 6; drying procedure: overnight at 20 ^{o}C and ~40% RH).

Tests done in duplicates from membranes of the same batch.

Permeance values of dried crosslinked membrane were lower in 2 out 3 solvents tested, although in both of these cases (MeCN and THF), the permeance values were above 1.5 L.h^{-1}. m^{-2}.bar^{-1}, indicating that much of internal porosity was still retained. Dry non-crosslinked membrane without glycerol treatment failed to show any permeation in 2 hours at 40 bar of transmembrane pressure, indicating that the structural changes due to hornification rendered the membrane impermeable.

As discussed in section 5.1.2, it is generally accepted from polymer/biopolymer field of knowledge that cellulosic hornification can be described as an increase in the degree of crosslinking within the fibre microstructure. The exact mechanism is yet to be ascertained, with some authors believe this crosslinking as an irreversible or partially irreversible connection of interfibril hydrogen bonding, whilst others view this as lactone bridge formation in lignocellulosic materials.[120] It can be concluded that cellulose crosslinking through acetal or hemiacetal linkages formed by reaction of glyoxal did not result in nearly as much reduction in internal porosity as crosslinking due to hornification. Crosslinking by glyoxalisation can therefore be considered as a feasible treatment to provide protection against hornification of cellulose membranes.

Crosslinking to Make 'Tighter' Membrane

Studies of polystyrene (PS) rejection showed that crosslinked cellulose membranes yielded lower molecular weight cut-off (MWCO) than their non-crosslinked versions.

Membrane 27-1 was shown to have a MWCO of ca. 6300 Da (extrapolated) whilst MWCO of its crosslinked version, 27-1X, was 5200 Da (Figure 4). Similar 'tigthening' effect from crosslinking was also seen from membrane 32 with 29% rejection of PS 5200, compared that to 59% from its crosslinked version, Figure 42.
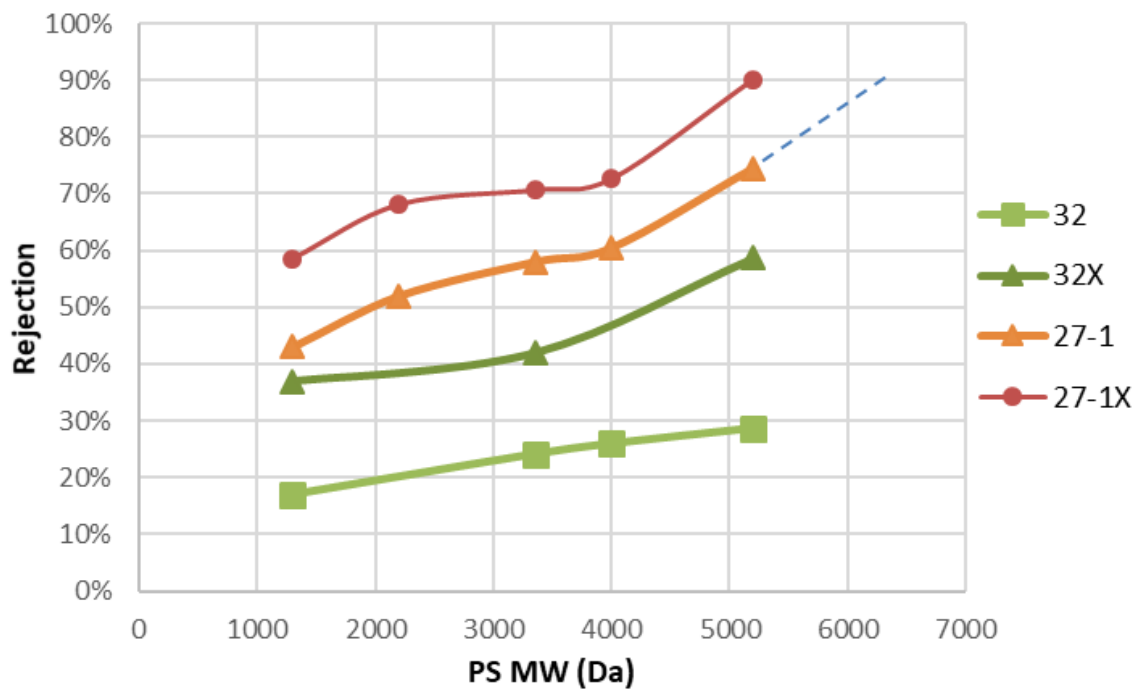
Figure 42. Rejection of PS of two crosslinked cellulose membranes and their non-crosslinked versions (membrane ID ending with 'X' denotes crosslinked version)

Permeance values of the aforementioned non-crosslinked and crosslinked membrane pairs also showed a slight decrease in flux when the membranes were crosslinked (Figure **43**), consistent with the increase in PS rejections. These results suggest that interfibril linkage bonds formed during crosslinking caused reduction in internal porosity of crosslinked cellulose membranes causing them to be 'tighter' than their non-crosslinked versions.
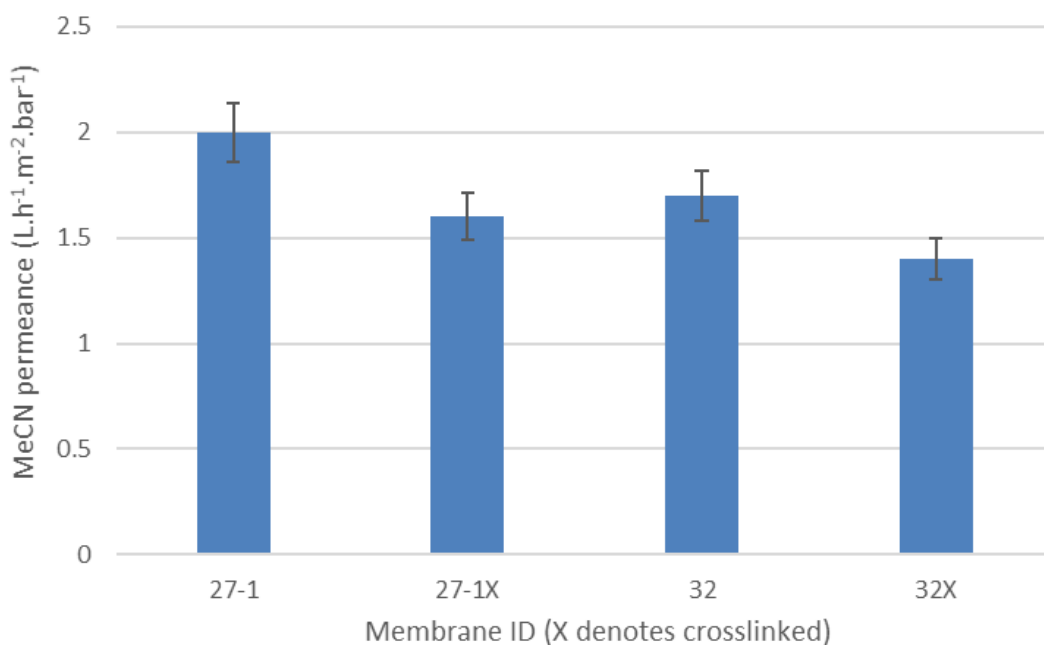
Figure 43. Acetonitrile permeance values of non-crosslinked membranes and their crosslinked versions. Tests done in duplicates from membranes of the same batch.

6.2.2 Physical Properties & Characterisation of Cellulose Membranes

Surface Zeta Potential Measurements

Membrane surface characterisation is important for the development of new membranes. Surface zeta potential measurements can help to correlate surface charge with membrane performance and to understand and control membrane fouling.

Surface zeta potential (SZP) values of cellulose membranes were measured, including Whatman 42 filter paper, which was used as the backing layer for these membranes. These results are presented in Figure 44.

Whatman 42 filter paper yielded the most negative SZP, -42 mV, whilst non-crosslinked cellulose membranes (membranes 27-1 and 32) yielded SZP values between -21 and -4 mV, respectively. This is consistent with a report from Navard and co-workers when they reported SZP values of between -7 to -10 mV for regenerated cellulose fibres made from cellulose-[EMIm][OAc]

solution.[123] It is noteworthy that crosslinking could change SZP to a more positive value. By crosslinking membrane 27-1, its SZP increased from -21 to +6 mV although in membrane 32, crosslinking did not change the SZP significantly (from -4 to -2 mV, a change that was still within the error range).
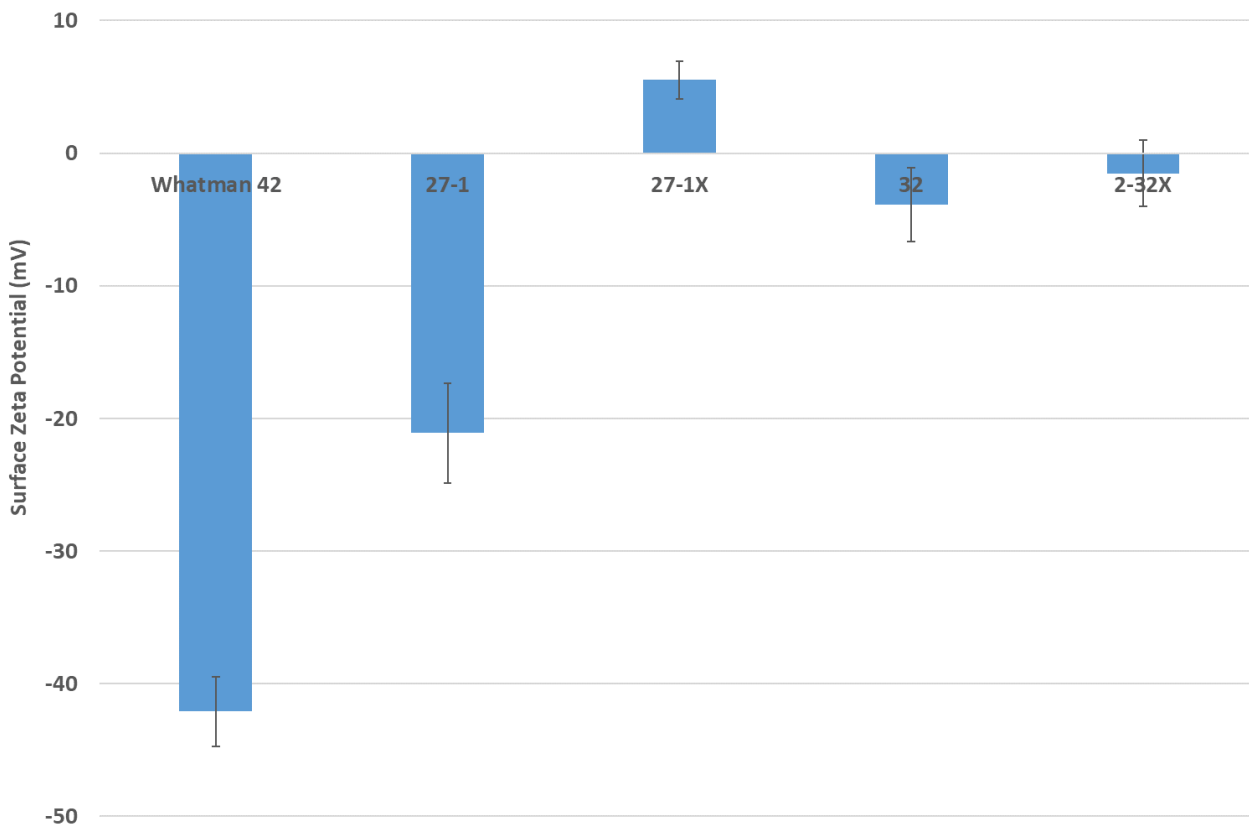
Figure 44. Surface Zeta Potential Measurements ('X' at the end membrane ID denotes crosslinked version). Tests done in duplicates from membranes of the same batch.

These SZP measurements also showed that membrane 32 yielded a considerably less negative surface charge than membrane 27-1 (-4 and -21 mV, respectively). As outlined in Table 1 in Chapter 4, the difference between membranes 27-1 and 32 was in the composition of the casting solution, membrane 27-1 was cast using 31:69 [EMIm][OAc]:1-methylimidazole (mol/mol) solvent system, whilst the solvent system for membrane 32 was 57:43 [EMIm][OAc]:γ-butyrolactone.

Despite the differences in surface zeta potential values, these were not found to impact the membranes' rejection performance. This seemed to confirm the conclusion from the dye

rejection tests, where the principal solute rejection mechanism was determined to be by surface adsorption mechanism (see Section 5.2.2). However, the results seemed to suggest that by using different co-solvent in the organic electrolyte solution (OES), one could manipulate the surface charge of the cellulose membrane to a limited extent. This could be useful when surface charge effect is desired (i.e. Donnan exclusion).

Captive Bubble Contact Angle Measurements

Water contact angle measurement (i.e. sessile method) in cellulose membrane is problematic because untreated cellulose membrane taken from volatile non-solvent bath experiences hornification upon drying very quickly, rendering the surface property different than that of the active layer of a functional cellulose membrane. Glycerol treatment solves the drying out problem, but the presence of glycerol on the surface will affect the water contact angle measurement. Additional problems such as the capillary force due to porosity of the membrane and variation of contact angle with respect of time can further complicate this technique.

Captive bubble contact angle technique, Figure 45, with the cellulose membrane immersed under water was therefore employed to characterise the hydrophilicity/hydrophobicity of the surface. The smaller the angle θ, the more hydrophilic (less hydrophobic) the surface is, and vice versa.
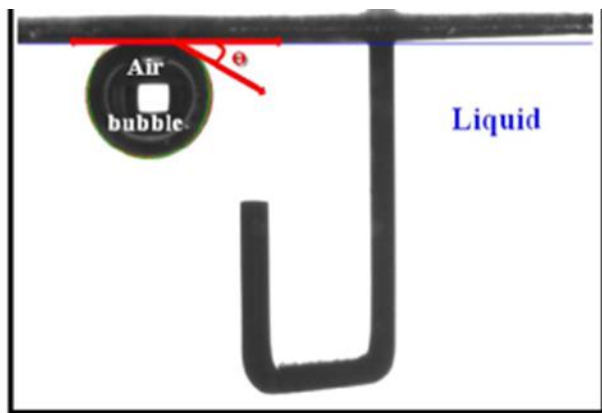
Figure 45. Captive Bubble Contact Angle

116

Captive bubble contact angle (CBCA) measurements (Figure 46) showed that membrane 32 showed smaller CBCA than membrane 27-1 (57° and 91°, respectively), which suggests that hydrophilicity/hydrophobicity of cellulose membrane could be tuned, to some extent, by employing different co-solvent in the casting solution. Membrane 27-1 was cast using 31:69 [EMIm][OAc]:1-methylimidazole (mol/mol) solvent system, whilst the solvent system for membrane 32 was 57:43 [EMIm][OAc]:γ-butyrolactone.

CBCA measurements also showed that crosslinking seemed to have an effect of making the membrane surface more hydrophilic, as indicated by the change in CBCA in membrane 27-1 to its crosslinked version, 27-1X (from 91° to 34°) and membrane 32 to its crosslinked version, 32X (from 57° to 50°). To investigate the effect from this change in surface energy to solvent permeation, flux tests were conducted with acetonitrile (MeCN), a hydrophilic solvent and with hexane, a hydrophobic solvent, at 22°C and 30 bar transmembrane pressure. The flux values were then expressed in terms of the ratio of that of MeCN to that of hexane, to discount the effect of non-relevant factors such as the differences in thickness or pore sizes between the non-crosslinked & crosslinked test membrane pieces. The CBCA values and MeCN/hexane flux ratios of the two non-crosslinked & crosslinked membrane pairs are presented in Figure 46.
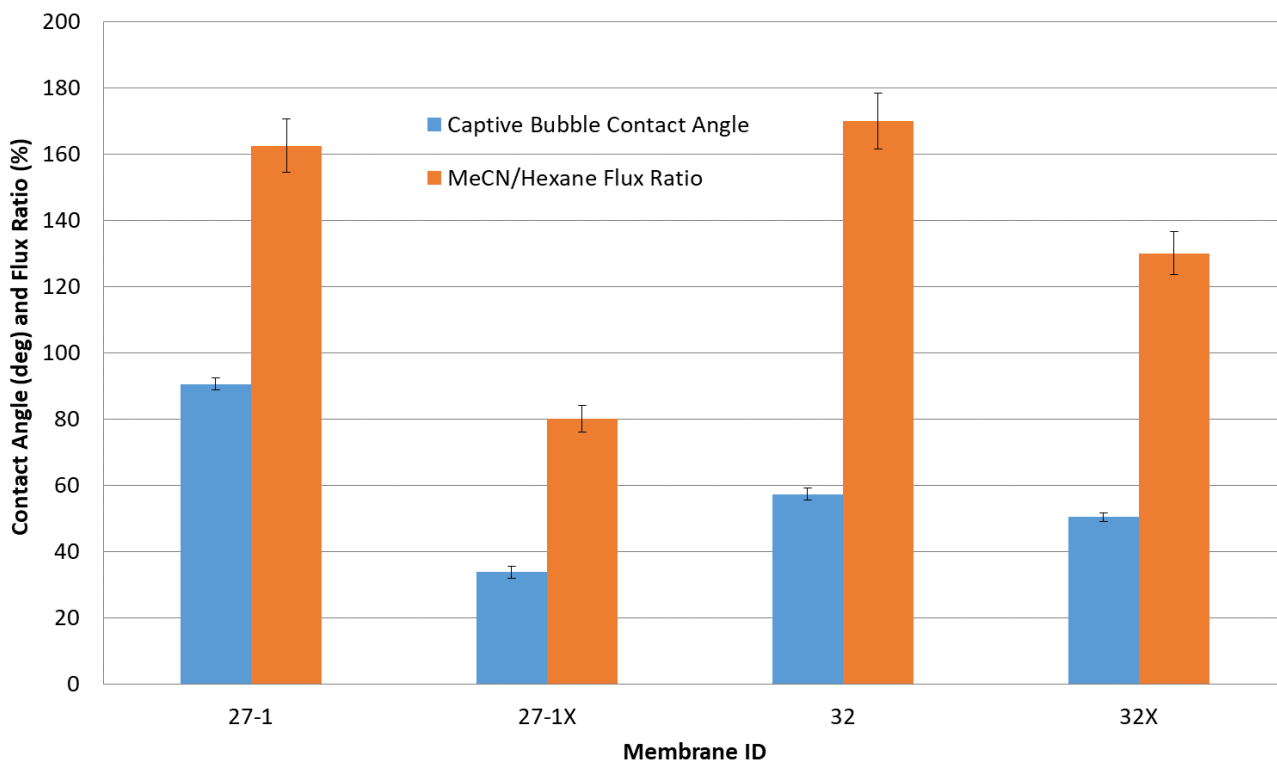
Figure 46. Captive bubble contact angle measurements and ratio of acetonitrile to hexane flux values. Tests done in duplicates from membranes of the same batch.

A trend was revealed that as a membrane surface became more hydrophilic (smaller CBCA), the MeCN/hexane flux ratio decreased. In other words, the results seemed to suggest that as cellulose membrane became more hydrophilic from crosslinking, it seems to favour transport of hexane (a hydrophobic solvent) over that of MeCN (a hydrophilic solvent). This might seem counter intuitive at first, but this can perhaps be **partially** explained by the fact that the dominant transport model in this case is the pore flow model (as discussed in section 5.3.1). In the pore flow model, solvent's viscosity has the greatest influence on the solvent permeability through a membrane. As it was previously shown that crosslinking seemed to produce a 'tighter' membrane (smaller pore sizes), the effect of viscosity on permeability became even more pronounced, and therefore hexane, having lower viscosity than MeCN, became easier to transport. This is, of course, a simplistic explanation, as it does not account for the difference in the chemical nature of MeCN and hexane (polar and non-polar compounds) as well as ignoring the difference in the membrane surface

energies shown by CBCA values. A better explanation would include the solution-diffusion transport model to account for the polymer-solvent interaction, which will require further investigations.

Young's Modulus Measurements

Young's modulus, also known as the elastic modulus, is a measure of the stiffness of a solid material. It defines the relationship between stress and strain in a material. Dynamic mechanical analysis (DMA) was conducted to obtain the Young's moduli on some of membrane samples (i.e. cellulose layer with the Whatman 42 filter paper backing layer) under wet condition, as well as the filter paper itself. Non-crosslinked and crosslinked samples of these were measured and the results are tabulated in Table 21.

Table 21. Young's Moduli from Dynamic Mechanical Analysis (tested under wet condition)

Sample	E* (MPa)	Error (±)
Whatman 42 filter paper	261	65
Whatman 42 filter paper, crosslinked	365	57
Membrane 25 (non-crosslinked)	43	3
Membrane 25X (crosslinked)	66	6

The Young's modulus measurements showed that Whatman 42 (W42) filter paper was considerably higher (stiffer) than that of cellulose polymer, as expected. However, the Young's moduli measurement of the cellulose membrane samples, which had W42 filter paper as the backing layer, yielded values of approximately one order of magnitude less (43 to 66 MPa) than those of the W42 filter paper on its own (261-365 MPa), which meant that the cellulose membrane material (cellulose layer + W42 filter paper) was considerably more elastic than W42 filter paper. This meant that the cellulose layer interacted with the filter paper to form a composite material, yielding a lower Young's moduli than the filter paper's. Two parallel layers of completely non-interacting materials (e.g. rubber on a steel plate) would yield a higher resultant Young's modulus of the stiffer material. In this our case, the resultant Young's moduli of the

cellulose membrane (with W42 filter paper as a backing layer) yielded lower Young's moduli, which suggested that the two layers interacted or that the W42 was modified during the process of membrane-making.

The explanation of the cellulose membrane acted as a composite is probably misleading because of the way the membrane was prepared. Composite material typically has homogenous composition or developed from homogenous mixture such as fibres or filler in a matrix. Our cellulose membranes, even accounting for penetration of the cellulose solution to the filter paper backing layer during the casting process, do not have a structure of a homogenous composite. Based on the SEM pictures in the subsequent section, our cellulose membranes have distinct two-layer structure.

Based on the Young's moduli, crosslinking seemed to make the membrane (and the filter paper) stiffer (less elastic). This is consistent with the report from Eichhorn and co-workers when they reported that wet glyoxalised (crosslinked) bacterial cellulose (BC) showed higher Young's modulus than that of non-crosslinked BC.[118] They also reported wet mechanical properties (e.g. failure stress) of the BC networks are improved by glyoxalisation.[118] This enhancement of mechanical properties is attributed to the interfibril covalent bonds formed by glyoxal crosslinking. Therefore, crosslinked cellulose membranes offer enhanced mechanical properties to produce more robust membranes for demanding applications.

6.2.3   Porometry

Due to hornification of cellulose upon drying, the commonly used nitrogen absorption methods to measure pore sizes (or pore size distribution) were ruled out since these methods require dry samples. Three 'wet' techniques of measuring pore sizes were thus employed: differential scanning calorimetry (DSC) thermoporometry, nuclear magnetic resonance NMR) cryoporometry, and bubble point porometry. The first two are variants of thermoporometry, a calorimetric method that determines pore size based on the melting or crystallization point depression of a liquid confined in a pore. The liquid used in both thermoporometry techniques was water and both techniques involve freezing the liquid and let the temperature rise in a controlled manner and making use of the Gibbs–Thomson effect: small crystals of a liquid in the pores melt at a lower temperature than the bulk liquid and that the melting point depression is inversely proportional

to the pore size. The physical basis for the shift is that the equilibrium temperature for a solid–liquid phase transition is determined by the radius of curvature of the interface between the solid and liquid phases.[37] A liquid held inside a porous material is finely divided; therefore, the radius of curvature is closely related to the pore size.[37]

DSC is suited for precise measurement of the relatively small temperature shifts because of its sensitivity to exothermic freezing and endothermic melting transitions.

Nuclear magnetic resonance (NMR) cryoporometry measures the quantity of water that has melted, as a function of temperature, making use of the fact that the T2 relaxation time in ice is much shorter than that in mobile liquid water.

DSC thermoporometry measurements of membrane ID 6X (crosslinked) indicated that there are two main pore sizes: one group at around 2-3 nm and the other at around 40-50 nm (Figure 47). These results were corroborated by pore sizes distribution profile obtained from NMR cryoporometry measurements (Figure 48).
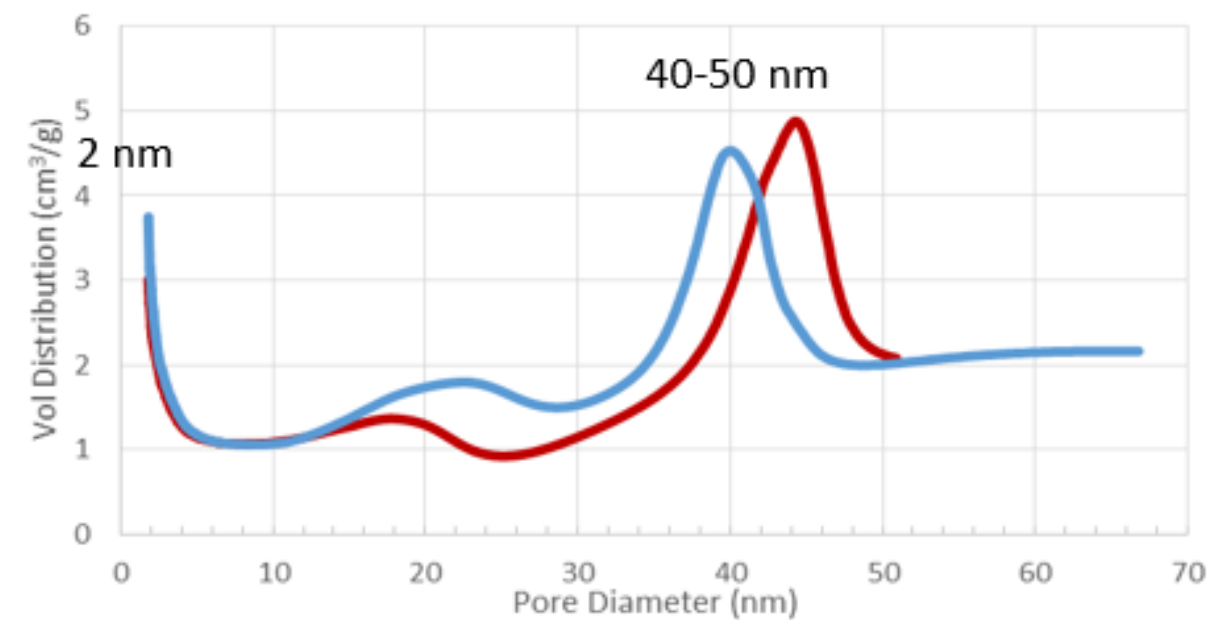
Figure 47. Pore size distribution of membrane 6 (crosslinked) processed from DSC thermoporometry measurements. Blue and red curves indicate two independent runs using two samples of the membrane ID 6X (crosslinked).
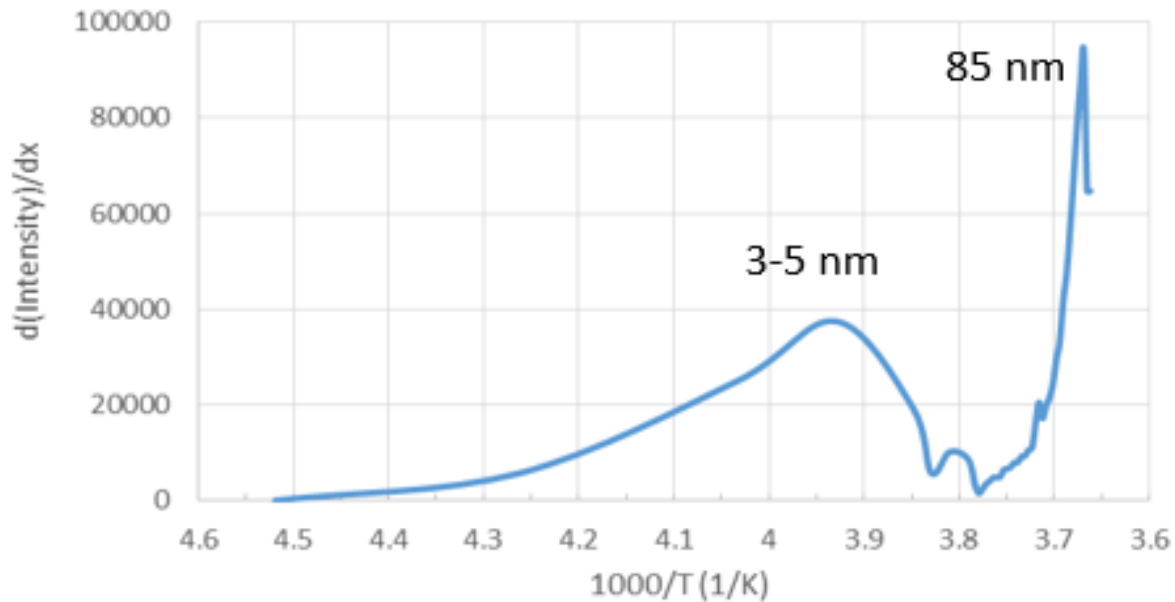
Figure 48. Effective pore size distribution of membrane 6X (crosslinked) processed from NMR cryoporometry measurement. The two peaks observed are converted to the pore sizes (3-4 nm and 85 nm) using correlation table A1 from Petrov *et. al.*[39]
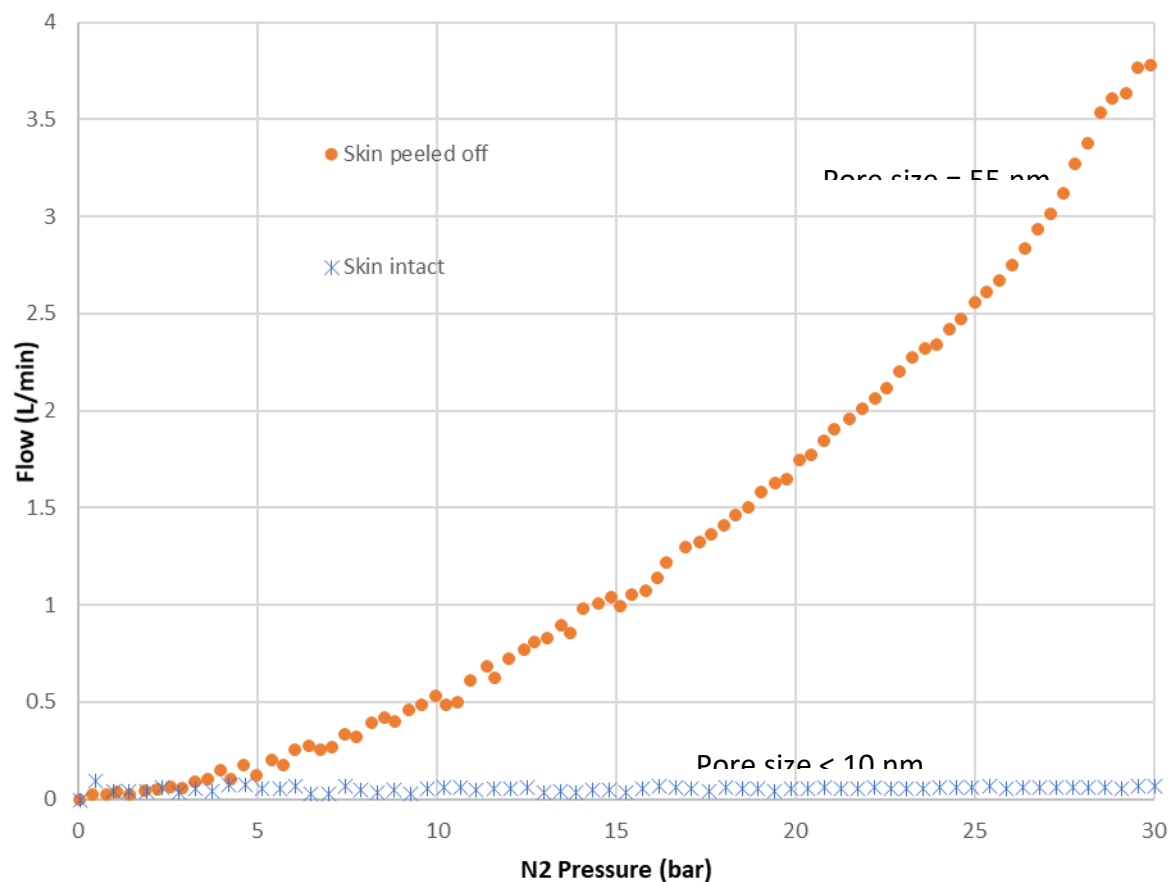
Figure 49. Bubble point pore size measurement using POROLUX 1000 for membrane 76X (crosslinked). Orange circles are measurement of membrane with the top layer (skin) of the membrane peeled off. Blue crosses are measurements from the same membrane with the skin intact. See experimental section for details on POROLUX 1000 measurements.

Capillary flow porometry (also called bubble point porometry) technique was also employed using POROLUX 1000 instrument. A membrane sample is wetted with liquid of low surface tension and low vapour pressure and subjected to increasing pressure using an inert gas (nitrogen in this case). When the pressure gets higher than the surface tension of the liquid in the largest pore, it pushes liquid out progressively through smaller and smaller pores until all the pores are emptied. By monitoring gas pressure and flow and knowing the relevant properties of the wetting liquid, pore sizes can be calculated. The wetting liquid used was a proprietary one called Porefil™, which is a fluorocarbon compound.

Figure 49 shows PORORLUX 1000 measurements where a sample of crosslinked membrane was tested with its top layer intact and the results showed that there was no gas flow, indicating that the membrane pores were smaller than 10-15 nm, the lower limit of measurement using this technique. However, when the skin of the membrane was removed, accomplished by sticking and lifting adhesive tapes on the surface of the membrane two or three times, measurements showed that the bubble point pore size was 55 nm. This is in close agreement with DSC thermoporometry and NMR cryoporometry results of the larger sized pores. Porometry measurements then showed that the cellulose membranes had skinned asymmetric membrane typical of those produced from non-solvent induced phase inversion method.

6.2.4 Scanning Electron Microscopy (SEM)

It is difficult to obtain images of cellulose membranes that are accurate with regards to their pore structure from scanning electron microscopy (SEM) due to fact that samples must be completely dry in the sample chamber and that the membranes undergo hornification upon drying. One workaround was to freeze dry the membrane samples, hoping that the pore structure would be somewhat preserved. Below are series of SEM images from membrane 27-1 sample that had been freeze dried.
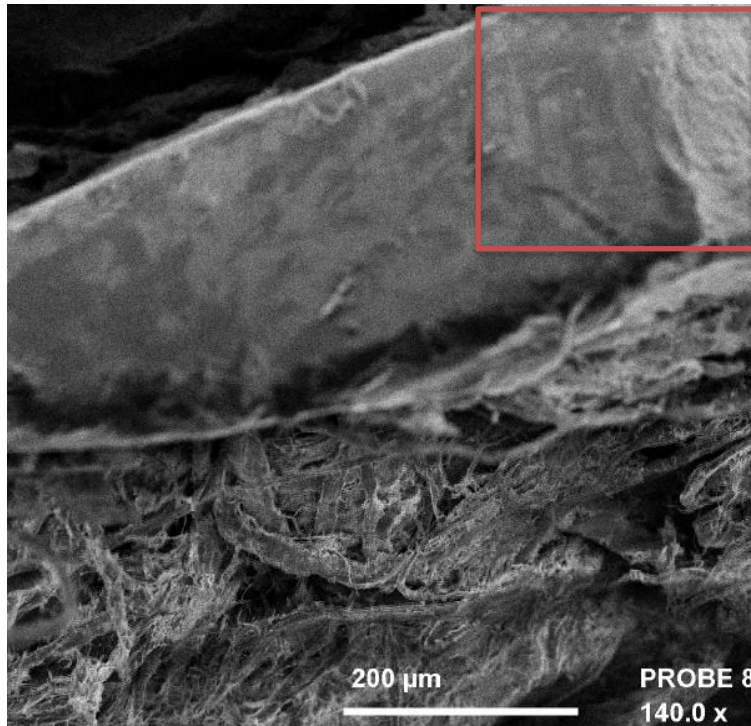
Figure 50. The bottom, fibrous layer is the filter paper backing layer and the dense top layer is the active cellulose layer. Based on this image, the thickness of the active layer was approximately between 100 to 200 μm. The rectangle is the area where the next image was zoomed in on.
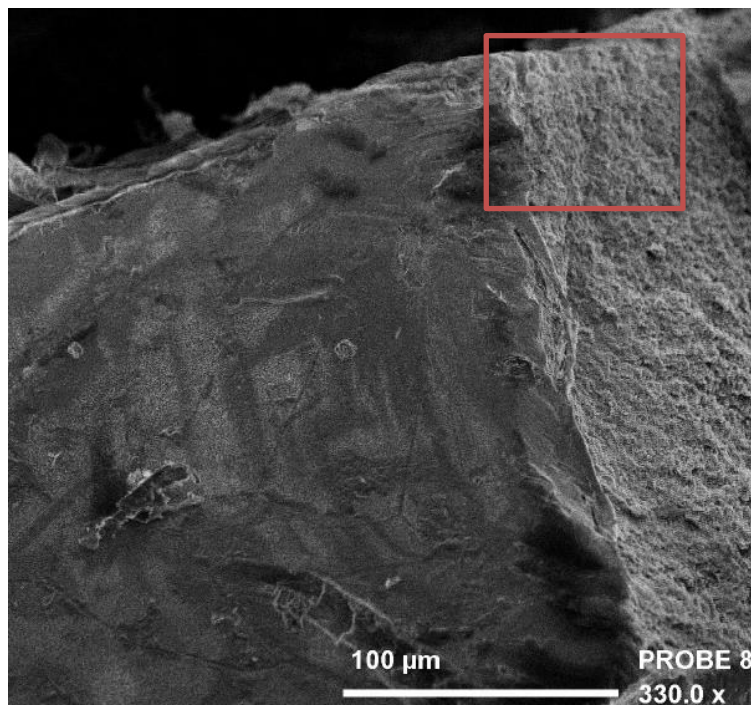
Figure 51. Zooming in on the active layer showing the two faces. The rectangle is the area where the next image was zoomed in on.
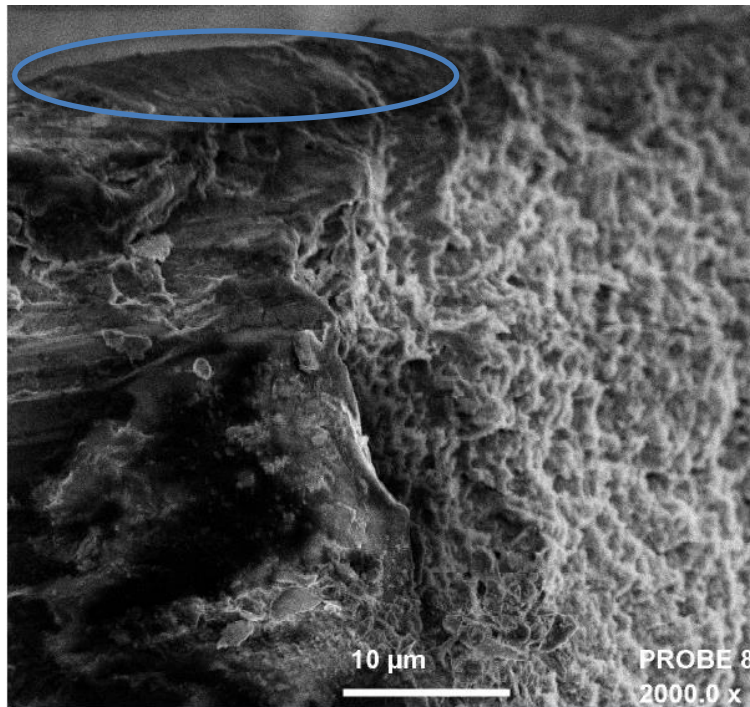
Figure 52. Zooming in further to the top part of the active layer revealed that there were unidirectional, channel-like passages underneath what seems to be a **dense skin layer** (circled on the figure) on top of the membrane. This skin is very thin compared to the bulk of the active layer.
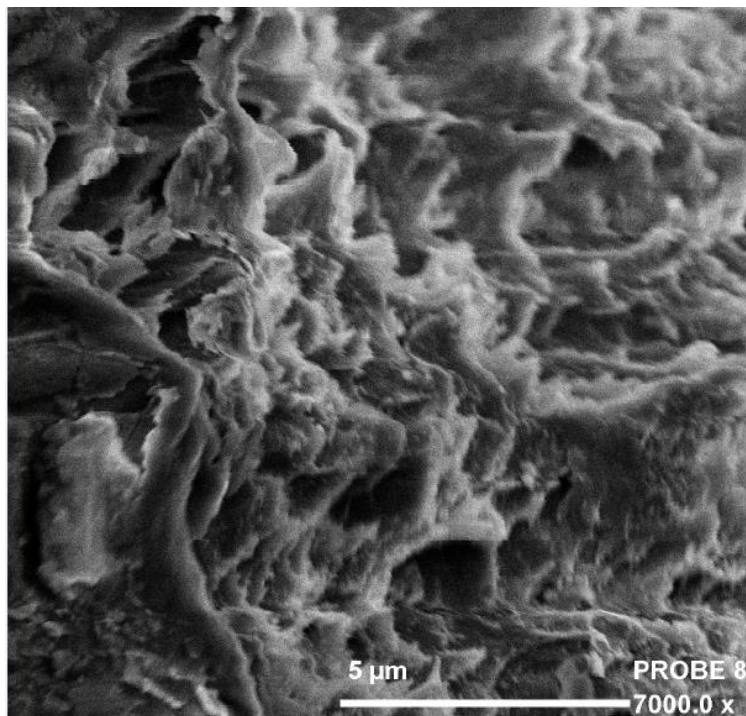
Figure 53. At even higher magnification, the charging/micro movement effect from the equipment becoming significant, yielding blurry image.

6.2.5 Thermal stability from Thermogravimetric Analysis

Thermal stability studies from Thermogravimetric Analysis (TGA) were carried out for non-crosslinked and crosslinked membranes without the filter paper backing layer, i.e. just the active cellulose layer. The results showed that the crosslinked membrane has slightly lower decomposition temperature than the non-crosslinked version (185 vs 205 deg C, Table 22). These results are consistent with typical results obtained by other researchers in the group, showing that crosslinked cellulose samples typically have lower thermal stability compared to non-crosslinked ones.

Table 22. Decomposition Temperature of crosslinked and non-crosslinked membranes from TGA

Membrane ID (X denotes crosslinked)	Decomposition Temperature from TGA (°C)
6	205
6X	185

6.2.6   Conclusion

Crosslinking is a viable way to combat the hornification of cellulose upon drying in cellulose membranes. Hornification needs to be prevented as hornified cellulose membranes offer near zero permeability to liquids. As shown in Chapter 5, glycerol post-treatment is a viable method of preserving non-crosslinked cellulose membranes. However, the protection that glycerol affords is only available as long as the glycerol has not been rinsed or washed away. This poses handling issues as it means that when a membrane has been used for filtration (glycerol has been washed away), it needs to be constantly kept in a wet state. Results from this chapter showed that dried, crosslinked cellulose membranes by glyoxalisation resisted hornification and retained their permeabilities when dried.

Studies of polystyrene (PS) rejection showed crosslinking produced tighter cellulose membranes, with one membrane showing a decrease of PS MWCO from ca. 6300 Da (non-crosslinked) to 5200 Da (crosslinked). Permeability was lower in crosslinked version, as expected, with one test showed 20% reduction in the acetonitrile permeance value compared to that of the non-crosslinked version. These results suggest that interfibril linkage bonds formed during crosslinking caused reduction in internal porosity.

The effect of crosslinking on the surface zeta potential (SZP) of the membranes are inconclusive, with one membrane showed a significant increase (from negative to positive charge) when crosslinked, but another membrane showed insignificant change. Differences in SZP values did not seem to have a meaningful effect to the membranes' rejection performance, consistent with the conclusion of surface adsorption as the primary rejection mechanism. Using a different co-solvent, however, one could manipulate the surface charge of the cellulose membrane to a limited extent. This could be useful when surface charge effect is desired (i.e. Donnan exclusion). However, a follow-up study needs to be carried out to ascertain this phenomenon.

Captive bubble contact angle (CBCA) measurements suggests that hydrophilicity/hydrophobicity of cellulose membrane could be tuned, to some extent, by employing different co-solvent in the casting solution, with a change of 34 degree in CBCA was recorded in one instance. Crosslinking did show to affect CBCA results, by making the membrane surface more hydrophilic. However, permeation tests using a hydrophilic liquid (acetonitrile) and a hydrophobic one (hexane) could not confirm this effect because of the difference in their viscosities. This is due to the previously

established assertion that the dominant transport model in cellulose membrane is the pore flow model, where liquid viscosity is the single biggest influence factor on the permeability.

Based on Young's modulus measurements from Dynamic Mechanical Analysis (DMA), crosslinking seemed to make cellulose membranes stiffer (less elastic). This is in agreement with the literature. This enhancement of mechanical properties is attributed to the interfibril covalent bonds formed by glyoxal crosslinking. Therefore, crosslinked cellulose membranes offer enhanced mechanical properties to produce more robust membranes for demanding applications.

The porometry techniques (DSC thermoporometry, NMR cryoporometry and capillary flow) indicated that membrane's structure was integrally skinned asymmetric form, with a dense, thin skin on the membrane surface, with less than 5 nm pore size, and a more porous structure underneath it, with pore sizes ranging from 40 to 85 nm. Scanning electron microscopy (SEM) images seemed to confirm the assertion of skinned asymmetric structure, although pore sizes were unable to be confirmed.

Thermogravimetric analysis showed thermal stability of cellulose membranes of ca. 200 $^{\circ}$C (slightly less when crosslinked), showing good thermal stability upper limit for potential high temperature nanofiltration applications.

The results and findings gathered during these characterisation tests, combined with the results and findings from the membrane permeation studies in Chapter 5, met the 3rd objective of this thesis as outlined in Section 1.6.

Overall Conclusion

Investigation and tests on cellulose dissolution using [EMIm][OAc]-based OESs provided a know-how on preparation of high concentration cellulose solutions, which is a prerequisite for casting cellulose membranes using NIPS technique. From the cellulose dissolution results based on multiple co-solvents, coupled with analysis of solvent parameters from the works of Catalán and Laurence and co-workers, two 'green' cellulose co-solvents were discovered: γ-butyrolactone and γ-valerolactone. The latter, along with 1-methylimidazole, which was found to be the most effective cellulose co-solvent, were the primary co-solvents used to prepare cellulose solutions for membrane castings.

Resistance of the membranes to different classes of organic solvent, including to the dipolar aprotic solvents, was excellent, as expected from cellulose. Extended exposure to these solvents, as well as transmembrane pressure of up 60 bar have been shown to pose no visual or performance degradation to the membranes, meeting the objective of creating 'robust' membranes.

The dominant transport mechanism seemed to be pore-flow model, at least for hydrophilic, solvents with low cellulose interaction. This means that viscosity plays a significant role in determining flux. Water and other cellulose-swelling solvents, such as DMSO, were found to have very low flux, pointing to OSN applications and excluding aqueous UF or NF applications. Flux comparison to commercial OSN membranes indicated comparable performances (refer to Table 17 for flux comparisons). MWCO of cellulose membranes tested by PS oligomers showed values of >6500 Da, indicating that these membranes can be considered as 'tight' UF membranes. Nevertheless, separation performances for polar compounds with MW as low as 320 Da were found to be very high, provided that the solvent used is a low interacting (non-swelling) one. The rejection mechanism was concluded to be solute-membrane adsorptive interaction. Although this rejection mechanism brought up fouling concern, facile desorption was proved possible by washing or permeating solvent with moderate (or high) affinity towards cellulose, such as methanol, achieving up to 95% cleaning efficiency.

Hornification of cellulose upon drying posed a problem, however, employing glycerol post-casting treatment circumvented, but not eliminated the problem. Crosslinking was found to be a more permanent way to combat the hornification issue. Crosslinked cellulose membranes by retained their permeabilities when dried, with the cost of lower permeability compared to the non-crosslinked version, with one test shows 20% reduction in acetonitrile flux. The reduction in permeability caused reduction in MWCO, producing 'tighter' membranes.

Porometry measurements and SEM images indicated that the membranes had integrally skinned asymmetric form, with a dense, thin skin on the membrane surface, with less than 5 nm pore size, and a more porous structure underneath it, with pore sizes ranging from 40 to 85 nm. Thermal stability was shown to be approximately ca. 200 $^{\circ}$C.

All these characteristics provided cellulose membranes an opportunity to complement the current OSN membrane portfolio.

References

1   M. A. S. Azizi Samir, F. Alloin and A. Dufresne, *Biomacromolecules*, 2005, **6**, 612–26.

2   Y. Habibi, L. a Lucia and O. J. Rojas, *Chem. Rev.*, 2010 **110**, 3479–500.

3   D. Klemm, B. Heublein, H.-P. Fink and A. Bohn, *Angew. Chemie Int. Ed.*, 2005, **44**, 3358–3393.

4   R. P. Swatloski, S. K. Spear, J. D. Holbrey and R. D. Rogers, *J. Am. Chem. Soc.*, 2002, 4974–4975.

5   L. Jiang and J. Zhang, in *Handbook of Biopolymers and Biodegradable Plastics - Properties, Processing and Applications*, ed. S. Ebnesajjad, Elsevier, 2013.

6   K. M. Gupta, Z. Hu and J. Jiang, *Polymer (Guildf).*, 2011, **52**, 5904–5911.

7   D. Klemm, D. Schumann, F. Kramer, N. Heßler, D. Koth and B. Sultanova, *Macromol. Symp.*, 2009, **280**, 60–71.

8   A. Pinkert, K. N. Marsh and S. Pang, *Ind. Eng. Chem. Res.*, 2010, **49**, 11121–11130.

9   C. Felgueiras, N. G. Azoia, C. Gonçalves, M. Gama and F. Dourado, *Front. Bioeng. Biotechnol.* , 2021, 9, 202.

10   D. Ciechanska, E. Wesoeowska and D. Wawro, *Handbook of Textile Fibre Structure, Volume 2 - Natural, Regenerated, Inorganic and Specialist Fibres*, Woodhead Publishing, 2009.

11   B. Kirchner, in *Topics in Current Chemistry: Ionic Liquids*, ed. B. Kirchner, Springer, 2009.

12   M. Gericke, P. Fardim and T. Heinze, *Molecules*, 2012, **17**, 7458–502.

13   S. S. Y. Tan and D. R. Macfarlane, in *Topics in Current Chemistry: Ionic Liquids*, ed. B. Kirchner, Springer, 2009.

14   A. Pinkert, K. N. Marsh, S. Pang and M. P. Staiger, *Chem. Rev.*, 2009, **109**, 6712–28.

15   L. Feng and Z. Chen, *J. Mol. Liq.*, 2008, **142**, 1–5.

16   R. Rinaldi, *Chem. Commun. (Camb).*, 2011, **47**, 511–3.

17   K. Ohira, K. Yoshida, S. Hayase and T. Itoh, *Chem. Lett.*, 2012, **41**, 987–989.

18   K. Ohira, Y. Abe, M. Kawatsura, K. Suzuki, M. Mizuno, Y. Amano and T. Itoh, *ChemSusChem*, 2012, **5**, 388–391.

19   M. Gericke, T. Liebert, O. A. El Seoud and T. Heinze, *Macromol. Mater. Eng.*, 2011, **296**, 483–493.

20   Y. Zhao, X. Liu, J. Wang and S. Zhang, *J. Phys. Chem. B*, 2013, **117**, 9042–9049.

21   J.-M. Andanson, E. Bordes, J. Devémy, F. Leroux, A. a. H. Pádua and M. F. C. Gomes, *Green Chem.*, 2014, **16**, 2528.

22   D. M. Rein, R. Khalfin, N. Szekely and Y. Cohen, *Carbohydr. Polym.*, 2014, **112**, 125–33.

23   Relative permittivity, http://en.wikipedia.org/wiki/Relative_permittivity.

24   IUPAC Compendium of Chemical Terminology, 2nd ed. (the 'Gold Book'), http://goldbook.iupac.org/D01751.html.

25   P. Vandezande, L. E. M. Gevers and I. F. J. Vankelecom, *Chem. Soc. Rev.*, 2008, **37**, 365–405.

26   M. Mulder, *Basic Principles of Membrane Technology*, Kluwer Academic Publishers, 2nd ed., 1997.

27   L. G. Peeva, M. Sairam and A. G. Livingston, in *Comprehensive Membrane Science and Engineering - Volume 2*, eds. E. Drioli and L. Giorno, Elsevier B.V., 2010, pp. 91–113.

28   Membrane Separation in Aqueous Environment, http://www.sulzer.com/en/Products-and-Services/Separation-Technology/Membrane-Technology/Membrane-Separation-in-Acqueous-Environment.

29   M. F. J. Solomon, Y. Bhole and A. G. Livingston, *J. Memb. Sci.*, 2012, **423–424**, 371–382.

30   Organic   Solvent   Nanofiltration   (OSN),   http://www.sulzer.com/en/Products-and-Services/Separation-Technology/Membrane-Technology/Organic-Solvent-Nanofiltration-OSN.

31   K. Vanherck, P. Vandezande, S. O. Aldea and I. F. J. Vankelecom, *J. Memb. Sci.*, 2008, **320**, 468–476.

32   C. Jimenez-Gonzalez, C. S. Ponder, Q. B. Broxterman and J. B. Manley, *Org. Process Res. Dev.*, 2011, **15**, 912–917.

33   A. V Volkov, G. A. Korneeva and G. F. Tereshchenko, *Russ. Chem. Rev.*, 2008, **77**, 983–993.

34   Y. H. S. Toh, F. W. Lim and A. G. Livingston, *J. Memb. Sci.*, 2007, **301**, 3–10.

35   C. Cuissinat, P. Navard and T. Heinze, *Carbohydr. Polym.*, 2008, **72**, 590–596.

36   A. R. Mahajan and S. R. Mirgane, *J. Thermodyn.*

37   M. R. Landry, *Thermochim. Acta*, 2005, **433**, 27–50.

38   E. Rojo, M. S. Peresin, W. W. Sampson, I. C. Hoeger, J. Vartiainen, J. Laine and O. J. Rojas, *Green Chem.*, 2015, **17**, 1853–1866.

39   O. V. Petrov and I. Furo, *Prog. Nucl. Magn. Reson. Spectrosc.*, 2009, **54**, 97–122.

40   J. D. Jeon, S. J. Kim and S. Y. Kwak, *J. Memb. Sci.*, 2008, **309**, 233–238.

41   Y. Yuan and T. R. Lee, in *Springer Series in Surface Sciences*, eds. G. Bracco and B. Holst, Springer, 2013, vol. 51.

42   C. Causserand and P. Aimar, in *Comprehensive Membrane Science and Engineering, Volume 1*, Elsevier B.V., 2010, pp. 311–335.

43   G. Shlieout, K. Arnold and G. Müller, *AAPS PharmSciTech*, 2002, 45–54.

44   M. T. Clough, K. Geyer, P. a. Hunt, S. Son, U. Vagt and T. Welton, *Green Chem.*, , DOI:10.1039/C4GC01955E.

45   C. Olsson, A. Hedlund, A. Idström and G. Westman, *J. Mater. Sci.*, 2014, **49**, 3423–3433.

46   D. Rabari, N. Patel, M. Joshipura and T. Banerjee, *J. Chem. Eng. Data*, 2014, **59**, 571–578.

47   276855   -   Dimethyl   sulfoxide, http://www.sigmaaldrich.com/catalog/product/sial/276855?lang=en&region=GB.

48   L. C. Fidale, N. Ruiz, T. Heinze and O. A. El Seoud, *Macromol. Chem. Phys.*, 2008, **209**, 1240–1254.

49   A. C. O'Sullivan, *Cellulose*, 1997, **4**, 173–207.

50   O. A. El Seoud, H. Nawaz and E. P. G. Arêas, *Molecules*, 2013, **18**, 1270–1313.

51   F. Huo, Z. Liu and W. Wang, *J. Phys. Chem. B*, 2013, **117**, 11780–11792.

52   B. Kosan, C. Michels and F. Meister, *Cellulose*, 2008, 59–66.

53   J. Vitz, T. Erdmenger, C. Haensch and U. S. Schubert, *Green Chem.*, 2009, **11**, 417.

54   J. Catalán, *J. Phys. Chem. B*, 2009, **113**, 5951–5960.

55   C. Laurence, J. Legros, A. Chantzis, A. Planchat and D. Jacquemin, *J. Phys. Chem. B*, 2015, **119**, 3174–3184.

56   WHO, *Gamma-butyrolactone (GBL) Critical Review Report*, Geneva, 2014.

57   J. S. Luterbacher, J. M. Rand, D. M. Alonso, J. Han, J. T. Youngquist, C. T. Maravelias, B. F. Pfleger and J. A. Dumesic, *Science (80-.).*, 2014, **343**, 277–280.

58   I. T. Horváth, H. Mehdi, V. Fábos, L. Boda and L. T. Mika, *Green Chem.*, 2008, **10**, 238–242.

59   Y. H. See-Toh, M. Silva and A. Livingston, *J. Memb. Sci.*, 2008, **324**, 220–232.

60   J. P. Robinson, E. S. Tarleton, C. R. Millington and A. Nijmeijer, *Membr. Technol.*, 2004, 5–12.

61   C. J. Davey, Z.-X. Low, R. H. Wirawan and D. A. Patterson, *J. Memb. Sci.*, 2017, **526**, 221–228.

62   Solvent Resistent Membranes, http://www.solsep.com/SRM.htm, (accessed 9 July 2017).

63   G. Yang, L. Zhang and H. Feng, *J. Memb. Sci.*, 1999, **161**, 31–40.

64   X. Xiong, J. Duan, W. Zou, X. He and W. Zheng, *J. Memb. Sci.*, 2010, **363**, 96–102.

65   V. Romero, M. I. Vazquez and J. Benavente, *J. Memb. Sci.*, 2013, **433**, 152–159.

66   Z. Karim, A. P. Mathew, M. Grahn, J. Mouzon and K. Oksman, *Carbohydr. Polym.*, 2014, **112**, 668–676.

67   H. Ma, C. Burger, B. S. Hsiao and B. Chu, *J. Memb. Sci.*, 2014, **454**, 272–282.

68   A. Mautner, K. Y. Lee, P. Lahtinen, M. Hakalahti, T. Tammelin, K. Li and A. Bismarck, *Chem Commun*, 2014, **50**, 5778–5781.

69   A. Mautner, K. Y. Lee, T. Tammelin, A. P. Mathew, A. J. Nedoma, K. Li and A. Bismarck, *React. Funct. Polym.*, 2015, **86**, 209–214.

70   S. Livazovic, Z. Li, A. R. Behzad, K.-V. Peinemann and S. P. Nunes, *J. Memb. Sci.*, 2015, **490**, 282–293.

71   T. Puspasari, N. Pradeep and K.-V. Peinemann, *J. Memb. Sci.*, 2015, **491**, 132–137.

72   H. H. Wang, J. T. Jung, J. F. Kim, S. Kim, E. Drioli and Y. M. Lee, *J. Memb. Sci.*, 2019, **574**, 44–54.

73   S. Li, D. Wang, H. Xiao, H. Zhang, S. Cao, L. Chen, Y. Ni and L. Huang, *Carbohydr. Polym.*, 2021, **255**, 117352.

74   S. Loeb and S. Sourirajan, *Adv. Chem.*, 1963, 117–132.

75   Vidya Mahankali Burra, PhD Dissertation, Texas Tech University, 1993.

76   A. K. Hołda, B. Aernouts, W. Saeys and I. F. J. Vankelecom, *J. Memb. Sci.*, 2013, **442**, 196–205.

77   S. Darvishmanesh, J. C. Jansen, F. Tasselli, E. Tocci, P. Luis, J. Degrève, E. Drioli and B. Van der Bruggen, *J. Memb. Sci.*, 2011, **379**, 60–68.

78   K. Hendrix, G. Koeckelberghs and I. F. J. Vankelecom, *J. Memb. Sci.*, 2014, **452**, 241–252.

79   G. Szekely, M. F. Jimenez-Solomon, P. Marchetti, J. F. Kim and A. G. Livingston, *Green Chem.*, 2014, **16**, 4440–4473.

80   L. Broens, F. W. Altena, C. A. Smolders and D. M. Koenhen, *Desalination*, 1980, **32**, 33.

81   A. Nazet, S. Sokolov, T. Sonnleitner, T. Makino, M. Kanakubo and R. Buchner, *J. Chem. Eng. Data*, 2015, **60**, 2400–2411.

82   E. Gale, R. H. Wirawan, R. L. Silveira, C. S. Pereira, M. A. Johns, M. S. Skaf and J. L. Scott, *ACS Sustain. Chem. Eng.*, 2016, **4**, 6200–6207.

83   J. P. Robinson, E. S. Tarleton, C. R. Millington and A. Nijmeijer, *J. Memb. Sci.*, 2004, **230**, 29–37.

84   M. E. Williams, J. A. Hestekin, C. N. Smothers and D. Bhattacharyya, *Ind. Eng. Chem. Res.*, 1999, **38**, 3683–3695.

85   D. R. Paul, in *Comprehensive Membrane Science and Engineering*, 2010.

86   S. Zeidler, U. Kätzel and P. Kreis, *J. Memb. Sci.*, 2013, **429**, 295–303.

87   A. Malakhov and A. Volkov, *Sep. Sci. Technol.*, 2015, **6395**, 2198–2210.

88   V. N. Burganos, in *Comprehensive Membrane Science and Engineering*, 2010.

89   P. Silva, S. Han and A. G. Livingston, *J. Memb. Sci.*, 2005, **262**, 49–59.

90   R. Machado, D. Hasson and R. Semiat, *J. Memb. Sci.*, 2000, **166**, 63–69.

91   H. Strathmann, L. Giorno and E. Drioli, in *Comprehensive Membrane Science and Engineering - Volume 1*, eds. E. Drioli and L. Giorno, Elsevier B.V., 2010, pp. 91–112.

92   B. Van der Bruggen, J. Geens and C. Vandecasteele, *Sep. Sci. Technol.*, 2002, **37**, 783–797.

93   D. Bhanushali, S. Kloos, C. Kurth and D. Bhattacharyya, *J. Memb. Sci.*, 2001, **189**, 1–21.

94   D. Bhanushali, S. Kloos and D. Bhattacharyya, *J. Memb. Sci.*, 2002, **208**, 343–359.

95   H. J. Zwijnenberg, S. M. Dutczak, M. E. Boerrigter, M. A. Hempenius, M. W. J. Luiten-

Olieman, N. E. Benes, M. Wessling and D. Stamatialis, *J. Memb. Sci.*, 2012, **390**–**391**, 211–217.

96   B. Van Der Bruggen, J. C. Jansen, A. Figoli, J. Geens, K. Boussu and E. Drioli, *J. Phys. Chem. B*, 2006, **110**, 13799–13803.

97   J. Geens, K. Boussu, C. Vandecasteele and B. Van der Bruggen, *J. Memb. Sci.*, 2006, **281**, 139–148.

98   Y. Zhao and Q. Yuan, *J. Memb. Sci.*, 2006, **279**, 453–458.

99   R. Rohani, M. Hyland and D. Patterson, *J. Memb. Sci.*, 2011, **382**, 278–290.

100   P. Marchetti, M. F. J. Solomon, G. Szekely and A. G. Livingston, *Chem. Rev.*, 2014, **114**, 10735–10806.

101   A. W. Mohammad, Y. H. Teow, W. L. Ang, Y. T. Chung, D. L. Oatley-Radcliffe and N. Hilal, *Desalination*, 2015, **356**, 226–254.

102   N. A. A. Sani, W. J. Lau, N. A. H. M. Nordin and A. F. Ismail, *Chem. Eng. Res. Des.*, 2016, **115**, 66–76.

103   S. Hermans, H. Mariën, C. Van Goethem and I. F. Vankelecom, *Curr. Opin. Chem. Eng.*, 2015, **8**, 45–54.

104   Y. H. See Toh, X. X. Loh, K. Li, a. Bismarck and a. G. Livingston, *J. Memb. Sci.*, 2007, **291**, 120–125.

105   S. Postel, C. Schneider and M. Wessling, *J. Memb. Sci.*, 2016, **497**, 47–54.

106   K. J. Liu and J. L. Parsons, *Macromolecules*, 1969, **2**, 529–533.

107   O. A. El Seoud, L. C. Fidale, N. Ruiz, M. L. O. D'Almeida and E. Frollini, *Cellulose*, 2008, **15**, 371–392.

108   Viscosity, http://macro.lsu.edu/HowTo/solvents/viscosity.htm, (accessed 28 May 2017).

109   J. Sangster, *J. Phys. Chem. Ref. Data*, 1989, 18, 1111–1229.

110   M. J. Kamlet, J.-L. M. Abboud, M. H. Abraham and R. W. Taft, *J. Org. Chem.*, 1983, 2877–2887.

111   C. Reichardt, *Chem. Rev.*, 1994, **94**, 2319–2358.

112   Y.-L. Lin and C.-H. Lee, *Ind. Eng. Chem. Res.*, 2014, **53**, 6798–6806.

113   S. Darvishmanesh, J. Degrève and B. Van der Bruggen, *Phys. Chem. Chem. Phys.*, 2010, **12**, 13333.

114   P. Wu and M. Imai, *Desalin. Water Treat.*, 2013, **51**, 5237–5247.

115   A. K. Hołda and I. F. J. Vankelecom, *J. Memb. Sci.*, 2014, **450**, 499–511.

116   C. Kaewprasit, E. Hequet, N. Abidi and J. P. Gourlot, *J. Cotton Sci.*, 1998, **173**, 164–173.

117   TAKESHI MATSUURA and S. Sourirajan, *J. Appl. Polym. Sci.*, 1971, **15**, 2905–2927.

118   F. Quero, M. Nogi, K. Lee, G. Vanden Poel, A. Bismarck, A. Mantalaris, H. Yano and S. J. Eichhorn, *ACS Appl. Mater. Interfaces*, 2011, 490–499.

119   C. Schramm and B. Rinderer, *Anal. Chem.*, 2000, **72**, 5829–5833.

120   J. M. B. Fernandes Diniz, M. H. Gil and J. A. A. M. Castro, *Wood Sci. Technol.*, 2004, **37**, 489–494.

121   Å. Östlund, A. Idström, C. Olsson, P. T. Larsson and L. Nordstierna, *Cellulose*, 2013, **20**, 1657–1667.

122   Q. Q. Wang, Z. He, Z. Zhu, Y. H. P. Zhang, Y. Ni, X. L. Luo and J. Y. Zhu, *Biotechnol. Bioeng.*, 2012, **109**, 381–389.

123   P. Navard, F. Wendler, F. Meister and M. Bercea, *Preparation and Properties of Cellulose Solutions*, 2012.

APPENDIX A – CELLULOSE SOLUBILITY TESTING DATA

EMIM Ac/PC (min XIL for dissolution = 0.2)
70 C

						wt % cellulose						
X_{IL}	Trial 1 - Y	Trial 1 - N	Midpoint	Trial 2 - Y	Trial 2 - N	Midpoint	Trial 3 - Y	Trial 3 - N	Midpoint	Avg - Y	Avg - N	Midpoint
0.2	3.32	4.07	3.70	4.28	4.81	4.55	4.27	4.91	4.59	3.96	4.60	4.28
0.3	7.85	9.07	8.46	8.69	8.93	8.81	8.65	8.86	8.76	8.40	8.95	8.68
0.4	10.31	11.00	10.66	9.49	10.43	9.96	10.01	10.53	10.27	9.94	10.65	10.30
0.5	11.49	12.10	11.80	12.80	13.76	13.28				12.15	12.93	12.54
0.6	9.10	10.71	9.91	12.26	12.80	12.53	12.77	12.97	12.87	11.38	12.16	11.77
0.7	10.70	11.09	10.90	13.45	14.04	13.75				12.08	12.57	12.32
0.8	15.78	16.35	16.07	15.08	15.64	15.36				15.43	16.00	15.71
0.9	19.85	20.62	20.24	19.88	20.69	20.29				19.87	20.66	20.26
1												21.66

EMIM Ac/DMSO (min XIL for dissolution = 0.08 [Rinaldi])
70 C

						wt % cellulose						
X_{IL}	Trial 1 - Y	Trial 1 - N	Midpoint	Trial 2 - Y	Trial 2 - N	Midpoint	Trial 3 - Y	Trial 3 - N	Midpoint	Avg - Y	Avg - N	Midpoint
0.02												
0.052	3.15	3.47	3.31	3.98	4.22	4.10	3.42	3.69	3.56	3.52	3.79	3.66
0.077				6.83	7.14	6.99	6.56	7.04	6.80	6.70	7.09	6.89
0.11	10.4	11.21	10.81	10.38	11.49	10.94	10.9	11.27	11.09	10.56	11.32	10.94
0.15	12.79	13.10	12.95	12.05	12.41	12.23				12.42	12.76	12.59
0.20	15.46	15.77	15.62	15.64	16.46	16.05	15.09	15.52	15.31	15.40	15.92	15.66
0.25	17.21	17.70	17.46	19.14	19.60	19.37				18.18	18.65	18.41
0.30	20.00	20.38	20.19	19.60	20.16	19.88	19.50	19.86	19.68	19.70	20.13	19.92
0.40	20.90	21.39	21.15	18.75	19.74	19.25	19.84	20.33	20.09	19.83	20.49	20.16
0.50	21.18	21.50	21.34	21.37	21.85	21.61	21.15	21.49	21.32	21.23	21.61	21.42
0.60	22.00	22.53	22.27	22.41	22.94	22.68	22.33	22.76	22.55	22.25	22.74	22.50
0.70	22.83	23.15	22.99	23.09	23.28	23.19	22.68	23.23	22.96	22.87	23.22	23.04
0.85	22.22	22.92	22.57	22.92	23.62	23.27	23.53	24.51	24.02	22.89	23.68	23.29
0.93	22.77	23.10	22.94	23.06	23.44	23.25	23.70	24.08	23.89	23.18	23.54	23.36
1.00	20.30	21.22	20.76	22.51	22.95	22.73	21.12	21.86	21.49	21.31	22.01	21.66

EMIM Ac/DMI (min XIL for dissolution = 0.18 [Rinaldi])
70 C

						wt % cellulose						
X_{IL}	Trial 1 - Y	Trial 1 - N	Midpoint	Trial 2 - Y	Trial 2 - N	Midpoint	Trial 3 - Y	Trial 3 - N	Midpoint	Avg - Y	Avg - N	Midpoint
0.21	9.92	10.51	10.22	10.52	11	10.76	10.76	11.37	11.07	10.40	10.96	10.68
0.3	16.03	16.32	16.18	15.58	16.14	15.86	16.04	16.55	16.30	15.88	16.34	16.11
0.4	19.08	19.41	19.25	18.84	19.33	19.09	18.89	19.28	19.09	18.94	19.34	19.14
0.56	21.79	22.15	21.97	21.26	21.76	21.51	21.76	22.23	22.00	21.60	22.05	21.83
0.7	22.68	23.28	22.98	22.80	23.36	23.08	22.59	23.12	22.86	22.69	23.25	22.97
0.85	24.26	24.84	24.55	24.40	24.65	24.53	24.02	24.27	24.15	24.23	24.59	23.40
1.00	20.30	21.22	20.76	22.51	22.95	22.73	21.12	21.86	21.49	21.31	22.01	21.66

EMIM Ac/1-methylimidazole (min XIL for dissolution = 0.08)
70 C

												wt % cellulose
X_{IL}	Trial 1 - Y	Trial 1 - N	Midpoint	Trial 2 - Y	Trial 2 - N	Midpoint	Trial 3 - Y	Trial 3 - N	Midpoint	Avg - Y	Avg - N	Midpoint
0.07	5.06	5.95	5.51	5.13	6.09	5.61				5.10	6.02	5.56
0.15	14.27	15.49	14.88	13.85	14.81	14.33	14.7	15.21	14.96	14.27	15.17	14.72
0.2	17.6	18.47	18.04	18.89	20.17	19.53	18.52	19.07	18.80	18.34	19.24	18.79
0.3	20.94	22.22	21.58	20.72	21.99	21.36	22.13	22.47	22.30	21.26	22.23	21.75
0.4	22.13	23.14	22.64	21.52	22.84	22.18	22.4	22.73	22.57	22.02	22.90	22.46
0.5	19.71	23.17	21.44	21.55	24.08	22.82	23.97	24.38	24.18	21.74	23.88	22.81
0.65	20.80	22.69	21.75	23.48	23.96	23.72	22.35	23.03	22.69	22.21	23.23	22.72
0.8	23.11	23.92	23.52	22.84	23.68	23.26				22.98	23.80	23.40
1.00	20.30	21.22	20.76	22.51	22.95	22.73	21.12	21.86	21.49	21.31	22.01	21.66

EMIM Ac/sulfolane (min XIL for dissolution = 0.23 [Rinaldi])
70 C

												wt % cellulose
X_{IL}	Trial 1 - Y	Trial 1 - N	Midpoint	Trial 2 - Y	Trial 2 - N	Midpoint	Trial 3 - Y	Trial 3 - N	Midpoint	Avg - Y	Avg - N	Midpoint
0.28				10.82	12.66	11.74	11.3	12.82	12.06	11.06	12.74	11.90
0.4	15.7	16.7	16.20	15.42	17.17	16.30	16.26	17.54	16.90	15.79	17.14	16.47
0.55	17.11	18.96	18.04	18.49	19.09	18.79	17.68	18.6	18.14	17.76	18.88	18.32
0.7	21.41	21.93	21.67	20.3	20.78	20.54	20.31	20.71	20.51	20.67	21.14	20.91
1.00	20.30	21.22	20.76	22.51	22.95	22.73	21.12	21.86	21.49	21.31	22.01	21.66

EMIM Ac/γ-valerolactone (min XIL for dissolution = 0.26)
70 C

												wt % cellulose
X_{IL}	Trial 1 - Y	Trial 1 - N	Midpoint	Trial 2 - Y	Trial 2 - N	Midpoint	Trial 3 - Y	Trial 3 - N	Midpoint	Avg - Y	Avg - N	Midpoint
0.2												
0.31	9.75	11.24	10.50	6.01	9.12	7.57	9.59	10.15	9.87	8.45	10.17	9.31
0.42	14.93	15.84	15.39	14.33	14.91	14.62	14.25	15.03	14.64	14.50	15.26	14.88
0.50	16.44	17.09	16.77	16.79	17.3	17.05	16.93	17.35	17.14	16.72	17.25	16.98
0.58	19.09	19.58	19.34				18.28	18.49	18.39	18.69	19.04	18.86
0.70	20.24	20.85	20.55	19.74	19.99	19.87	19.57	19.87	19.72	19.85	20.24	20.04
0.85	19.51	20.24	19.88	20.19	20.62	20.41	20.54	20.76	20.65	20.08	20.54	20.31
1.00												21.66

EMIM Ac/DMAc
70 C

												wt % cellulose
X_{IL}	Trial 1 - Y	Trial 1 - N	Midpoint	Trial 2 - Y	Trial 2 - N	Midpoint	Trial 3 - Y	Trial 3 - N	Midpoint	Avg - Y	Avg - N	Midpoint
0.07												
0.15	6.51	7.61	7.06	7.14	7.35	7.25	6.62	6.99	6.81	6.76	7.32	7.04
0.25	13.19	13.58	13.39	11.95	12.74	12.35	12.36	12.78	12.57	12.50	13.03	12.77
0.36	16.03	16.84	16.44	15.79	16.68	16.24	15.65	16.21	15.93	15.82	16.58	16.20
0.50	17.90	19.12	18.51	18.27	18.55	18.41	18.24	18.52	18.38	18.14	18.73	18.43
0.65	20.39	21.32	20.86	21.03	21.61	21.32	20.43	20.71	20.57	20.62	21.21	20.92
0.80	21.28	21.68	21.48	20.78	21.08	20.93	20.63	20.86	20.75	20.90	21.21	21.05

EMIM Ac/DMF
70 C

												wt % cellulose		
X_{IL}	Trial 1 - Y	Trial 1 - N	Midpoint	Trial 2 - Y	Trial 2 - N	Midpoint	Trial 3 - Y	Trial 3 - N	Midpoint	Avg - Y	Avg - N	Midpoint
0.09												
0.15	8.89	9.78	9.34	8.20	9.67	8.94				8.55	9.73	9.14
0.21	13.53	14.29	13.91	12.99	14.10	13.55				13.26	14.20	13.73
0.28	15.16	16.05	15.61	14.30	15.53	14.92				14.73	15.79	15.26
0.35	17.85	18.53	18.19	18.35	19.14	18.75				18.10	18.84	18.47
0.44	20.05	20.79	20.42	18.14	19.71	18.93				19.10	20.25	19.67
0.60	20.91	21.56	21.24	20.53	21.52	21.03				20.72	21.54	21.13
1.00												21.66

EMIM Ac/TMU
70 C   Additional repeats

												wt % cellulose		
X_{IL}	Trial 1 - Y	Trial 1 - N	Midpoint	Trial 2 - Y	Trial 2 - N	Midpoint	Trial 3 - Y	Trial 3 - N	Midpoint	Avg - Y	Avg - N	Midpoint
0.45												
0.50	6.10	6.83	6.47	10.34	11.09	10.72	7.44	8.17	7.81	7.96	8.70	8.33
0.59	13.28	14.00	13.64	15.84	16.64	16.24				14.56	15.32	14.94
0.69	16.98	17.99	17.49	19.78	20.12	19.95				18.38	19.06	18.72
0.80	21.59	22.06	21.83	20.70	21.53	21.12				21.15	21.80	21.47
1.00												21.66

EMIM Ac/NMP
70 C

												wt % cellulose		
X_{IL}	Trial 1 - Y	Trial 1 - N	Midpoint	Trial 2 - Y	Trial 2 - N	Midpoint	Trial 3 - Y	Trial 3 - N	Midpoint	Avg - Y	Avg - N	Midpoint
0.20	9.65	10.93	10.29	10.10	10.57	10.34				9.88	10.75	10.31
0.30	14.07	14.61	14.34	14.46	14.82	14.64				14.27	14.72	14.49
0.40	18.12	18.71	18.42	18.37	19.24	18.81				18.25	18.98	18.61
0.50	19.73	20.52	20.13	20.09	20.76	20.43				19.91	20.64	20.28

EMIM Ac/γ-butyrolactone (min XIL for dissolution = 0.08)
70 C

												wt % cellulose		
X_{IL}	Trial 1 - Y	Trial 1 - N	Midpoint	Trial 2 - Y	Trial 2 - N	Midpoint	Trial 3 - Y	Trial 3 - N	Midpoint	Avg - Y	Avg - N	Midpoint
0.08	1.91	2.88	2.40	2.33	3.14	2.74				2.12	3.01	2.57
0.15	7.34	7.94	7.64	6.86	7.47	7.17				7.10	7.71	7.40
0.25	11.90	12.71	12.31	11.92	12.58	12.25				11.91	12.65	12.28
0.38	17.81	18.75	18.28	17.31	17.88	17.60				17.56	18.32	17.94
0.50	19.56	20.01	19.79	19.44	20.17	19.81				19.50	20.09	19.80
0.65	22.01	22.64	22.33	21.56	22.01	21.79				21.79	22.33	22.06
0.83	22.37	23.06	22.72	21.26	22.19	21.73				21.82	22.63	22.22

APPENDIX B – Density and Excess Molar Volume of EMIM AcO-based Organic Electrolyte Solutions

Density measurements of EMIM AcO-DMSO system at 20 deg C

Mole fract	Density (g.cm^{-3})	SD	% error	Molar Vol	Error prop.	Excess Molar Vol,
1.000	1.1004	0.00148	0.13%	154.68	0.21	0.00
0.900	1.1020	0.00033	0.03%	146.10	0.04	-0.20
0.758	1.1030	0.00051	0.05%	134.12	0.06	-0.30
0.687	1.1039	0.00037	0.03%	128.07	0.04	-0.38
0.546	1.1059	0.00057	0.05%	116.15	0.06	-0.54
0.417	1.1069	0.00050	0.05%	105.26	0.05	-0.57
0.364	1.1072	0.00055	0.05%	100.87	0.05	-0.57
0.301	1.1078	0.00034	0.03%	95.55	0.03	-0.59
0.251	1.1075	0.00016	0.01%	91.44	0.01	-0.53
0.205	1.1072	0.00069	0.06%	87.64	0.05	-0.48
0.156	1.1069	0.00020	0.02%	83.54	0.01	-0.42
0.103	1.1057	0.00058	0.05%	79.26	0.04	-0.31
0.056	1.1049	0.00043	0.04%	75.37	0.03	-0.23
0.000	1.1016	0.00049	0.04%	70.92	0.03	0.00

Density measurements of EMIM AcO-PC system at 20 deg C

Mole fract	Density (g.cm^{-3})	SD	% error	Molar Vol	Error prop.	Excess Molar Volu
1.000	1.1004	0.00148	0.13%	154.68	0.21	0.00
0.885	1.1089	0.00020	0.02%	146.42	0.03	-0.20
0.723	1.1208	0.00017	0.02%	135.00	0.02	-0.27
0.592	1.1323	0.00023	0.02%	125.76	0.03	-0.36
0.491	1.1399	0.00022	0.02%	118.90	0.02	-0.18
0.408	1.1484	0.00027	0.02%	113.11	0.03	-0.18
0.307	1.1625	0.00028	0.02%	105.80	0.03	-0.41
0.208	1.1759	0.00007	0.01%	98.89	0.01	-0.43
0.107	1.1885	0.00025	0.02%	92.02	0.02	-0.19
0.000	1.2046	0.00078	0.07%	84.75	0.06	0.00

Density measurements of EMIM AcO-PC system at 19 deg C (13 June 2015)

Mole fract	Density (g.cm^{-3})	SD	% error	Molar Vol	Error prop.	Excess Molar Volu
1.000	1.1037	0.00034	0.03%	154.22	0.05	0.00
0.854	1.1130	0.00024	0.02%	144.00	0.03	-0.05
0.705	1.1244	0.00047	0.04%	133.48	0.06	-0.15
0.589	1.1347	0.00032	0.03%	125.30	0.04	-0.24
0.471	1.1456	0.00033	0.03%	117.12	0.03	-0.24
0.362	1.1572	0.00038	0.03%	109.52	0.04	-0.23
0.256	1.1696	0.00020	0.02%	102.22	0.02	-0.18
0.166	1.1812	0.00040	0.03%	96.01	0.03	-0.10
0.096	1.1920	0.00022	0.02%	91.12	0.02	-0.09
0.000	1.2077	0.00014	0.01%	84.54	0.01	0.00

Karl-Fischer reading (water content) of neat PC: 1014 ppm, 1171 ppm.

Density measurements of EMIM AcO-DMI system at 20.5 deg C (12 Oct 2015)

Mole fract	Density (g.cm^{-3})	SD	% error	Molar Vol	Error prop.	Excess Molar Volu
0.000	1.0625	0.00047	0.04%	107.43	0.05	0.00
0.105	1.0695	0.00046	0.04%	112.24	0.05	-0.16
0.205	1.0755	0.00030	0.03%	116.83	0.03	-0.29
0.307	1.0811	0.00027	0.02%	121.52	0.03	-0.44
0.408	1.0855	0.00011	0.01%	126.24	0.01	-0.48
0.503	1.0889	0.00018	0.02%	130.71	0.02	-0.47
0.603	1.0921	0.00017	0.02%	135.49	0.02	-0.44
0.702	1.0942	0.00037	0.03%	140.31	0.05	-0.31
0.842	1.0973	0.00042	0.04%	147.03	0.06	-0.17
1.000	1.1004	0.00050	0.05%	154.68	0.07	0.00

Density measurements of EMIM AcO-GVL system at 20.0 deg C (12 Oct 2015)

Mole fract	Density (g.cm^{-3})	SD	% error	Molar Vol	Error prop.	Excess Molar Volu
0.000	1.0541			94.98		0.000
0.138	1.0668			102.94		-0.301
0.281	1.0770			111.24		-0.498
0.416	1.0842			119.23		-0.564
0.560	1.0896			127.90		-0.483
0.709	1.0948			136.87		-0.434
0.847	1.0980			145.28		-0.253
1.000	1.1007			154.64		0.000

Density measurements of EMIM AcO-TMU system at 21.2 deg C (12 Oct 2015)

Mole fract	Density (g.cm^{-3})	SD	% error	Molar Vol	Error prop.	Excess Molar Volu
0.000	0.966319579			120.21		0.000
0.150	0.993446728			125.10		-0.269
0.287	1.016260912			129.54		-0.510
0.414	1.035213565			133.80		-0.611
0.540	1.051926374			138.19		-0.577
0.700	1.071049358			143.76		-0.478
0.853	1.087073792			149.26		-0.240
1.000	1.101285055			154.56		0.000

Density measurements of EMIM AcO-1MI system at 19 deg C (28 Jun 2016)

Mole fract	Density (g.cm^{-3})	SD	% error	Molar Vol	Error prop.	Excess Molar Volu
0.000	1.0323			79.53		0.000
0.142	1.0588			89.39		-0.824
0.276	1.0730			99.15		-1.057
0.426	1.0830			110.49		-1.006
0.565	1.0896			121.05		-0.864
0.709	1.0953			132.01		-0.703
0.855	1.0991			143.28		-0.401
1.000	1.1015			154.52		0.000